

# D5.2.1



## **SPECIFICATIONS FOR BEACON WP5: TESTING, VERIFICATION AND VALIDATION OF MODELS STEP 2- large scale experiments**

### DELIVERABLE (D5.2.1) Report

Author(s): Jean Talandier, Andra

Contributions from Beacon partners

Reporting period: 01/06/17 – 30/11/18

Date of issue of this report: **30/11/2018**

Start date of project: **01/06/17**

Duration: 48 Months

This project receives funding from the Euratom research and training programme 2014-2018 under grant agreement No 745 942	
<b>Dissemination Level</b>	
<b>PU</b>	Public



**REVIEW**

<b>Name</b>	<b>Internal/Project/External</b>	<b>Comments</b>
Patrik Sellin	Project internal	
Mary Westermark	Project internal	

**DISTRIBUTION LIST**

<b>Name</b>	<b>Number of copies</b>	<b>Comments</b>
Athanasios Petridis (EC) Christophe Davies (EC)  Beacon partners		



# Content

<b>1</b>	<b>Introduction .....</b>	<b>5</b>
<b>2</b>	<b>EB - Engineered Barrier Emplacement Experiment.....</b>	<b>7</b>
2.1	Location and design.....	7
2.2	Main Materials and component of the experiment .....	8
2.2.1	Bentonite block bed .....	8
2.2.2	Granular Bentonite Material (GBM).....	9
2.2.3	Concrete bed .....	9
2.2.4	Dummy canister .....	9
2.2.5	Concrete plug and retaining wall .....	9
2.2.6	Hydration system .....	10
2.3	Instrumentation.....	11
2.3.1	Detailed Geometry .....	12
2.4	Surrounded host rock.....	13
2.4.1	Characteristics of the Opalinus Clay at Mont Terri .....	13
2.4.2	EDZ.....	14
2.5	Steps of the test.....	14
2.5.1	Installation .....	14
2.5.2	Hydration of buffer .....	14
2.5.3	Dismantling.....	15
2.6	Test cases.....	15
2.6.1	Main initial conditions .....	16
2.6.2	Evolution on a cross section .....	17
2.6.3	Evolution of the total structure.....	22
<b>3</b>	<b>FEBEX - Full-scale Engineered Barrier Experiment.....</b>	<b>23</b>
3.1	History of the Febex project .....	23
3.1.1	Installation of the test.....	23
3.1.2	Partial dismantling after five years .....	25
3.1.3	Final dismantling of the test.....	26
3.2	The Grimsel Test Site .....	26
3.2.1	The Febex area.....	27
3.2.2	Characteristic values of various granitic rocks .....	29
3.3	Main Materials and component of the experiment .....	32
3.3.1	Bentonite blocks .....	32
3.3.2	Heating system.....	33
3.3.3	Instrumentation .....	35
3.3.4	Installation .....	37
3.3.5	Concrete plug .....	38
3.3.6	Quality assurance and quality control .....	39
3.4	Test operation .....	39
3.4.1	Initial tests and start-up.....	39
3.4.2	Heating control and operation.....	39
3.5	Test case .....	40
3.5.1	Required outputs .....	40
<b>4</b>	<b>CRT - Canister Retrieval Test.....</b>	<b>45</b>
4.1	Geometry .....	45
4.2	Summary from installation report.....	51
4.3	Test schedule .....	53
4.3.1	Test start.....	53
4.3.2	End of the experiment .....	54
4.3.3	Heater power and filter pressure protocols .....	55
4.3.4	Rock anchors and heave of the lid .....	56
4.3.5	Comments about the installation and operating phase .....	58



4.4	Sensor position .....	62
4.4.1	Strategy for describing the position of each device .....	62
4.4.2	Position of each instrument in the bentonite .....	63
4.4.3	Instruments in the rock.....	68
4.5	Proposed cases for CRT .....	68
4.6	Reference case: Thermo-hydro-mechanical simulation of the entire engineered buffer in CRT.....	69
4.6.1	Loads, boundary conditions and initial conditions.....	69
4.6.2	Material properties .....	69
4.6.3	Results to present .....	70
4.6.4	Sensor data to compare with .....	71
4.7	Alternative case: Thermo-hydro-mechanical simulation of the engineered buffer at canister mid-height..	72
4.7.1	Geometry .....	72
4.7.2	Boundary conditions and initial conditions.....	73
4.7.3	Material properties .....	73
4.7.4	Results to present .....	74
4.7.5	Sensor data to compare with .....	74
<b>References.....</b>		<b>76</b>
<b>Appendix.....</b>		<b>78</b>
<b>1</b>	<b>THE FEBEX BENTONITE.....</b>	<b>78</b>
1.1	Origin and general properties .....	78
1.1.1	Origin and general aspects .....	78
1.1.2	Identification properties .....	79
1.1.3	Porosity .....	80
1.2	Parameter determination tests.....	81
1.2.1	Mechanical properties .....	81
1.2.2	Hydraulic properties.....	87
1.2.3	Thermal properties .....	95
1.3	Thermo-hydro-mechanical tests .....	97
1.3.1	Tests for calibration of models by backanalyses. Thermohydraulic cell. ....	97
1.3.2	Mechanical properties: oedometer tests with controlled suction .....	102
1.3.3	Tests to advance knowledge of the THM behaviour of expansive clays .....	105
1.3.4	Tests in thermo-hydraulic cells .....	108
<b>2</b>	<b>CRT - Material properties .....</b>	<b>112</b>
2.1	Bentonite buffer.....	112
2.2	Bentonite blocks .....	112
2.3	Bentonite pellets .....	112
2.4	Bentonite bricks.....	113
2.5	MX-80 properties .....	113
2.5.1	Thermal properties .....	113
2.5.2	Hydraulic properties.....	115
2.5.3	Mechanical properties .....	120
2.6	Rock properties.....	124
2.7	Concrete plug properties.....	124
2.8	Steel lid properties .....	125
2.9	Rock anchors properties .....	125



# 1 Introduction

The overall objective of the project is to evaluate the performance of an inhomogeneous bentonite barrier. Inhomogeneities are mainly due to initial distribution of dry density in link with technological voids, the simultaneous use of several forms of bentonite (for example, blocks and pellets), the setting up in granular form... Some external solicitations could also lead to heterogeneous evolution of these bentonite based engineered barriers such as non-uniform water flow or anisotropic stress field.

Understanding of swelling clay properties and fundamental processes that lead to its homogenization as well as improvement of capabilities for numerical modelling are essential for the assessment of the hydromechanical evolution and the resulting performances of the engineered barriers

The purpose of WP5 is to contribute to improvement of numerical models proposing several tests from small size tests (centimeters) to real scale experiments (several meters). The idea is to start with simple tests and progressively increase the complexity in terms of scale, coupled processes and initial/boundary conditions.

The present specifications describe step 2 of WP5 program. This second step is built in continuity with step 1. It is also dedicated to verification and validation of models. The objective of this task is to model existing large scale field tests to show the capacity of the models to reproduce in situ experiments. Based on the work in WP2, a selection of test cases from large scale experiments is considered. The main criteria of choices are:

- The experiments have to be well described and dismantled.
- The experiments have to be relevant to disposal concepts used by project partners
- The experiments should highlight the role of heterogeneities in bentonite component.

Based on these criteria and after discussions during the annual meeting in May 2018, 3 experiments have been selected:

- EB - Engineered Barrier Emplacement Experiment (EB experiment), dismantled after almost eleven years of operation, has been a long, well monitored, and full-scale demonstration of the use of Granular Bentonite Material as clay barrier. The experiment was carried out in a gallery excavated in the Opalinus clay of the Mont Terri Underground Research Laboratory. The EB experiment was designed in order to demonstrate a new emplacement technique of the bentonite barrier according to the Swiss concept and to represent the saturation phase with an artificial hydration of the barrier and under isothermal conditions. It is being used as benchmark for Decovalex2019.
- FEBEX - Full-scale Engineered Barrier Experiment in Crystalline Host Rock, is a research and demonstration project that was initiated by ENRESA (Spain). The aim of the project is to study the behaviour of near-field components in a repository for high-level radioactive waste in granite formations. The main objectives of the project can be grouped in two areas:
  - Demonstration of the feasibility of constructing the engineered barrier system in a horizontal configuration according to the Spanish concept for deep geological storage, and analysis of the technical problems to be solved for this type of disposal method,
  - Better understanding of the thermo-hydro-mechanical (THM) and thermo-hydro-geochemical (processes in the near field, and development and validation of the modelling tools required for interpretation and prediction of the evolution of such processes.

Last section of FEBEX was dismantled after 18 years of heating and natural hydration. It is being used as a benchmark in Decovalex2019 and in the EBS Task Force framework.

- CRT - Canister Retrieval Test (CRT) is a project that was initiated by SKB at Äspö Hard Rock Laboratory. The Canister Retrieval Test was a full scale field experiment simulating a deposition hole in a high level radioactive waste repository of KBS-3V. It was designed to demonstrate the ability to retrieve a deposited canister at full buffer saturation. This in-situ experiment was carried out from 1999 to 2006. The experiment consisted of a cylindrical



deposition hole hosting a canister encapsulated in clay buffer. Cables attached between the host rock and a plug on top of the buffer retained the buffer vertically and simulated the reaction force of a tunnel backfill. The canister was equipped with heaters to simulate the thermal activity of nuclear waste and strips of plastic filter were installed at the deposition hole's wall and connected to a water supply to provide a controllable simulated groundwater inflow. CRT was dismantled after 5 years of heating and artificial hydration. It was used as a benchmark in the EBS Task Force (2007-2012).

The originality of this second task of WP5 is to revisit some of existing experiments integrating the role of the heterogeneities in bentonite behaviour.

Each group involved in this task will model one or several tests selected (see Table 1-1).

*Table 1-1 Selected experiments and choices of Beacon participants*

	EB	FEBEX	CRT
UPC	X	X	
ULG	X		
BGR		X(1)	X(2)
CU-CTU			X
LEI		X	
ClayTechnology		X(1)	X(2)
ICL	X	X	X
Quintessa		X	

## 2 EB - Engineered Barrier Emplacement Experiment

### 2.1 Location and design

The experiment has been carried out in a short gallery excavated for this purpose, identified as “EB niche”. It is located at the end of the DI niche and it is parallel to the “new gallery” of the Mont Terri Underground Rock Laboratory, on its shaly facies section (Figure 2-1).

The EB niche is 15 m long. It has a horseshoe section, 2.55 m high and 3 m wide (Figure 2-2). The aim was to install a dummy canister, of the same dimensions and weight than the reference canister, on the top of a bentonite blocks bed. The remaining gap between the canister and the rock was backfilled with bentonite pellets.

The experimental area was isolated by a concrete plug (Figure 2-3). To accelerate the hydration process an artificial system was installed. This system is comprised of a combination of pipes and mats arranged around the canister. To monitor the evolution of the experiment, different sensors and a data acquisition system were installed, including remote access.

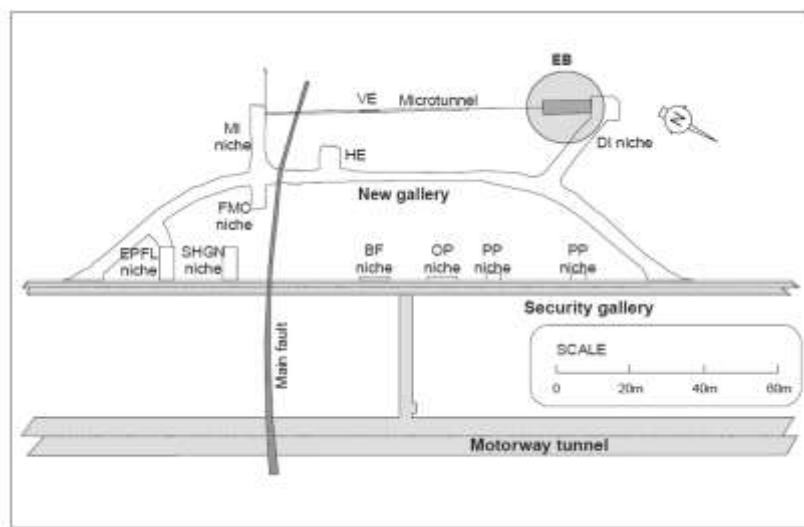


Figure 2-1 Location of EB Niche in Mont Terri URL

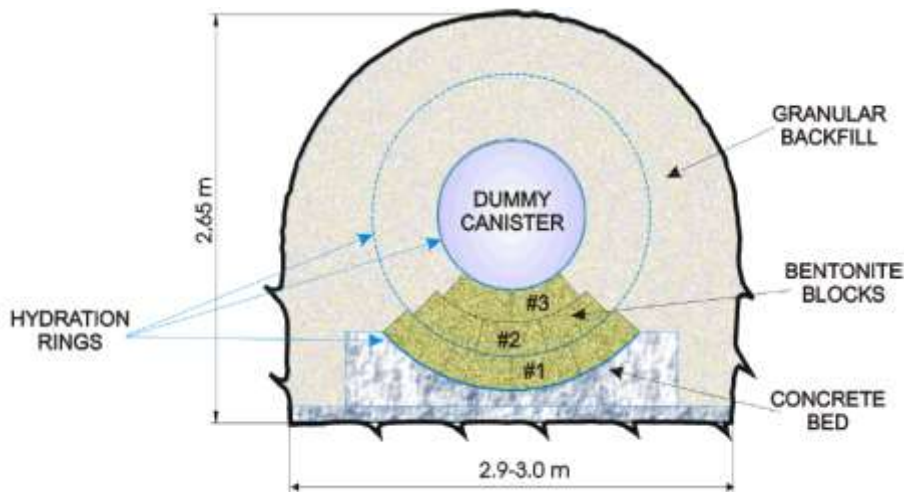


Figure 2-2 EB cross section

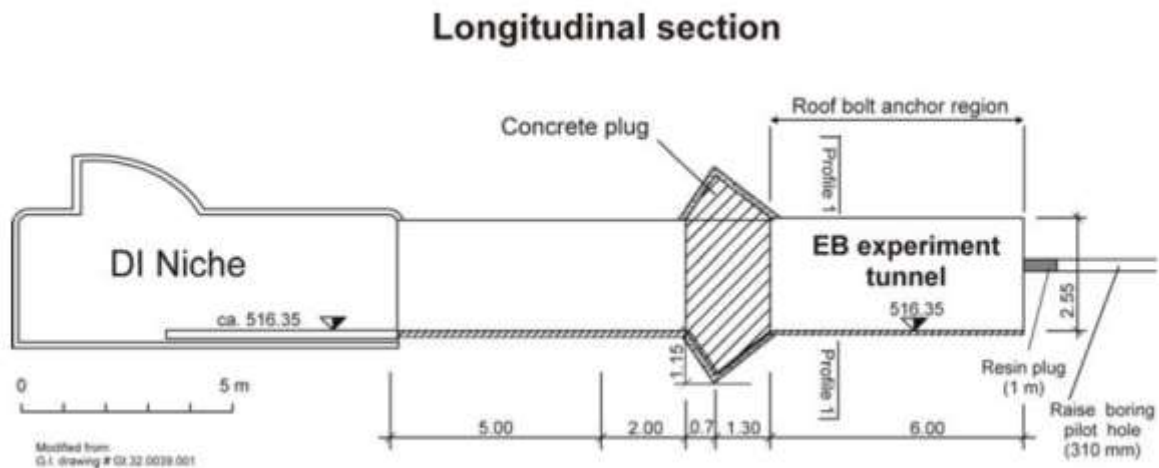


Figure 2-3 EB niche, longitudinal section

## 2.2 Main Materials and component of the experiment

Main component and materials are described in this section. Information are coming from Mayor et al., 2005. More details can be found in this document.

### 2.2.1 Bentonite block bed

The blocks, coming from the FEBEX project, have a dry density of 1,69 g/cm<sup>3</sup> and the water content was 14,36 %. The dimensions of blocks are given in Table 2-1 and Figure 2-4. The bentonite blocks bed is composed by three layers (#1, #2 and #3); see Figure 2-2 for their position.

Table 2-1 Characteristics of bentonite blocks

Block type	a (mm)	b (mm)	c (mm)	Thickness (mm)	R (mm)	r (mm)	$\alpha$ (°)	Weight (kg)
#1	470,0 <sup>+2,0</sup> <sub>-3,0</sub>	380,0 <sup>+2,0</sup> <sub>-4,0</sub>	214,0 <sup>+2,0</sup> <sub>-3,0</sub>	125,0 <sup>+2,0</sup> <sub>-2,0</sub>	1,133	919	24°	22,1
#2	473,0 <sup>+2,0</sup> <sub>-5,0</sub>	361,0 <sup>+2,0</sup> <sub>-4,0</sub>	214,0 <sup>+2,0</sup> <sub>-3,0</sub>	125,0 <sup>+2,0</sup> <sub>-2,0</sub>	917	703	30°	21,8
#3	478,0 <sup>+2,0</sup> <sub>-2,0</sub>	330,0 <sup>+2,0</sup> <sub>-4,0</sub>	214,0 <sup>+2,0</sup> <sub>-3,0</sub>	125,0 <sup>+2,0</sup> <sub>-2,0</sub>	701	487	40°	21,3

The hydromechanical properties for compacted bentonite are give in appendix based on FEBEX project.

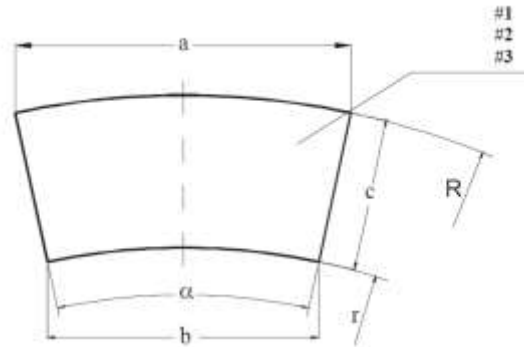


Figure 2-4 Dimensions of FEBEX bentonite blocks

### 2.2.2 Granular Bentonite Material (GBM)

The volume was filled with granular bentonite material prepared from Spanish Serrata bentonite. The average water content was 4.17 percent with a minimum of 3.52 percent and a maximum of 4.81 percent. The grain size analyses performed show a wide grading band. The average values are presented in Table 2-2

Table 2-2 Results from grain size analysis

Average percent passing	Size							
	10 mm	6,3 mm	5 mm	2 mm	1 mm	0,5 mm	0,25 mm	0,125 mm
	95	50	45	40	22	14	10	8

The total mass emplaced was about 40.2 T in an estimated available volume of about 28.4 m<sup>3</sup>. The obtained mean dry density ( $\rho_d$ ) of the GBM was 1,36 g/cm<sup>3</sup>. It has to be noted that it is 3% lower compared to what was expected.

The hydromechanical properties for compacted bentonite are give in appendix based on hoffmann et al., 2007).

### 2.2.3 Concrete bed

The concrete bed is of same length than the dummy canister and with a circular shape. It does not contain any steel re-enforcement due to geophysical requirements. The circular shape of the concrete bed allows to use bentonite blocks of the FEBEX project. It will be considered in the modelling work and its hydromechanical properties defined.

### 2.2.4 Dummy canister

The dummy canister used in the experiment is similar in weight and dimensions to the one in the ENRESA and NAGRA reference concepts, and has a length of 4,54 m and a diameter of 0,97 m. It was made of carbon steel and filled of a barite emulsion, density 2,65 g/m<sup>3</sup>, to obtain the needed weight, being the empty weight of 4000 kg and the final weight approximately 11000 kg

### 2.2.5 Concrete plug and retaining wall

The test section was sealed with a concrete plug of 2 meters long. This concrete plug is placed just behind a retaining wall with a thickness of 20 centimetres. The concrete plug is anchored in OPA on a thickness of 1.15 meters (see its shape on Figure 2-3).

**2.2.6 Hydration system**

The EB hydration system has two separated parts: test and service area. Test area components of the hydration system include the hydration tubes and geotextile hydration mats. Figure 2-5 shows the distribution of tubes and hydration mats around the canister and between the bentonite blocks. A water distribution system feeds the hydration tubes and geotextile mats at different levels: floor level, canister level and top level. also includes the elements of support (Kevlar® cables and Nylon® rods). The water used is synthetic and its composition is chemically equivalent to the Opalinus Clay formation water.

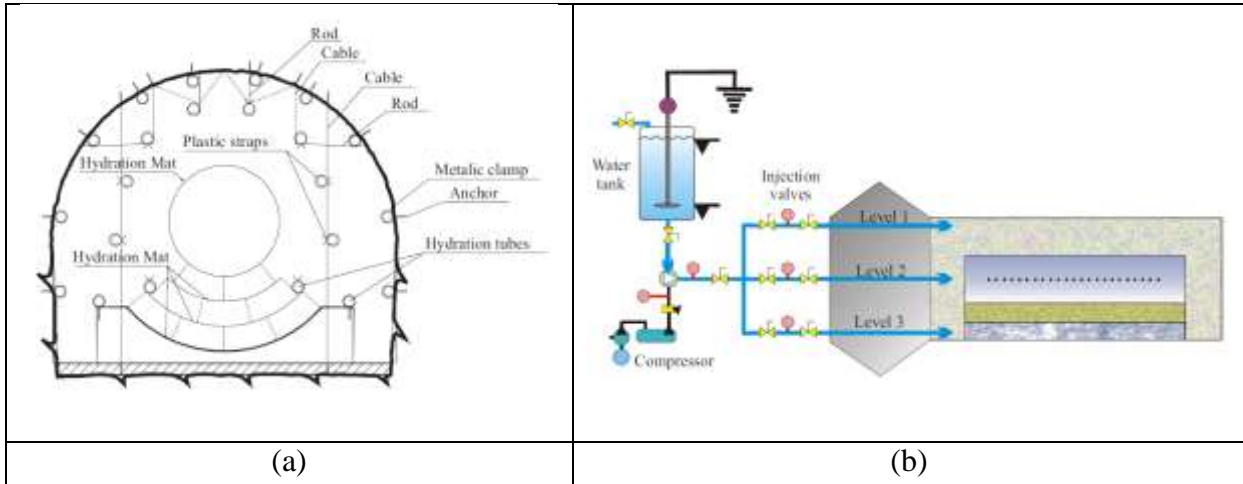


**Figure 2-5** (a) Scheme of Hydration system and support (cross-section). Position of hydration tubes, hydration mats and bentonite blocks, (b) Scheme of the hydration system (general layout)

37 injection tubes were arranged in a three layer configuration. Additionally, a pervious mat was used to cover the tubes, canister and the bentonite blocks in order to favour the water distribution in these zones. A cross section of the tunnel showing a schematic view of the hydration system is illustrated in Figure 2-6a. Tubes were connected in such a way that the water flows into buffer materials from the floor to the roof of the excavation as indicated in Figure 2-6b. In order to favour the injection process and to allow the air existing in the buffer and in the water injection system to escape, the upper tube was connected to the access gallery.

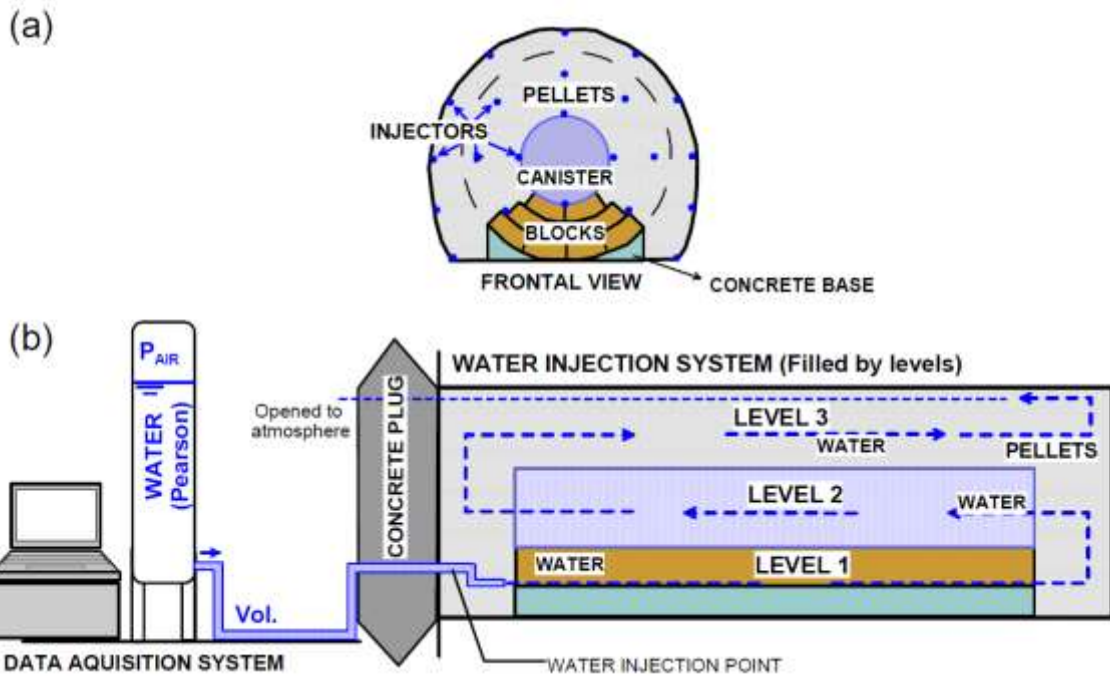


Figure 2-6 Hydration system

## 2.3 Instrumentation

To monitor the relative humidity, temperature, pore and total pressure and displacements, sensors were installed in different sections along the niche. The idea was to be able to monitor rock mass evolution around the niche and buffer evolution. So, several types of sensors were installed in the buffer and in the clay rock:

- For measurements in the rock mass:
  - 20 Piezometers
  - 8 Capacitive humidity sensors
  - Extensometers
  - Seismic sensors
  - Electrode chains
- For measurements in the bentonite buffer:
  - 8 Total pressure cells
  - Extensometers (for canister displacements)
  - 8 Capacitive humidity sensors

Distribution of sensors in the Niche are presented on Figure 2-7. More details about exact position of sensors are given in appendix.

For hydrogeological characterization of the surrounded rock several boreholes were drilled to depths of approximately 0.3 to 3 m vertical, horizontal and at an angle of 30° from the horizontal. The boreholes have a diameter of 30mm. An example of such boreholes is given for section C2 on Figure 2-8

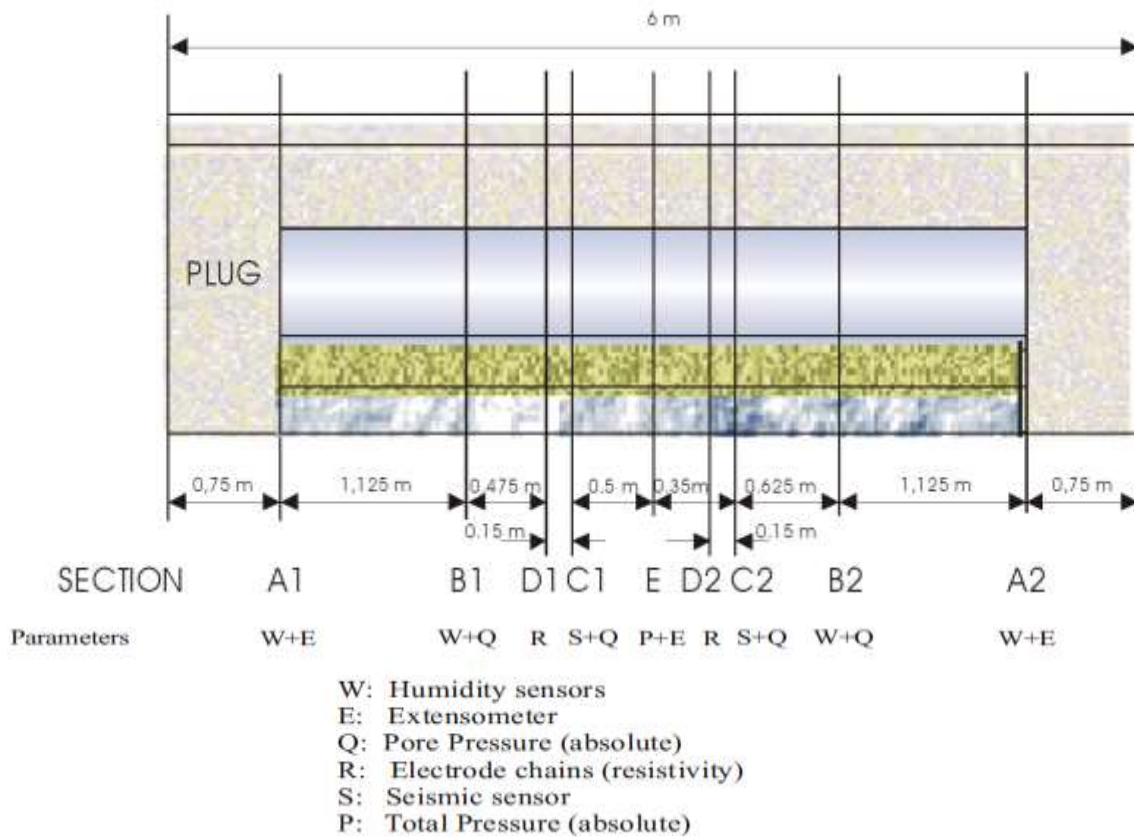


Figure 2-7 Position of instrumented sections in EB Niche

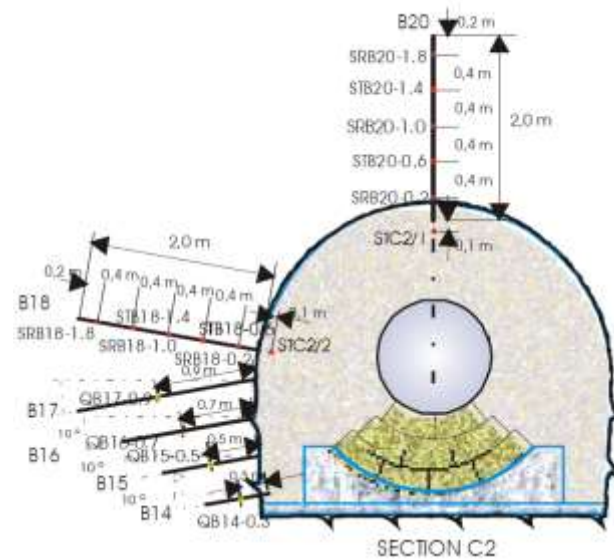


Figure 2-8 Boreholes in the rock in section C2

### 2.3.1 Detailed Geometry

Dimensions of the all the components are given on Figure 2-9 for a current section. Longitudinal dimensions are presented on Figure 2-3.

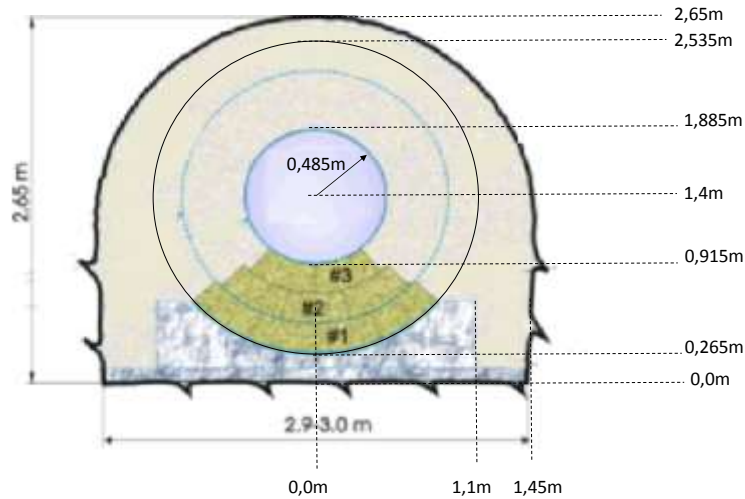


Figure 2-9 Dimensions on a perpendicular cut

## 2.4 Surrounded host rock

### 2.4.1 Characteristics of the Opalinus Clay at Mont Terri

The main hydromechanical properties of Opalinus Clay are summarised in Table 2-3. More details about the geological environment of Mont Terri can be found in Bossard and Thury (2008).

Table 2-3 Hydromechanical parameter for OPA (Bossard and Thury, 2008)

Parameter	Range	Best estimate
Density, bulk saturated [g/cm <sup>3</sup> ]	2.40 - 2.53	2.45
Water content [saturated wt%]	5.0 - 8.9	6.6
Water loss porosity at 105°C [vol%]	12.6 - 21.1	16.2
Porosity, total physical [vol%]	14.0 - 24.7	18.3
Hydraulic conductivity [m/s]	2E-14 - 1E-12	2E-13
Thermal conductivity [W/mK]	1.0 - 3.1	1.7
Thermal conductivity parallel to bedding [W/mK]	-	2.1
Thermal conductivity normal to bedding [W/mK]	-	1.2
Heat capacity [J/Kg K]	-	860
Total dissolved solids in porewater [g/l]	5 - 20	-
Young's modulus normal to bedding [MPa]	2100 - 3500	2800
Young's modulus parallel to bedding [MPa]	6300 - 8100	7200
Poisson's ratio normal to bedding [-]	0.28 - 0.38	0.33
Poisson's ratio parallel to bedding [-]	0.16 - 0.32	0.24
Shear modulus [MPa]	800 - 1600	1200
Uniaxial compressive strength normal to bedding [MPa]	23.1 - 28.1	25.6
Uniaxial compressive strength parallel to bedding [MPa]	4.0 - 17.0	10.5
Uniaxial tensile strength normal to bedding [MPa]	-	1
Uniaxial tensile strength parallel to bedding [MPa]	-	2
Cohesion [MPa]	2.2 - 5	3.6
Internal friction angle [°]	23 - 25	24

### 2.4.2 EDZ

Following, “in situ” geophysical and hydraulic measurements were performed, to characterize the EDZ. From these field surveys, it was concluded that the EDZ reaches a depth of about 0.7 m in the roof of the test section, while at the sidewalls only extends to 0.1 m depth.

The hydraulic conductivity of EDZ fractures is thus many orders of magnitude higher (estimated five to eight orders) compared to undisturbed Opalinus Clay with a mean hydraulic conductivity of  $2 \cdot 10^{-13}$  m/s. (Bossard et al., 2004).

Several boreholes have been drilled to depths of approximately 0.3 to 0.9 m at an angle of 30° from the horizontal. The schematic borehole configuration is shown on Figure 2-10a

The initial hydrogeological characterization has been performed in two campaigns around the EB niche, followed by three campaigns of test after buffer installation. Figure 2 6b shows the evolution of hydraulic conductivity in the rock at different locations at several times. The permeability tend to decrease with time as expected due to self-sealing. Origin of water was not identified. It could come from artificial hydration of buffer or from the clay rock itself.

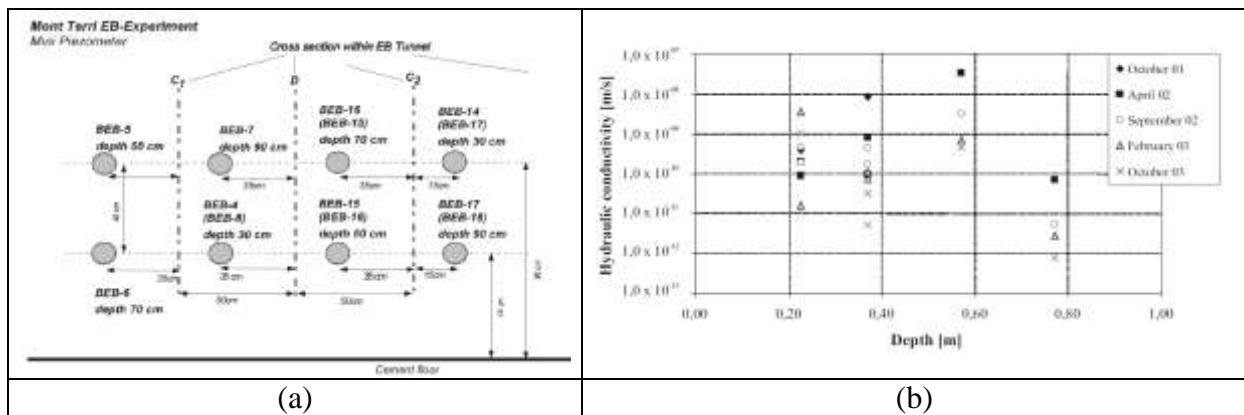


Figure 2-10 (a) Schematic borehole configuration, (b) Hydraulic conductivity measured before buffer installation and at the beginning of hydration buffer test as a function of depth from the tunnel wall

## 2.5 Steps of the test

### 2.5.1 Installation

The installation of the experiment was carried out in several steps. The instrumentation was installed from November 2001 to February 2002: in-rock pore pressure sensors, rock displacement sensors and some rock relative humidity sensors, canister displacement sensors, relative humidity sensors in bentonite and total pressure cells. The artificial hydration system was installed in March 2002. The installation of the experiment was finished in April 2002, including the retaining wall, the concrete plug and the data acquisition system.

### 2.5.2 Hydration of buffer

The artificial hydration of the bentonite buffer started in May 2002 and ended in June 2007. There was an initial hydration phase with an important amount of water injected (6,700 litres in two days) that was stopped after several water stains appeared on the wall. After that, and from September 2002 to June 2007, there were different hydration phases with continuous water injection. Daily injection rate is shown on Figure 2-11 and the temporal evolution of the injection pressure on Figure 2-12.

After June 2007 and till the end natural hydration of the buffer occurred with water coming from the host rock.

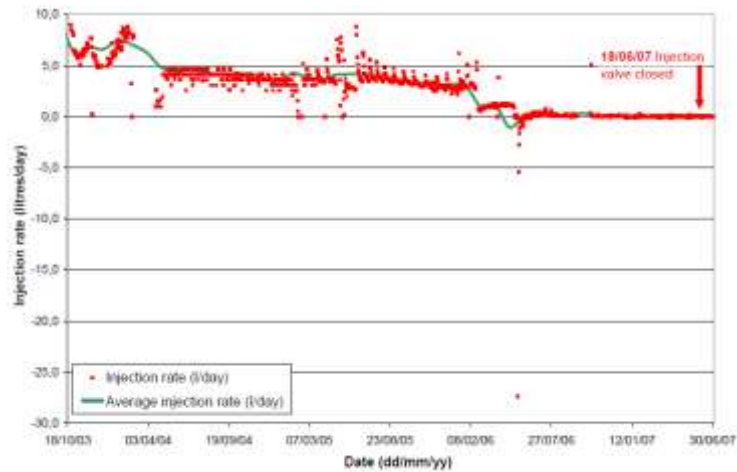


**Figure 2-11** Daily injection rate versus average daily injection rate

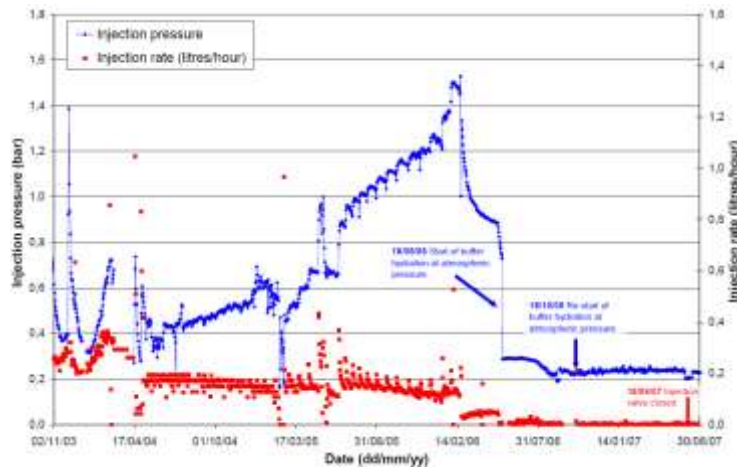


**Figure 2-12** Injection rate versus injection pressure from the start of continuous injection

For several reasons, it was not possible to be sure that all injected water goes in the bentonite. The inflow coming from the host rock is not possible to estimate. The total volume of injected water (18882 Litres) is just given as an indicative information.

### 2.5.3 Dismantling

The dismantling and sampling operations<sup>3</sup> began on October 19th, 2012 and were finished on February 1st, 2013 (approximately a period of 100 days).

The main objective of the dismantling of the EB experiment has been to know about the real status of the GBM used after its artificial saturation: degree of saturation, permeability, density, aspect, homogeneity, etc. It has been also important to check the status of the bentonite blocks that support the canister, the rock in contact with the buffer, with especial interest in the EDZ, and the degree of saturation of the concrete in the vicinity of the buffer (plug and blocks support). Therefore, the activities of the dismantling have been coordinated with a sampling programme intended to analyse parameters such as dry density, water content, permeability... in the laboratories of the different organizations as well as in an onsite laboratory.

## 2.6 Test cases

Two stages of modelling are proposed for EB experiment:

- Evolution on a cross section 2D perpendicular to the axis of the canister
- Evolution of the EB experiment total structure

**2.6.1 Main initial conditions**

Main properties and initial conditions for GBM are given in Table 2-4

*Table 2-4 Material properties for GBM (from Hoffmann et al, 2007)*

$\rho_s$ (Mg/m <sup>3</sup> )	$w_P$ (%)	$w_L$ (%)	% of particles < 75 $\mu$ m
<i>FEBEX Ca-bentonite</i>			
2.7	47	93	85
$\rho_d$ (Mg/m <sup>3</sup> )	$e_0$	$w_0$ (%)	Initial suction (MPa)
<i>Pellets</i>			
1.95	0.38	3-4	250-300

$\rho_s$ : mineral density;  $\rho_d$ : dry density;  $e_0$ : initial void ratio;  $w_0$ : initial water content;  $w_L$ : liquid limit;  $w_P$ : plastic limit.

The initial water content of the blocks ranged between 12.5 and 15.5 % for a suction between 100 to 200MPa (see Figure 2-13).

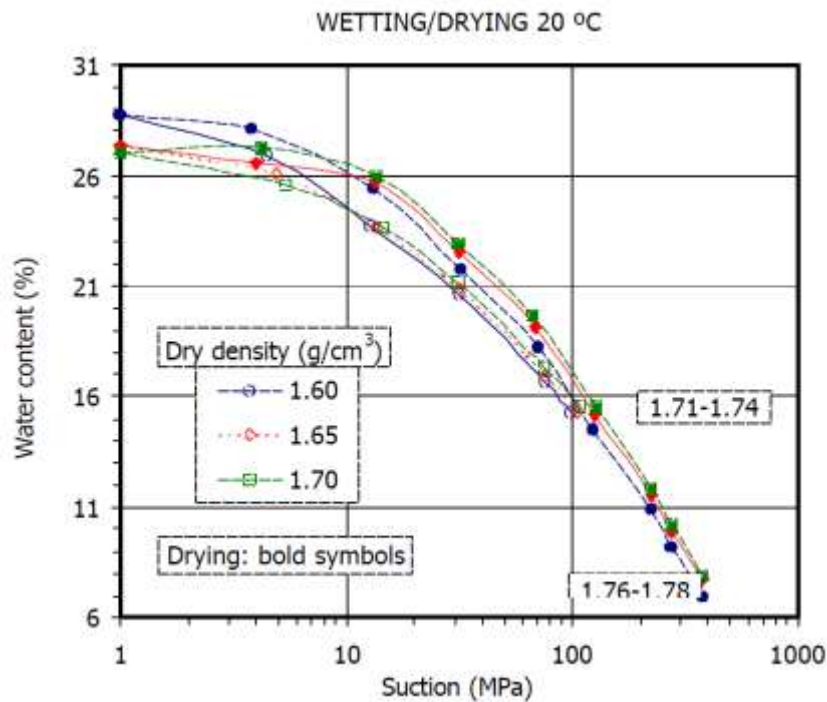


*Figure 2-13 Retention curves at constant volume in a wetting/drying path for the FEBEX bentonite compacted at different dry densities. The dry densities at the end of drying are indicated in g/cm<sup>3</sup> (Lloret et al. 2004)*

Mean relative humidity in the niche after excavation and before installation of materials is about 75%. The excavation finished on June 2001 and GBM was installed in April 2002.

**2.6.2 Evolution on a cross section**

The objective is to calibrate the model on cross section E (see Figure 2-7) during the saturation phase. Results showed that the evolution of the structure could not be handled without taking into account the behaviour in the longitudinal dimension. This first cross section model is made to bring qualitative elements to understand the behaviour of the structure. It will allow to detail the homogenization of the granular mixture in contact with compacted blocs which is the major point for the BEACON project.

**Main results after dismantling**

On Figure 2-14 and Figure 2-15, dry density, water content and water saturation are presented after dismantling.

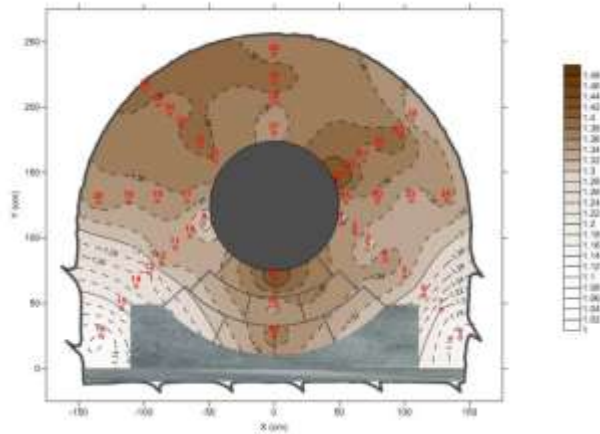


*Figure 2-14 Dry density – section E*

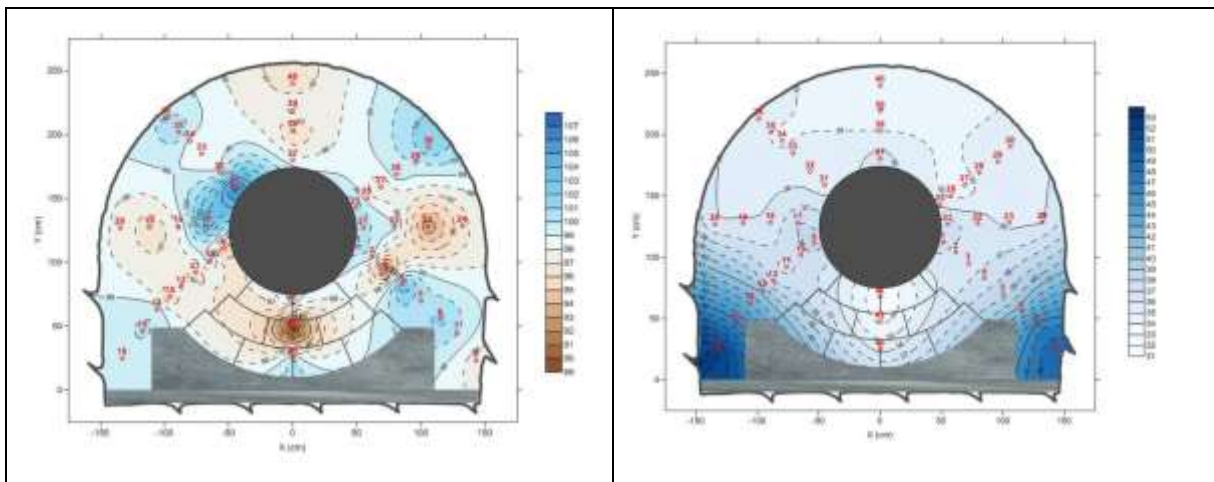


*Figure 2-15 Water saturation and water content section E*

**Measures during hydration**

Some measures have been done in section E: displacement in host rock and total pressure in the buffer. Pore pressure evolution in the rock should be deduced from measurements in other sections.(C1 and C2).

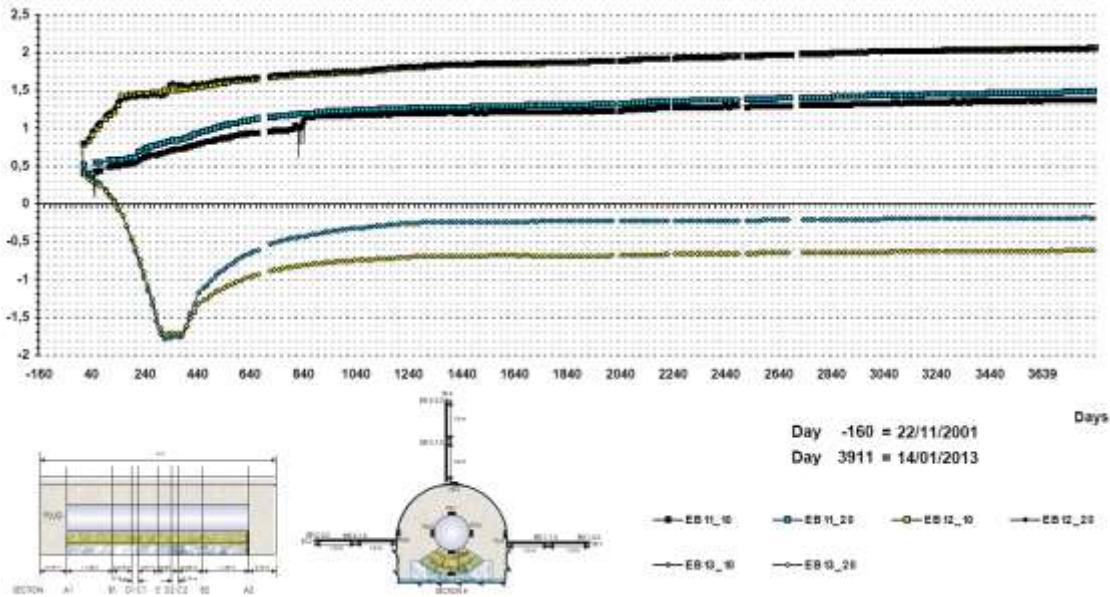


**Figure 2-16** Displacement in the rock (mm)

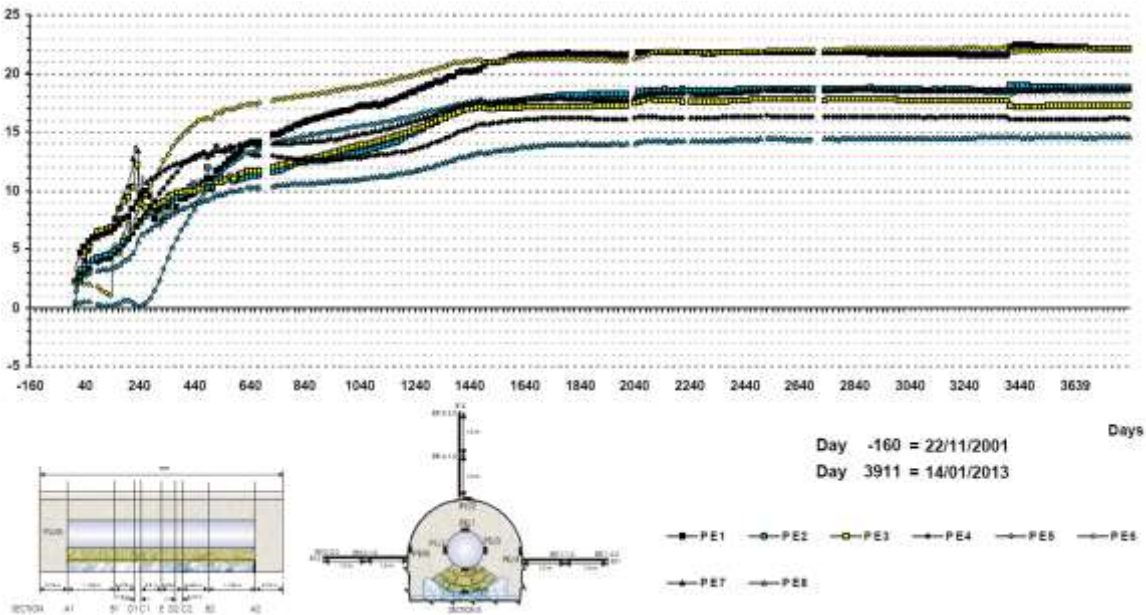


**Figure 2-17** Total pressure in the buffer (bars)

**Geometry proposed for the 2D test**

It is proposed for this part of the exercise to model a section of the experiment. On Figure 2-18, the geometry and boundary conditions are represented. Numerical points are indicated in Table 2-5.

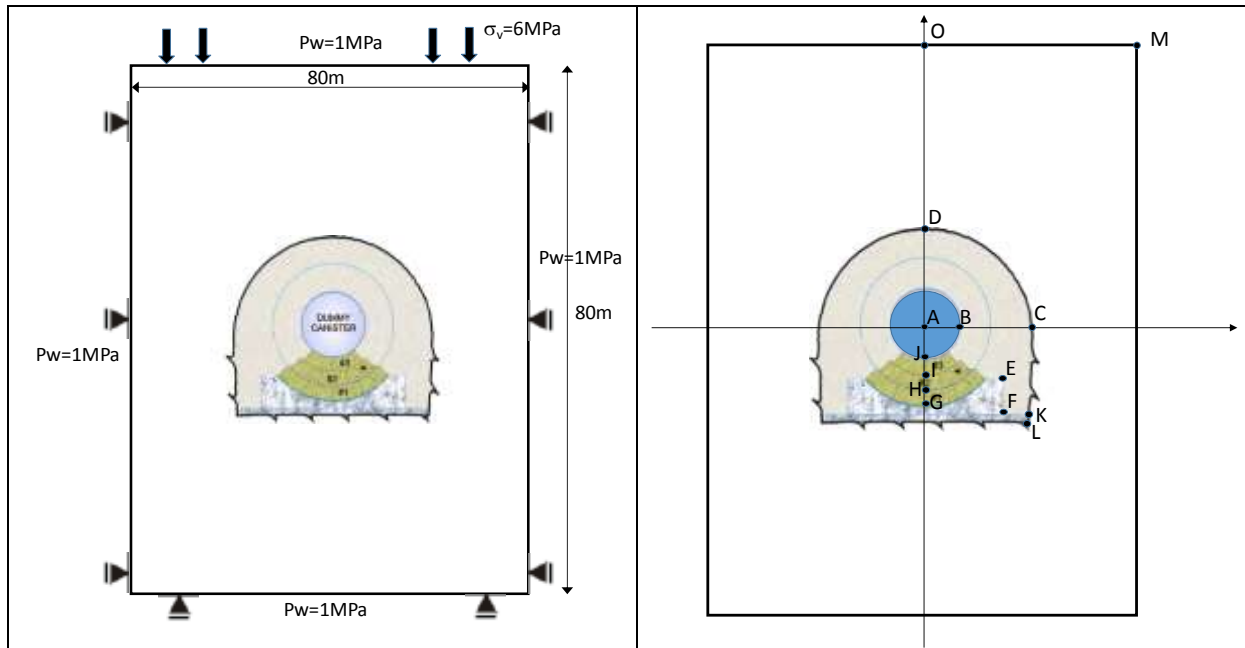


Figure 2-18 Model geometry and boundary conditions for 2d case

Table 2-5 Initial geometry for a perpendicular section of the niche

Point	X	Y
A	0	0
B	0.485	0
C	1.45	0
D	0	1.25
E	1.1	-0.76
F	1.1	-1.3
G	0	-1.135
H	0	-0.917
I	0	-0.701
J	0	-0.485
K	1.45	-1.3
L	1.45	-1.4
M	40	40
O	0	40



**Outputs**

Simulations should be done between the end of excavation of the niche and until dismantling.

Main outputs required

- Iso-value maps for water content, dry density and saturation at the end of the simulation.
- Water content and dry density evolution at several locations:

**Table 2-6**      *Location of the points for history output*

	X	Y
S1	-1.4	0
S2	-1.2	0
S3	1.2	0
S4	1.4	0
S5	1.6	0
S6	-1.25	-0.8
S7	-1.25	-0.2
S8	-0.9	-0.4
S9	0	-1.5
S10	0	-1.135
S11	0	-0.917
S12	0	-0.701
S13	0	-0.485
S14	1.25	-0.2
S15	1.25	-0.8
S16	0	0.917
S17	0	1.2

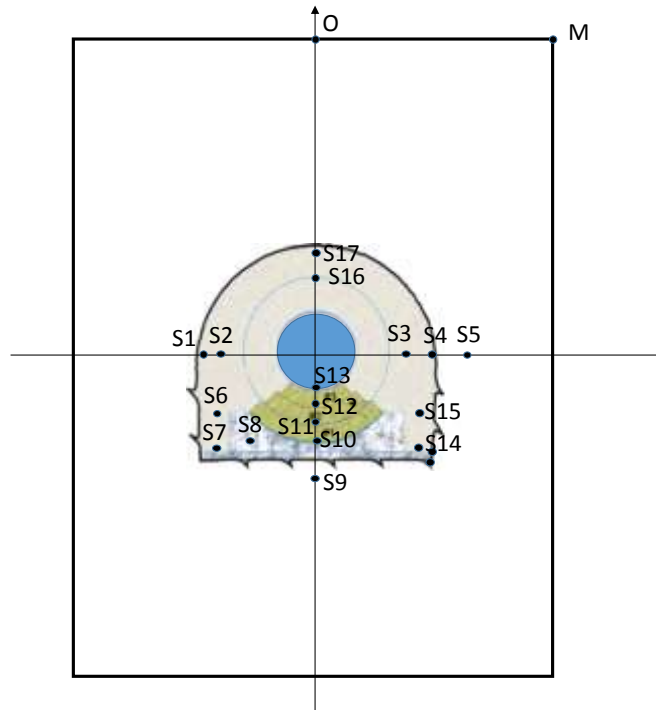


*Figure 2-19 Graphical representation for point locations*

- Total pressure evolution on points PE1 to PE8 (from Figure 2-17)
- Pore pressure in the rock on points EB11 to EB13 from Figure 2-16



### 2.6.3 Evolution of the total structure

A model of the global structure should be performed in this stage of work. Due to the fact that a part of water implied in the saturation process of the bentonite came from the rock, it is suggested to take a part of it in the domain.

#### **Required outputs**

It is proposed to produce as an output the variables measured by the sensors installed in EB niche and at the same location (see Table 2-7). To complete, this set of outputs, at the same location water content, dry density and total pressure should be produced.

*Table 2-7 Sensors installed in EB experiment and quantity measured*

sensor	section	material	variable	units
EA11	A1	canister	hor. displacement	mm
EA12	A1	canister	vert. displacement	mm
WB11	B1	GBM	rel. humidity	%
WB12	B1	GBM	rel. humidity	%
WB13	B1	B Block	rel. humidity	%
WB14	B1	B Block	rel. humidity	%
PE1	E	GBM/canister	total pressure	bar
PE2	E	GBM/rock	total pressure	bar
PE3	E	GBM/canister	total pressure	bar
PE4	E	GBM/rock	total pressure	bar
PE5	E	B Block/canister	total pressure	bar
PE6	E	B Block/concrete	total pressure	bar
PE7	E	GBM/canister	total pressure	bar
PE8	E	GBM/rock	total pressure	bar
WB21	B2	GBM	rel. humidity	%
WB22	B2	GBM	rel. humidity	%
WB23	B2	GBM	rel. humidity	%
WB24	B2	GBM	rel. humidity	%
EA21	A2	canister	hor. displacement	mm
EA22	A2	canister	vert. displacement	mm

On each identified section, iso-values at several time steps should be produced for dry density and water content. Excel files with output format will be supplied.



## 3 FEBEX - Full-scale Engineered Barrier Experiment

FEBEX (Full-scale Engineered Barrier Experiment in Crystalline Host Rock) was a research and demonstration project that was initiated by Enresa (Spain). The aim of FEBEX (Full-scale Engineered Barrier Experiment) was to study the behaviour of components in the near-field for a high-level radioactive waste (HLW) repository in crystalline rock. The project was based on the Spanish reference concept for disposal of radioactive waste in crystalline rock (AGP Granito): the waste canisters are placed horizontally in drifts and surrounded by a clay barrier constructed from highly-compacted bentonite blocks (Enresa 1995). The main objectives of the project were:

- Demonstration of the feasibility of constructing the engineered barrier system in a horizontal configuration according to the Spanish concept for deep geological storage (AGP), and analysis of the technical problems to be solved for this type of disposal method.
- Better understanding of the thermo-hydro-mechanical (THM) and thermo-hydro-geochemical (THG) processes in the near field, and development and validation of the modelling tools required for interpretation and prediction of the evolution of such processes.

### 3.1 History of the Febex project

The project started in 1994 and has been supported by the European Commission through consecutive contracts, identified as FEBEX I for the period January 1996 to June 1999, and FEBEX II, from September 2000 to December 2004. Afterwards, NF-PRO continued the project from January 2005 to December 2007. Finally, in January 2008, the in-situ test was transferred from Enresa to the FEBEXe Consortium, which supported it until final dismantling was completed.

#### Project Time Activities

- FEBEX I 1995 - 1999 Design, construction with heating initiated in 1997
- FEBEX II 2000 - 2004 Continued saturation and partial dismantling of In Situ Test (2002)
- NF-PRO 2005 - 2007 Continued saturation
- FEBEXe 2008 - 2014 Ongoing saturation and planned final dismantling for In Situ Test
- FEBEX-DP 2014 - 2017 Final dismantling of the In Situ Test

The major milestones for the In Situ Test were:

- 25/10/95: Start of tunnel boring machine excavation of FEBEX tunnel
- 01/07/96: Start of FEBEX Engineered Barrier System (EBS) construction
- 15/10/96: End of EBS construction
- 27/02/97: Start of heating<sub>2</sub>
- 28/02/02: Switch-off of Heater # 1
- 02/04/02: Start of partial dismantling
- 26/07/02: End of partial dismantling
- 24/04/15: Switch-off of Heater # 2
- 05/08/15: Completion of dismantling

#### 3.1.1 Installation of the test

The installation of the in-situ test was carried out at the GTS. A horizontal drift with a diameter of 2.28 m was excavated in the Grimsel granodiorite especially for this experiment using a tunnel boring machine (TBM). Two electrical heaters, of the same size and of a similar weight as the reference canisters, were placed in the axis of the drift. Figure 3-1 shows the dimensions and layout of the test components schematically. The gap between the heaters and the rock was backfilled with compacted

bentonite blocks, for a distance of 17.40 m and this required a total 115'716 kg of bentonite. The blocks were arranged in vertical slices consisting of concentric rings. In the heater areas, the interior ring was in contact with the steel liner, whereas in the non-heater areas a core of bentonite blocks replaced the heaters (Figure 3-2). The thickness of the bentonite barrier in the heater areas was 65 cm (distance from liner to granite). The bentonite slices were numbered from the back of the gallery towards the front, and those in which sensors were installed were called "instrumented section" and given a distinctive reference letter. The backfilled area was sealed with a plain concrete plug placed into a recess excavated in the rock and having a length of 2.70 m and a volume of 17.8 m<sup>3</sup>.

A total of 632 instruments, located in both the bentonite buffer and the host rock, were installed in a number of instrumented sections. They monitored relevant parameters such as temperature, humidity, total and pore pressure, displacements, etc. The instruments were of many different kinds and their characteristics and positions were fully described in Fuentes-Cantillana & García- Siñeriz (1998).

A Data Acquisition and Control System (DACS) located in the service area of the FEBEX drift collected the data provided by the instruments. This system recorded and stored information from the sensors and also controlled the power applied to the electrical heaters, in order to maintain a constant temperature at the heaters/bentonite interface. The DACS allowed the experiment to be run in an automated mode, with remote supervision from Madrid. Data stored at the local DACS were periodically downloaded in Madrid and used to build the experimental Master Data Base. The construction of the concrete plug was completed in October 1996, and the heating operation started on February 28, 1997. A constant temperature of 100°C was maintained at the heater/bentonite interfaces, while the bentonite buffer was slowly hydrating with water naturally flowing from the rock.

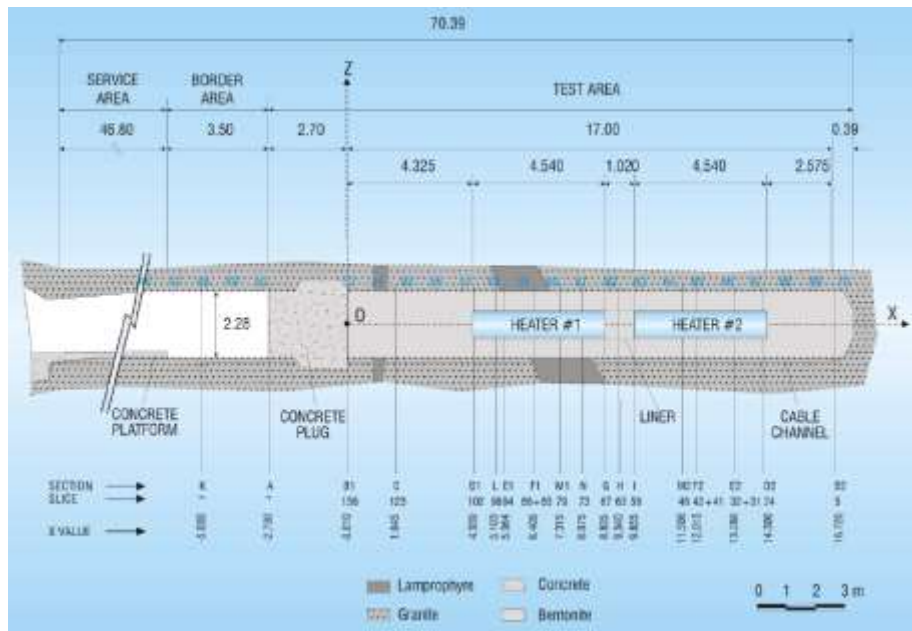


Figure 3-1 Initial general layout of the FEBEX in-situ test (dimensions in m).

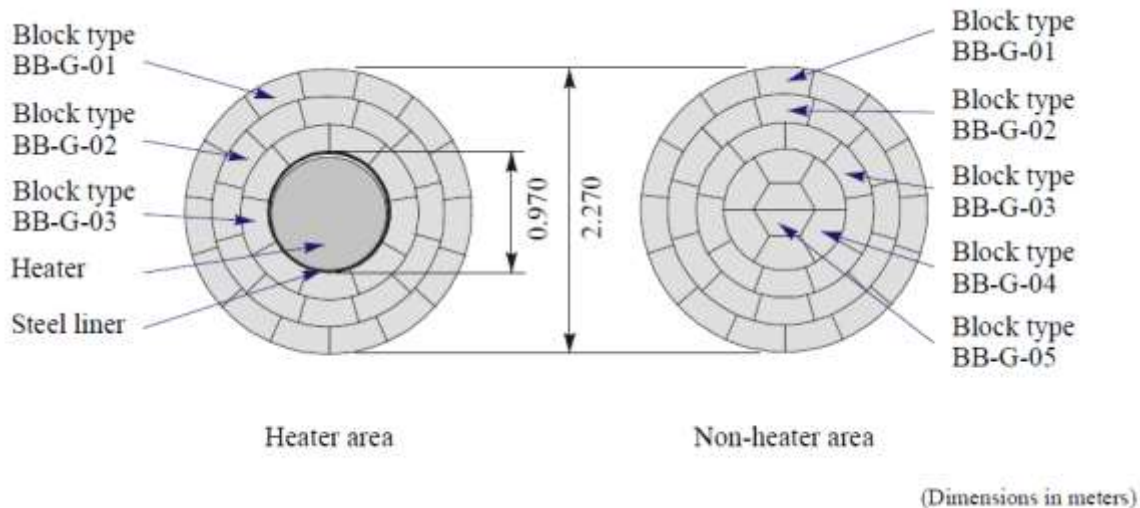


Figure 3-2 Geometry of the clay barrier in the FEBEX in-situ test at GTS (Enresa 2000)

### 3.1.2 Partial dismantling after five years

A partial dismantling of the FEBEX in-situ test was carried out during the summer of 2002, after 5 years of continuous heating. The operation included the demolition of the concrete plug, the removal of the section of the test corresponding to the first heater, and the resealing of the remaining tunnel with a new shotcrete plug. A large number of samples from all types of materials were taken for analysis during this partial dismantling. A number of instruments were also subsequently dismantled and inspected. The description of the partial dismantling operation is given in B arcena et al. (2003).

The configuration of the test, after completing the partial dismantling operation and construction of the full plug length, is shown in Figure 3-3. It shows how the buffer and all components were removed up to a distance of 2 metres from Heater #2 to minimise disturbance of the nondismantled area. A dummy steel cylinder with a length of 1 m was inserted in the void left by Heater #1 in the centre of the buffer.

Additional sensors were also introduced in boreholes drilled in the buffer parallel to the drift. To simplify this operation, the new shotcrete plug was constructed in two phases: an initial temporary plug measuring just 1 m in length, that was built immediately after dismantling, and a second section to complete the plug up to a length of 3 m as planned in the experimental design. The new plug differed from the FEBEX I plug in that it was constructed without a recess excavated in the rock and was installed by shotcreting.

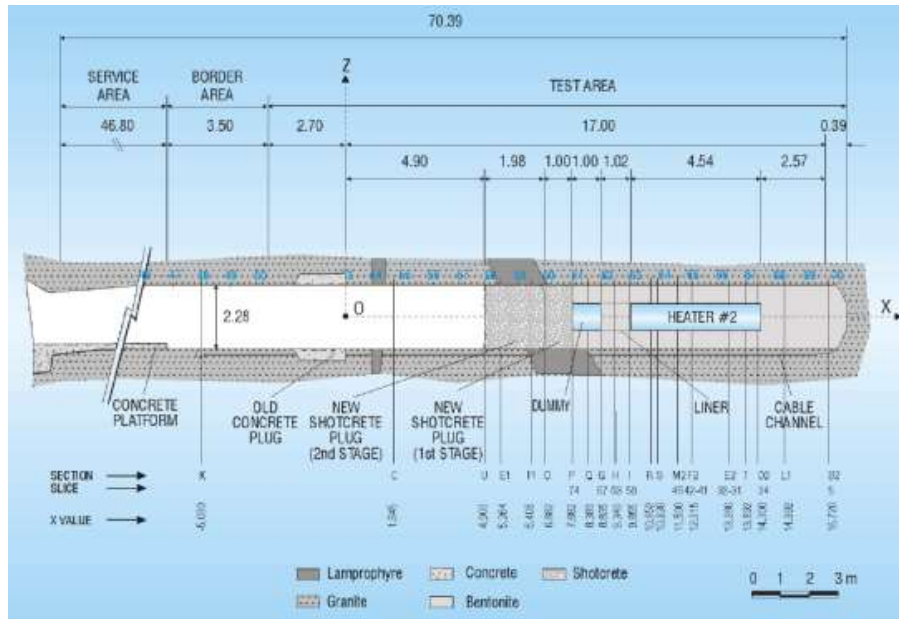


Figure 3-3 Layout of the FEBEX in-situ test after the partial dismantling (dimensions in m)

### 3.1.3 Final dismantling of the test

The objective of the second dismantling operation, carried out throughout 2015, was to dismantle all the remaining parts of the *in-situ* test, including Heater #2. Many sensors were in operation until the end of the experiment, which allowed to follow the evolution of some thermo-hydronechanical variables during the second operational phase (Martínez et al. 2016).

The dismantling operation included carrying out a complete sampling of the bentonite, rock, relevant interfaces, sensors, metallic components and tracers to allow the analysis of the barriers' condition after 18 years of heating and natural hydration, as described in NAB 16-11 (García-Siñeriz et al. 2016).

All details about the sampling program are given in NAB 15-14 (Bárcena & García-Siñeriz 2015). Following the same terminology used during installation of the experiment and during the first dismantling, the term bentonite "slice" refers to the vertical slices of bentonite blocks as they were installed. These were numbered during the installation of the barrier in 1997 as they were put in place: from slice 1, at the back of the gallery, to slice 136, at the front of the barrier in contact with the first concrete plug, the last one installed. The term "section" refers to the vertical sampling sections in which samples of any kind were taken during dismantling. They were numbered from the entrance of the gallery towards the back of it, and the numbering started in the first dismantling. Hence, sampling Sections S1 to S30 were sampled in 2002, and sampling Sections S31 to S61 were sampled in 2015. For this reason, there were more slices than sampling sections, because not all the bentonite slices were sampled. A sampling section could also include two or three slices.

## 3.2 The Grimsel Test Site

The In Situ Test is located within the FEBEX drift at the Grimsel Test Site (GTS). The GTS is located at an elevation of about 1'730 m a.s.l., roughly 400 to 450 m beneath the Juchlistock mountain top in Central Switzerland. The host rocks are the leucocratic Central Aare Granite and Grimsel Granodiorite in the southern section of the Central Aar Massif. During the Alpine Orogeny (40 Ma), Aare Granite was subject to regional shear displacement and weak to intermediate metamorphism. The latter caused significant foliation whereas the shear movement resulted in the development of cataclastic and mylonitic shear zones. Within the GTS area up to twelve different shear and fracture sets can be observed in detailed drill core and surface evaluations (Keusen et al. 1989). The most important geological features in this environment are the two families of shear zones (K and S). Two large S-family shear zones have been assumed to act as the hydraulic boundaries of the FEBEX site. The inflows to the tunnels from these shear zones were approximately 60 and 23 mL/min respectively before installation (Alonso & Alcoverro 2005).

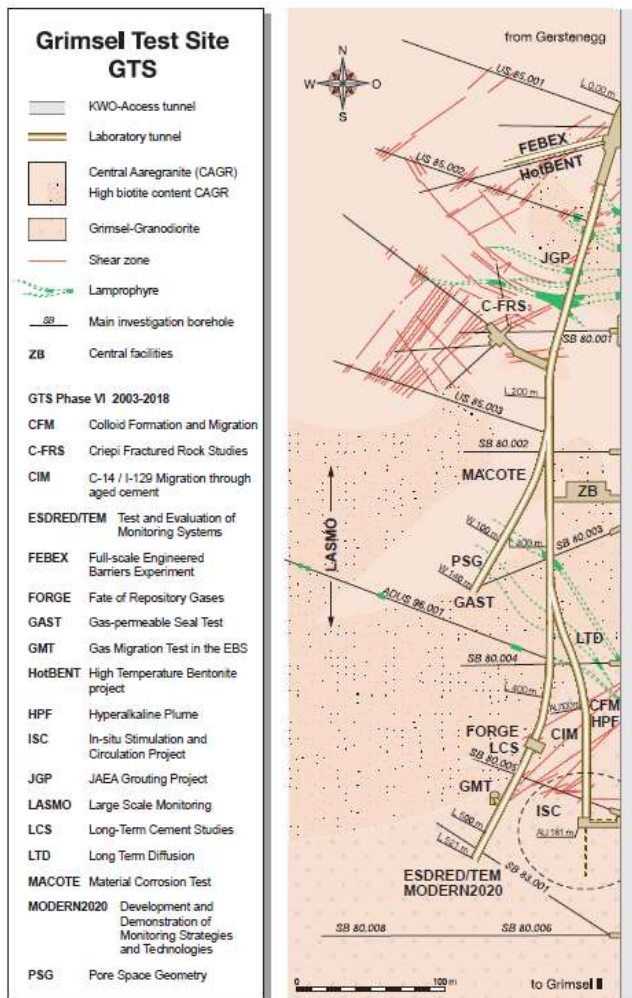


**Figure 3-4** Geological model of the Grimsel Test Site

### 3.2.1 The Febex area

The site of the FEBEX experiment was explored with 23 boreholes of depths ranging from 7 to 151 m (a total of about 750 m). Available data consist of a geological map of the tunnel wall, the borehole configuration, core descriptions and head monitoring in borehole intervals. Inflow measurements and hydraulic parameters obtained from hydraulic testing will be described separately in the next sections. The main reference to the geology of the FEBEX area is Pardillo et al. (1997).

Within this domain, some other geological features are worth mentioning: a shear zone, which actually crosses the FEBEX drift at a depth of about 20 m, and a lamprophyre dike, related to a major set of dikes. It intersects the GTS tunnel in the vicinity of the borehole BOUS 85.002, that is, close to the intersection of the S boundary. Figure 3-5 is a detailed description of geological features observed either in tunnel walls or borehole cores. In this figure, the N boundary of the FEBEX does not show up. However, the S boundary can be easily deduced by the density of fractures which constitute the shear zone. Also, the lamprophyres involved (black) can be traced between the FEBEX drift and the GTS tunnel. The shear zone intersected by the FEBEX drift is also shown.

Figure 3-6 and Figure 3-7 display the geological map of the drift. The last 17.4 m are of immediate concern for the FEBEX experiments because the heater and the bentonite block are installed in this section. Relevant geological features at the tunnel scale include:

- Lamprophyre dikes





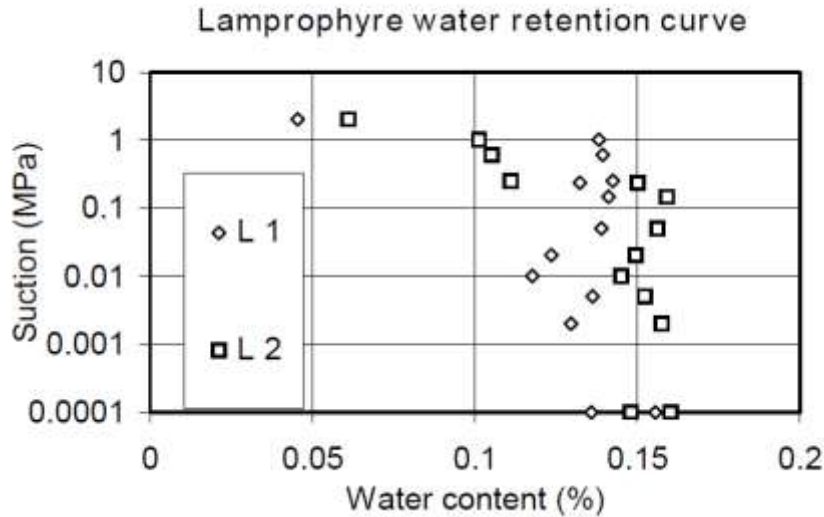


Figure 3-8 Water retention curves of lamprophyre (Pintado et al., 1997)

Table 3-1 Rock mechanical parameters of the main rocks at the Grimsel Test Site (Keusen et al., 1989). (\* refers to fractures).

parameter	granite (Central Aare)	granodiorite (Grimsel)	aplite	lamprophyre	units
density	2660±23.8	2706±13.6	2599±17.4	2909±31.0	kg/m <sup>3</sup>
porosity	0.4-1.0				vol %
uniaxial comp. strength	169.1±37.1	116.9±47.9	225.6±45.4	127.0±31.8	MPa
Young's modulus E <sub>50</sub>	53.3±11.0	47.3±15.4	60.2±8.9	42.4±8.5	GPa
Poisson's ratio	0.37±0.12 0.33±0.03	0.33±0.15	0.40±0.12	0.33±0.17	-
tensile strength	9.06±1.48	9.54±2.17	9.27±0.95	12.55±3.59	MPa
triaxial comp. strength (σ <sub>3</sub> ; σ <sub>1</sub> )	5.0 ; 263.0±29.9 10.0 ; 333.0±20.6 20.0 ; 410.0±63.8	5.0 ; 230.0±70.7 10.0 ; 287.0±24.7 20.0 ; 355.0±28.3	5.0 ; 297.0 10.0 ; 395.0 20.0 ; 455.0	5.0 ; 240.0 20.0 ; 226.0±44	MPa
friction angle	(*) 33	(*) 30±2 29	(*) 34 36	32.5±3.5	°
p-wave vel. (specimen)	3111±278	3351±388	2948±428	2120±480	m/s
p-wave vel. (whole rock)	5600±100	5600±100	5400-5700	5700-6100	m/s
thermal conductivity (wet)	2.58±0.19	2.66±0.19	3.31±0.35	2.21±0.45	W/m-K
thermal conductivity (dry)	3.34±0.35	3.22±0.29	5.32±0.49	2.71±0.60	W/m-K
permeability	5·10 <sup>-17</sup> (10 MPa) 3.5-4.5·10 <sup>-12</sup> (5-15 MPa) 5·10 <sup>-12</sup> (5-30 MPa)				m/s



**Table 3-2** *Properties of intact granite (Amiguet, 1985). (\* means in-situ stress condition)*

property	versus	mean value	range	units
bulk density		2640	2600-2680	kg/m <sup>3</sup>
grain density		2680	2650-2700	kg/m <sup>3</sup>
porosity		1.6	0.5-2.5	%
uniaxial compression strength		185	150-220	MPa
Young's modulus		60	45-75	GPa
Poisson's ratio		0.25	0.20-0.30	-
tensile strength		10	5-15	MPa
triaxial strength	conf. pressure			
	5 MPa	35	25-40	MPa
	10 MPa	45	35-55	MPa
	20 MPa	65	55-75	MPa
	50 MPa	105	95-120	MPa
	100 MPa	160	140-180	MPa
	200 MPa	240	200-280	MPa
angle of friction (natural joint)		32	25-40	°
p-wave velocity		*5600	5000-6200	m/s
s-wave velocity		*3400	3000-3600	m/s
coef. linear thermal expansion		8.0·10 <sup>-6</sup>	(5-12)·10 <sup>-6</sup>	K <sup>-1</sup>
coef. vol. thermal expansion		25·10 <sup>-6</sup>	(20-30)·10 <sup>-6</sup>	K <sup>-1</sup>
thermal conductivity		3.3	2.7-3.8	W/mK
specific heat		920	800-1250	J/kgK
permeability		10 <sup>-12</sup>	(0.1-5)·10 <sup>-12</sup>	m/s

### 3.3 Main Materials and component of the experiment

#### 3.3.1 Bentonite blocks

Figure 3-2 shows the geometry of the barrier in the heater and non-heater areas. In both areas, the three exterior crowns of the blocks are equal; in the heater area the interior crown of this group is in contact with the steel liner, while, in the non-heater area, the interior crown is in contact with a core of blocks. Five types of blocks form this barrier geometry: BB-G-01, BB-G-02, BB-G-03, BB-G-04, and BB-G-05. Figure 3-9 and Table 3-3 show the shapes and dimensions of the block types. The dry density specified in the design of the blocks was 1.70 g/cm<sup>3</sup>. This density was determined by taking into account the probable volume of the construction gaps and the need to have a barrier with an average dry density of 1.60 g/cm<sup>3</sup>. For a dry density of 1.60 g/cm<sup>3</sup>, the swelling pressure is of the order of 5 MPa, which is the value proposed in the AGP Granito. The water content of the blocks is that specified for the raw bentonite, 12.5% to 15.5%

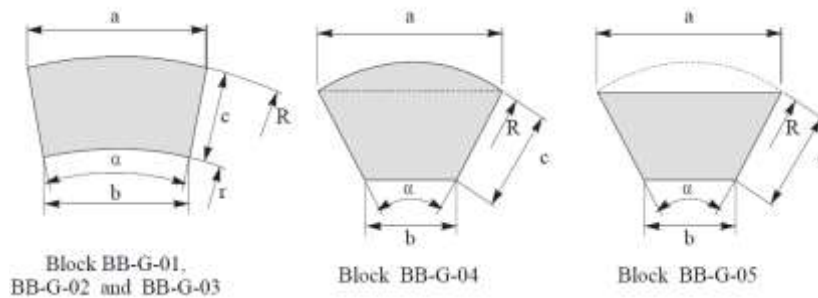


Figure 3-9 Shapes and dimensions of the blocks

Table 3-3 Dimensions for block fabrication

Type	a mm	b mm	c mm	thickness mm	R mm	r mm	$\alpha$ °
BB-G-01	470.0 (+2.0 -5.0)	380.0 (+2.0 -4.0)	214.0 (+2.0 -3.0)	125.0 (+2.0 -2.0)	1133	919	24
BB-G-02	473.0 (+2.0 -5.0)	361.0 (+2.0 -4.0)	214.0 (+2.0 -3.0)	125.0 (+2.0 -4.0)	917	703	30
BB-G-03	478.0 (+2.0 -5.0)	330.0 (+2.0 -4.0)	214.0 (+2.0 -3.0)	125.0 (+2.0 -4.0)	701	487	40
BB-G-04	483.0 (+2.0 -5.0)	240.0 (+2.0 -4.0)	240.0 (+2.0 -3.0)	125.0 (+2.0 -4.0)	485	—	60
BB-G-05	483.0 (+2.0 -5.0)	240.0 (+2.0 -4.0)	240.0 (+2.0 -3.0)	125.0 (+2.0 -4.0)	—	—	60

For the fabrication of blocks BB-G-01, BB-G-02, BB-G-03, and BB-G-04 it was necessary to design and manufacture moulds, whereas block BB-G-05 was obtained from BB-G-04 by machining the curved face with a saw. The blocks were fabricated in the REFRACTA, S. A. plant at Quart de Poblet (Province of Valencia, Spain), by compaction in a uniaxial hydraulic press under a pressure of 40 MPa to 45 MPa. A quality assurance program was applied in fabrication of the blocks: external appearance, dimensions, water content, and dry density were controlled. Table 5.2 shows the average values for the characteristics and the number of blocks fabricated for each type.



Taking into account the dimensions of the blocks of each type, the average values of water content and dry density are 14.4% and 1.69 g/cm<sup>3</sup>, respectively. A total of 7568 blocks were fabricated, with a total weight of 165 076 kg.

*Table 3-4 Average values of the physical properties and number of blocks fabricated*

	BB-G-01	BB-G-02	BB-G-03	BB-G-04	BB-G-05
weight per block (kg)	22.1	21.8	21.3	23.1	18.0
average water content (%)	14.49	14.07	14.87	13.69	13.07
average dry density (g/cm <sup>3</sup> )	1.69	1.69	1.69	1.70	1.70
number of units fabricated	2 898	2 310	1 614	562	184
total weight (kg)	64 046	50 358	34 378	12 982	3 312

### 3.3.2 Heating system

#### **General characteristics**

The test uses two electrical heaters inserted within a steel liner. The heaters reproduce the mechanical characteristics of the AGP Granito canister, simulating the thermal effects. The external dimensions of the heater are identical to those of the canister anticipated in the AGP Granito concept (a cylinder measuring 4.54 m in length with a diameter of 0.90 m) and the weight is of the same order (11 t). Both the material and the shape of the exterior body of the heaters are similar to those anticipated for the canister: carbon steel plate measuring 100 mm in thickness.

As regards the thermal aspect, the aim of the test is to subject the bentonite, at the point of contact with the steel liner, to a maximum constant temperature of 100°C, which is the maximum value anticipated in the reference concept. Nevertheless, in order to reach this value in a period of time compatible with the duration of the test, and maintain it in an isolated drift, it was necessary to increase the power of the heaters beyond the value anticipated in the AGP Granito concept for the maximum residual thermal power of the canisters, that is 1200 W. Following different analyses and modelling exercises, performed during the design phase of the experiment, the nominal power was fixed at 4,300 W per heater. This power will be the maximum required in the most unfavorable case of the clay barrier being totally saturated, with a certain margin of safety.

#### **Mechanical characteristics**

Figure 3-10 shows a general view of the final design of the heater. The exterior casing consists of a forged tube with a wall thickness of 100 mm, and two welded end covers of metal plate, each measuring 150 mm in thickness. The casing is of carbon steel without any treatment or covering, except shot-peening of the exterior surface.

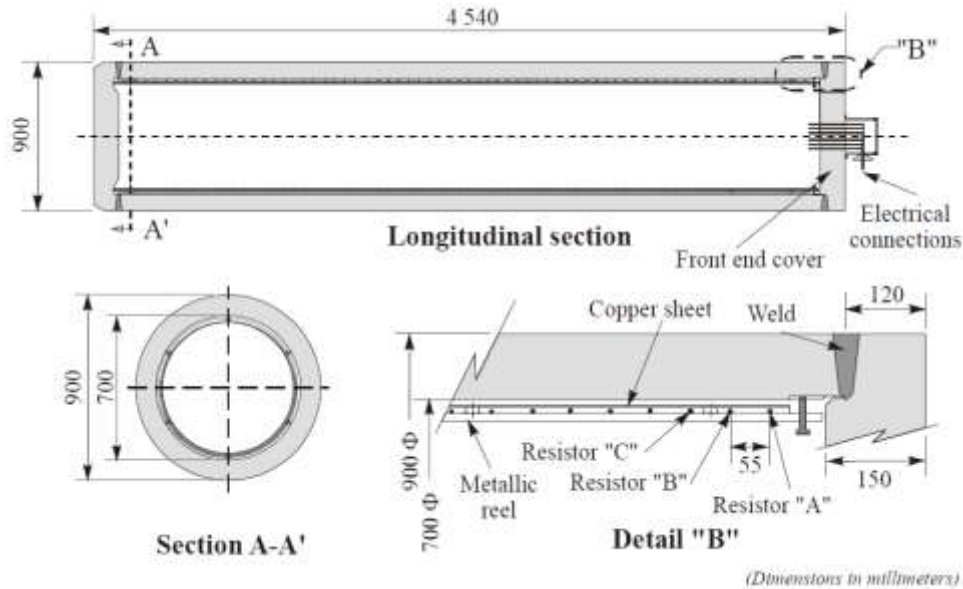


**Figure 3-10** Dimensions and construction details of the heaters

Inside the casing, the heating elements (resistances) are wound around a tube or reel measuring 660.4 mm in diameter and 12.7 mm in thickness. The assembly - reel and resistances - is covered with a copper sheet measuring 3 mm in thickness. This covering serves to distribute the temperatures more uniformly along the heater and to provide mechanical protection for the heating elements during heater assembly.

**Steel liner**

The “in situ” test faithfully reproduces the AGP Granito reference concept, which considers the existence of a continuous steel liner, common to all the canisters emplaced in the same drift. This steel liner consists of a perforated steel tube measuring 15 mm in thickness, providing the space into which the canister is inserted. Given that in the actual design of the AGP Granito concept no consideration is given to the retrievability of the canisters, the function of the steel liner terminates when the canister is introduced; therefore, the deformation of the liner due to swelling of the bentonite is not important.

The steel liner required for the test has a length of 10 m, corresponding to the length of the two heaters plus the 1-m separation between them. Thus, 11 segments of 1 m each were made, designed to be coupled by means of a male/female conical coupling measuring 100 mm in length, machined in the ends of each segment. The material of the steel liner is conventional alloyed steel for boilers and pressure vessels.

The inner diameter of the liner is 940 mm; thus there is a gap of 40 mm with respect to the outer diameter of the heaters, a value that was considered sufficient for correct insertion of the heaters, taking into account the normal errors of alignment in an installation operation of this type.

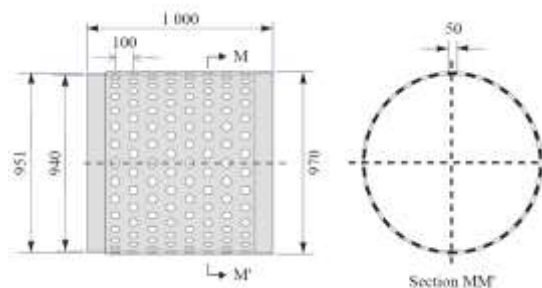


**Figure 3-11** Steel liner

**3.3.3 Instrumentation**

A total of 632 sensors were installed.

Table 3-6 indicates the variables measured, the types of sensors used and the locations of the sensors, by areas. The sensors in the clay barrier were grouped in a series of cross-sections, as indicated in Figure 3-12: sections A, B1, B2, C, D1, D2, E1, E2, F1, F2, G, H, I, K, L, M1, M2 and N. The sections with an identical letter have similar sensor configurations.

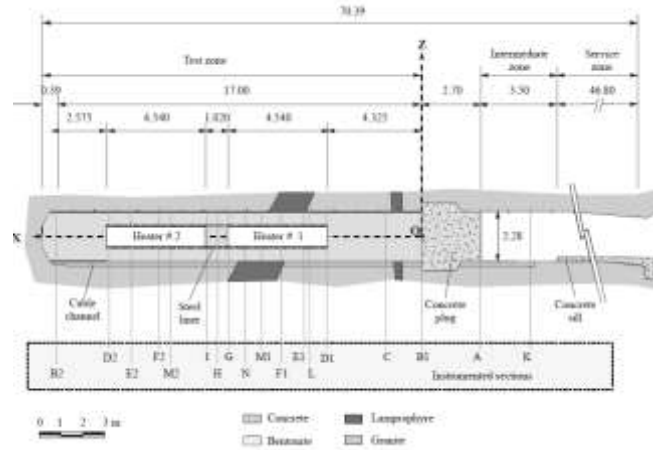


**Figure 3-12** Arrangement of the instrumented sections

The boreholes BOUS-1, BOUS-2, FBX-1, and FBX-2 were used, along with the 19 boreholes drilled from the interior of the drift, for instrumentation the rock, in particular for hydrogeological and mechanical variations. Other sensors, such as psychrometers and TDR probes were installed in smaller boreholes, drilled from the drift in areas closer to the wall (up to 2.5 m).

Two examples of the location of sensors in the clay barrier and in the surrounding rock are shown in Figure 3-13 and Figure 3-14, respectively. Each sensor is identified by a code of the type: AA-BBn-CC, where AA is the code of sensor type (see Table 3-5), BB is the designation of location type (borehole, instrumented section, etc.), n is the order number of section or borehole (where applicable) and CC is the order number within the corresponding section or borehole. The final locations of all sensors are identified by their coordinates, in the local reference system XYZ indicated in Figure 3-14.

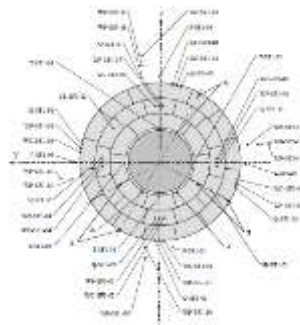


**Figure 3-13** Final location of sensors in instrumented cross-section F1.

**Table 3-5** Identification of sensor codes

code	sensor
T	Temperature
P	Total pressure
Q	Pore pressure



SH	Heater displacement
SB	Bentonite block displacement
S	Displacement (general)
3S	Crack meter
PP	Hydraulic pressure of packer in borehole
IT	Clinometer
GP	Gas pressure
GF	Gas flow
WC	Water content (capacitive type)
WP	Water content (psychrometer type)
WT	Water content (TDR type)
AP	Atmospheric pressure (in service zone)
A	Anemometer
V	Voltage meter
C	Electric current meter
Ω	Insulation meter

**Table 3-6** Installed sensors (G: granite; B: bentonite; C: heater; S: service zone)

Variable (or instrument)	type of sensor	area				total
		G	B	C	S	
Temperature	Thermocouple	62	91	36		189
Total pressure in borehole in rock (3-D)	Vibrating wire	4				4
Total pressure on rock surface	Vibrating wire	30				30
Total pressure on heater	Vibrating wire		6			6
Hydraulic pressure in borehole in rock	Piezoresistive	62				62
Packer pressure in borehole	Piezoresistive	62				62
Pore pressure in bentonite	Vibrating wire		52			52
Water content	Capacitive		58		1	59
Water content	Psychrometer	28	48			76
Water content	TDR	4	20			24
Extensometer in rock	Vibrating wire	2x3				6
Heater displacement	Vibrating wire		9			9
Expansion of bentonite block	Vibrating wire		8			8
Displacement within the bentonite barrier	Potentiometer		2x3			6
Clinometer	LVDT		6x2			12
Crack meter	LVDT	1x3				3
Gas pressure in the bentonite barrier	Magnetic		4			4
Gas flow	Manual measure		6			6
Atmospheric pressure	Piezoresistive				1	1
Velocity of ventilation air	Hot wire				1	1
Resistor intensity	Electric converter				6	6
Resistor voltage	Electric converter				6	6
<b>TOTAL</b>		<b>261</b>	<b>320</b>	<b>36</b>	<b>15</b>	<b>632</b>

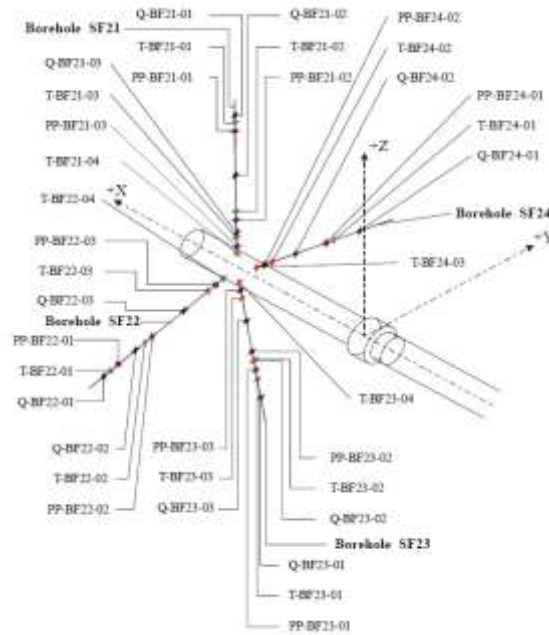


Figure 3-14 Location of sensors in boreholes SF21, SF22, SF23 and SF24

### 3.3.4 Installation

All the gaps existing between the blocks, both by design and as a result of manufacturing tolerances, accumulate at the top part of each slice, resulting in a total gap of approximately 2 to 3 cm. Figure 3-15 represents a typical cross-section of the drift. It may be seen that, for these reasons, the axis of the steel liner is off-center, displaced some 15 mm. Consequently, the heater is off-center by some 35 mm, the exact deviation depending on the actual diameter of the drift at each point.

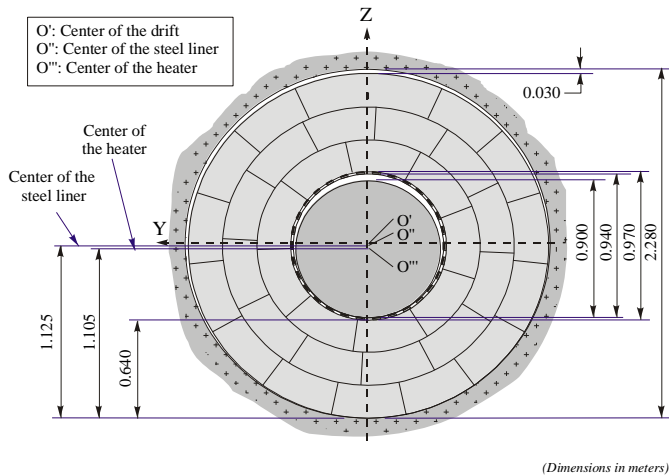
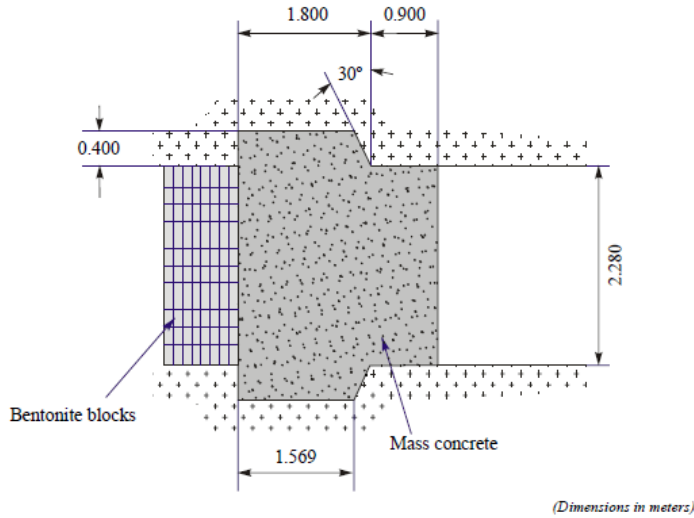


Figure 3-15 Typical cross section of the clay barrier

**3.3.5 Concrete plug**

The test zone was closed with a concrete plug, the geometry of which is shown in Figure 3-16. The plug was designed to resist the swelling pressure of the bentonite. No specification was included for the water tightness or gas tightness of the concrete plug. The plug was constructed with mass concrete, without any reinforcement, to facilitate the planned future dismantling. It was designed to withstand a total force of 2000 t, which corresponds to a swelling pressure of the bentonite of 5 MPa. The concrete used had a low value of hydration heat and minimum shrinkage. Table 3-7 shows the proportions used for the concrete mix.



**Figure 3-16** Longitudinal section of the concrete plug

The plug was concreted in three sections perpendicular to the axis of the drift, such that the filling of the upper part could be checked, at least for a part of the plug. The concrete was pumped from outside the drift and was compacted by vibration. This method did not allow for good concreting of the key, where a void remained, this subsequently being filled by means of injection. Table 3-8 shows the results obtained from the concrete control tests.

**Table 3-7** Concrete mix proportions used in plug construction

component	type	proportions kg/m <sup>3</sup>
cement	PCO “Sulfacem” (CEM I 32.5 HS)	160
silica fume	Sikafume HR	60
fine aggregate	Grimsel granite, 4 to 8 mm	660
coarse aggregate	Grimsel granite, 8 to 16 mm	430
sand	Quartz 0.1 to 5.6 mm	800
filler	limestone	170
water	city network	155
superplasticizer	Sikament-12+	13

**Table 3-8** Results of concrete control tests

water/cement ratio	0.99
water/total hydraulic materials ratio	0.72
slump (Abrams cone) (mm)	44



density (before setting) (kg/m <sup>3</sup> )	2394
air content (%)	0.4
28-day strength (MPa)	47.1

### 3.3.6 Quality assurance and quality control

Control of the dry density of the clay barrier was fundamental to its construction. The average dry density was to be no more than 1.60 t/m<sup>3</sup>, in order not to exceed the maximum swelling pressure of 5 MPa used in the calculations for the test components. On the other hand, it was required not to be less than the minimum considered tolerable, 1.4 t/m<sup>3</sup>. Furthermore, knowledge of the actual dry density obtained is necessary for modelling, as well as for the interpretation of the test results. For this reason, during the construction of the clay barrier, the real mass of bentonite placed and the volume of the drift occupied by each vertical slice of blocks was determined. From these values, the global dry density as well as the percentage of construction gaps for each slice were calculated. The profiles of dry density and construction gaps were drawn from each slice, these being shown in Figure 3-17.

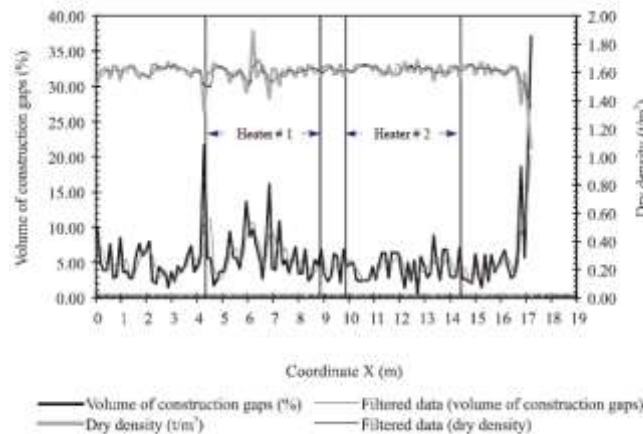


Figure 3-17 Profiles of dry density and volume of construction gaps in the clay barrier.

## 3.4 Test operation

### 3.4.1 Initial tests and start-up

The mechanical installation tasks were completed in 16 weeks between 1 July 1996 and 15 October 1996, two weeks ahead of schedule. The assembly and setting up of the data acquisition and control systems were prolonged more than anticipated, until 27 February 1997. Apart from some short duration tests, the heating (operational) stage began on 27 February 1997, the date identified as “day 0” on the time scale. The sequence of initiation was as follows:

- Throughout an initial period of 20 days a constant power of 1200 W per heater was applied, with the aim of identifying the thermal response of the system and adjusting the control algorithms.
- Over the next 33 days the power was increased to 2000 W per heater and maintained constant to approximate the temperature of 100 °C desired at the surface of the steel liner, but with a limitation on the rate of power increase to reduce thermally-induced stresses.
- Finally, on 21 April 1997 (day 53) the system was switched to the constant temperature control mode, allowing the power to fluctuate freely. Over a period of 8 days, three subsequent steps were performed to adjust the parameters of the control algorithm, the set points of the system being established successively at 95°C, 99°C, and 100 °C.

### 3.4.2 Heating control and operation

Beginning in day 61, the power control system has been automatically regulating the power in the two heaters independently, so as to maintain a constant temperature of 100°C at the hottest point of the steel liner/bentonite interface, as originally planned. The reference used by the power control

algorithm is the highest temperature value in the sensors located at the surface of the steel liner, which has always been at the center of the bottom line of the heater. Due to the shape of the heater casings, temperatures over 100 °C were observed at the lids, but these were discarded, as they are considered to be unique points.

With a view to increasing reliability, the heating system is redundant, and each heater has three independent heating elements, each having the rated nominal power of 4,300 W. During the test, only one of these elements, identified as Resistor A, has been used on each heater on a permanent basis, the other two being kept in reserve. The underlying reason for this was to check the operational life of these elements, which is inversely proportional to their external temperature. In any case, there has not been any failure of the elements after 1000 days (2 years and 9 months, in 27th of November, 2000) of continuous operation.

Approximately two years after the start of the experiment, the applied power at heater #2 started to increase slightly, maintaining the trend until the decommissioning of heater #1. A noticeable increase of about 5 % (about 100 W) was clearly seen during approximately two months after disconnecting heater #1. Since then, the applied power in heater #2 has been almost linear with time. Total increase in power seen from day 56 (24.04.1997) up to the switching off day was around 18.5 %.

### 3.5 Test case

The test case concerns only the evolution of the EBS around heater #2 on the period between 27<sup>th</sup> of February 1997 and 30<sup>th</sup> of August 2015. The data recorded on this period in the boreholes drilled in the rock and from the sensors installed in the bentonite are available in the report NAB16-019 (Martínez and al., 2016).

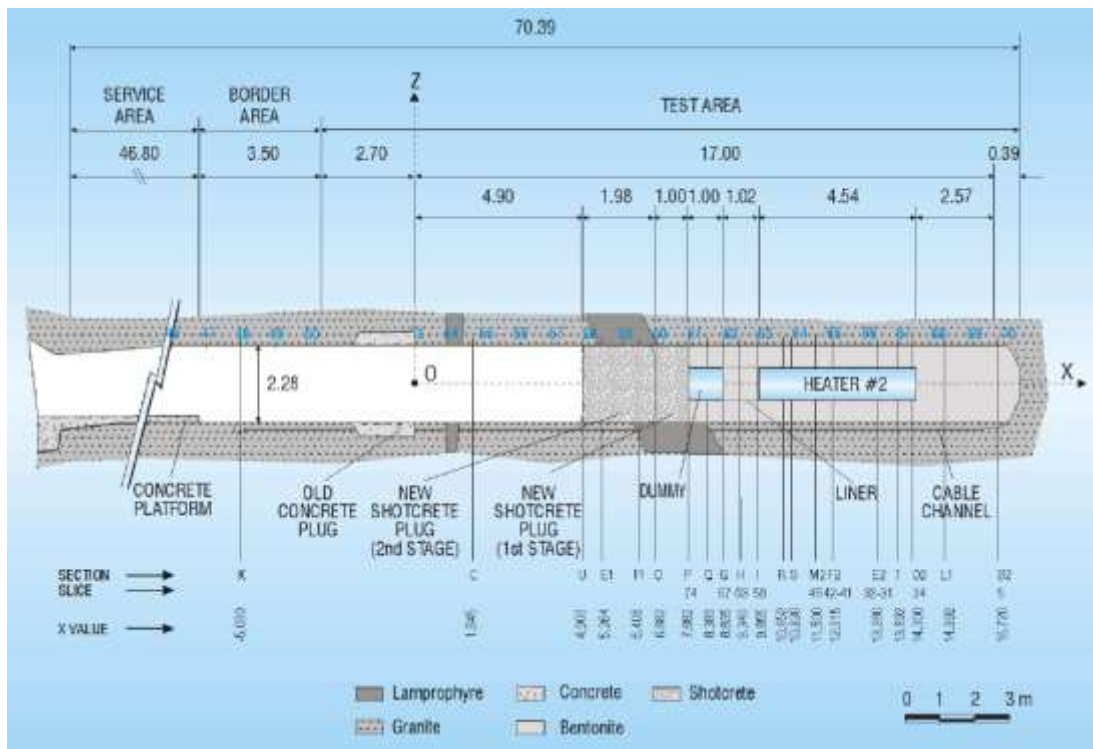


Figure 3-18 Domain of interest for the test case

#### 3.5.1 Required outputs

Results requested are: (1) distributions and evolutions of relative humidity; (2) distributions and evolutions of temperature; (3) evolutions of total stresses; (4) distribution and evolution of dry density, water content and degree of saturation. The objective is: (1) to show the ability of the model to



reproduce the global behavior of the structure during heating and hydration, (2) to follow on several locations points and some slices how the homogenization of the bentonite occurs.

**Location**

The computed variables (see Table 3-10 for the list) have to be produced at several locations. On 4 vertical sections: E2, F2, VS1, B2 (see Figure 3-20) at 12 points for sections E2 and F2, at 13 points for sections VS1 and B2 (see Figure 3-19, Table 3-9). On one horizontal section in the middle of the canister (HS1 at z=0 in plan XY). Point identifications should respect the following terminology: Variable-Section-Point-. For example, relative humidity function of time at point from section F2 will be identified: RH-F2-A1, RH-F2-A2...

**Table 3-9** Location of sections where outputs are required

Section	Location in x (m)
F2	12.015
E2	13.28
VS1 (S56)	14.52
B2	16.720

A1	0.485	
A2	0.918	
A3	1.135	

**Table 3-10** List of outputs and acronyms

Relative humidity	RH
Temperature	T
Water content	WC
Total Pressure	TP
Water Saturation	WS

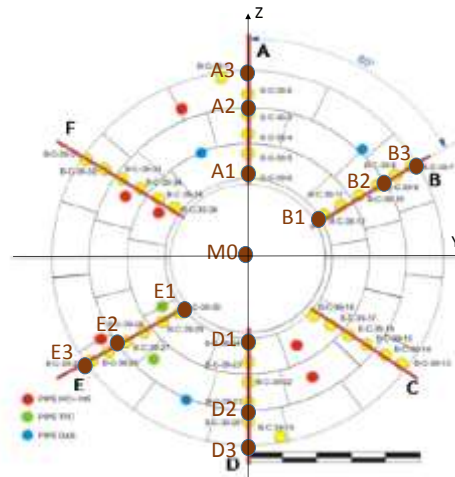


**Figure 3-19** Position of sampling radii and requested output locations in a section

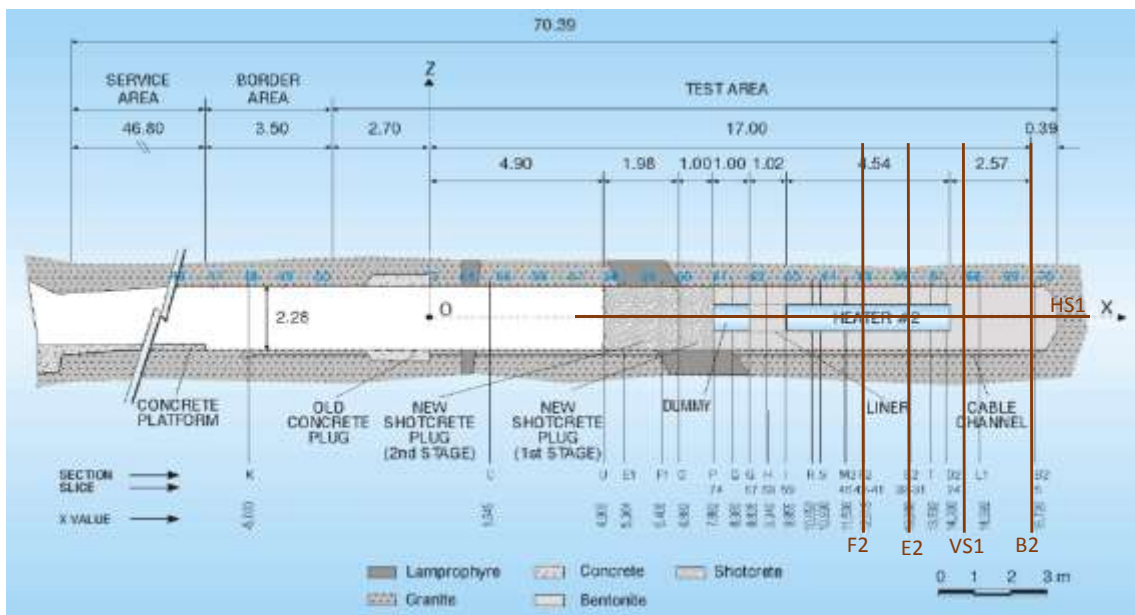


**Figure 3-20** Location of section where outputs are required

**Distribution and Evolution of relative humidity**

a) Evolution of relative humidity

The variation of relative humidity inside the bentonite along the radial distance is required. Four cross sections have been selected to give these outputs (their positions are shown in Figure 3-20):

Computed relative humidity as a function of radial distance on specific points will be given from time  $t=0$  (27/02/1997) to  $t=6758$  days (30/08/2015). Frequency is at least one value each 100 days, a minimum of 67 value for each point identify in Figure 3-19.

Four radial directions have been selected for this output, namely:

- RA: along positive axis Z (+z)
- RB: along a line with an angle of 30° from the horizontal and 60° vertical in positive domain for both Y and Z
- RD: along positive axis Z (-z)



- RE: along a line with an angle of 30° from the horizontal and 60°vertical in negative domain for both Y and Z

Sections concern by this output:

- Section F2: x = 12.015 m, Section E2: x = 13.44 m, Section VS: x=15.52, Section B2: x=16.720m

b) Distribution of relative humidity

Map of relative humidity should be produced at several times for the 4 sections: F2, E2, VS, B2.

for the following times : t1: t = 100 days, t2: t = 1000 days; t3: t = 1800 days, t4: t = 2500 days; t5: t = 4300 days, t6: t = 6758 days

**Distribution and evolution of temperature**

a) Distribution of temperature (radial direction)

The variation of temperature inside the bentonite along the radial distance is required. Four cross sections have been selected to give these outputs (their positions are shown in Figure 3-20):

Computed temperature as a function of radial distance on specific points will be given from time t=0 (27/02/1997) to t=6758 days (30/08/2015 ). Frequency is at least one value each 100 days, a minimum of 67 value for each point identify in Figure 3-19.

Four radial directions have been selected for this output, namely:

- RA: along positive axis Z (+z)
- RB: along a line with an angle of 30° from the horizontal and 60°vertical in positive domain for both Y and Z
- RD: along positive axis Z (-z)
- RE: along a line with an angle of 30° from the horizontal and 60°vertical in negative domain for both Y and Z

Sections concern by this output:

- Section F2: x = 12.015 m, Section E2: x = 13.44 m, Section VS: x=15.52, Section B2: x=16.720m

b) Distribution of temperature

Map of temperature (iso-values) should be produced at several times for the 4 sections: F2, E2, VS, B2.

for the following times : t1: t = 100 days, t2: t = 1000 days; t3: t = 1800 days, t4: t = 2500 days; t5: t = 4300 days, t6: t = 6758 days

**Evolution of total stresses**

The evolution of some specified stress along time, within the period (day 0 – day 6758) is required. The total stress component and the points selected are the following.

Section E2, Point E2G1 (x = 13.45 m; y = -0.28 m; z = -1.19 m). Radial stress ( $\sigma_r$ )

Section E2, Point E2H1 (x = 13.28 m; y = 0.00 m; z = -0.48 m). Radial stress ( $\sigma_r$ )

Section E2, Point E2G2 (x = 13.46 m; y = -1.19 m; z = 0.00 m). Radial stress ( $\sigma_r$ )

Section B2, Point B2G (x = 17.32 m; y = 0.26 m; z = 0.76 m). Axial stress ( $\sigma_x$ )



***Distribution and evolution of dry density, water content and degree of saturation***

a) Distribution of dry density, water content and Sw (radial direction)

The variation of dry density, water content and Sw inside the bentonite along the radial distance is required. Four cross sections have been selected to give these outputs (their positions are shown in Figure 3-20):

Computed dry density, water content and Sw as a function of radial distance on specific points will be given from time  $t=0$  (27/02/1997) to  $t=6758$  days (30/08/2015). Frequency is at least one value each 100 days, a minimum of 67 value for each point identify in Figure 3-19.

Four radial directions have been selected for this output, namely:

- RA: along positive axis Z (+z)
- RB: along a line with an angle of 30° from the horizontal and 60° vertical in positive domain for both Y and Z
- RD: along positive axis Z (-z)
- RE: along a line with an angle of 30° from the horizontal and 60° vertical in negative domain for both Y and Z

Sections concern by this output:

- Section F2:  $x = 12.015$  m, Section E2:  $x = 13.44$  m, Section VS:  $x=15.52$ , Section B2:  $x=16.720$ m

b) Distribution of dry density, water content and Sw

Map of dry density, water content and Sw (iso-values) should be produced at several times for the 4 vertical sections: F2, E2, VS, B2 and one horizontal section: HS1.

for the following times : t1:  $t = 100$  days, t2:  $t = 1000$  days; t3:  $t = 1800$  days, t4:  $t = 2500$  days; t5:  $t = 4300$  days, t6:  $t = 6758$  days

Comparison with measurements obtained after the final dismaling should be produced.



## 4 CRT - Canister Retrieval Test

### 4.1 Geometry

A schematic view of the experimental geometry is given in Figure 4-1 . More detailed drawings of the geometry of the CRT experiment is given by Figure 4-2 to Figure 4-6 below. Also the geometry of the TBT experiment is given in Figure 4-7.

The tunnel-profile has the approximate dimensions  $6 \times 6$  m with a horse shoe shaped profile. The experiments, CRT and TBT, are placed approximately at the tunnel center-line. The center of the TBT experiment is located = 6 m from the center of CRT.

In the hole 16 filter mats with a width of 10 cm are installed with uniform spacing, 0.15 m from the hole bottom up to 6.25 m height.

Ring-shaped or cylindrical bentonite blocks are placed in the hole. At the top of the canister bentonite bricks are filling up the volume between the canister top surface and the top surface of the upper most ring (R10). The height difference between the two surfaces was 220 - 230 mm. The volume between the bentonite blocks and the hole wall is filled with bentonite pellets and water.

An impermeable rubber mat was installed between C4 and the concrete plug. On top of the plug a steel lid was installed. The plug and lid can move vertically and are attached to the rock by nine rock anchors.

Each of the nine rock anchors, with 5 m fixed and free length, consists of 19 steel wires with a nominal area of  $98.7 \text{ mm}^2$ . The inclination of the anchors is 2.5:1 or  $\approx 22^\circ$ .

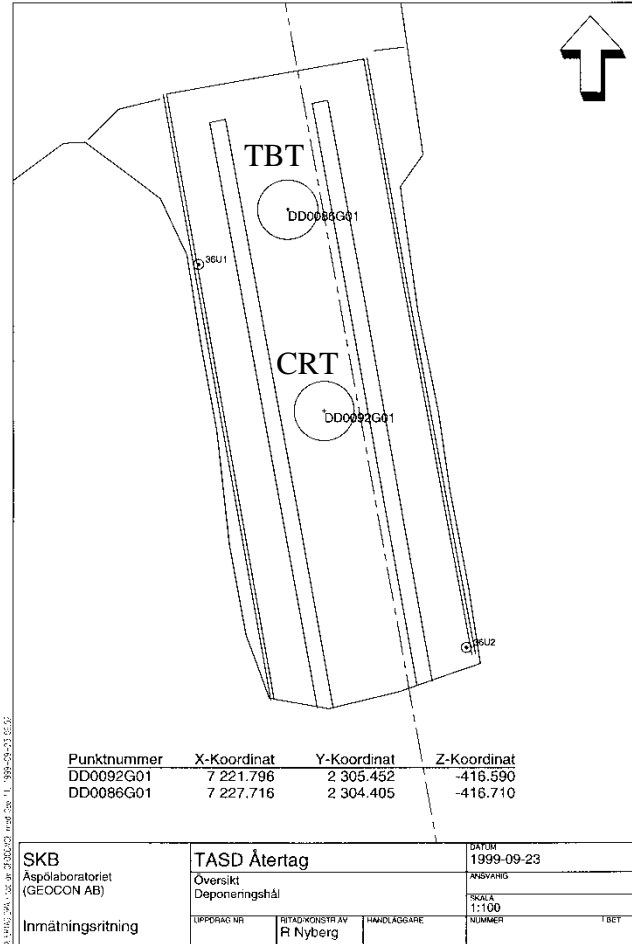
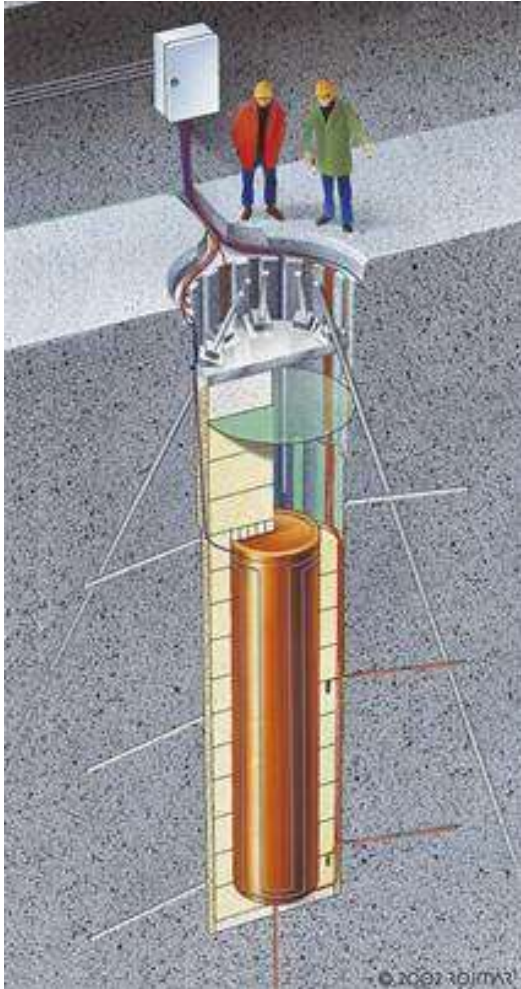


**Figure 4-1** Illustration of the experimental set-up of the Canister Retrieval Test and the location in the TASD tunnel.

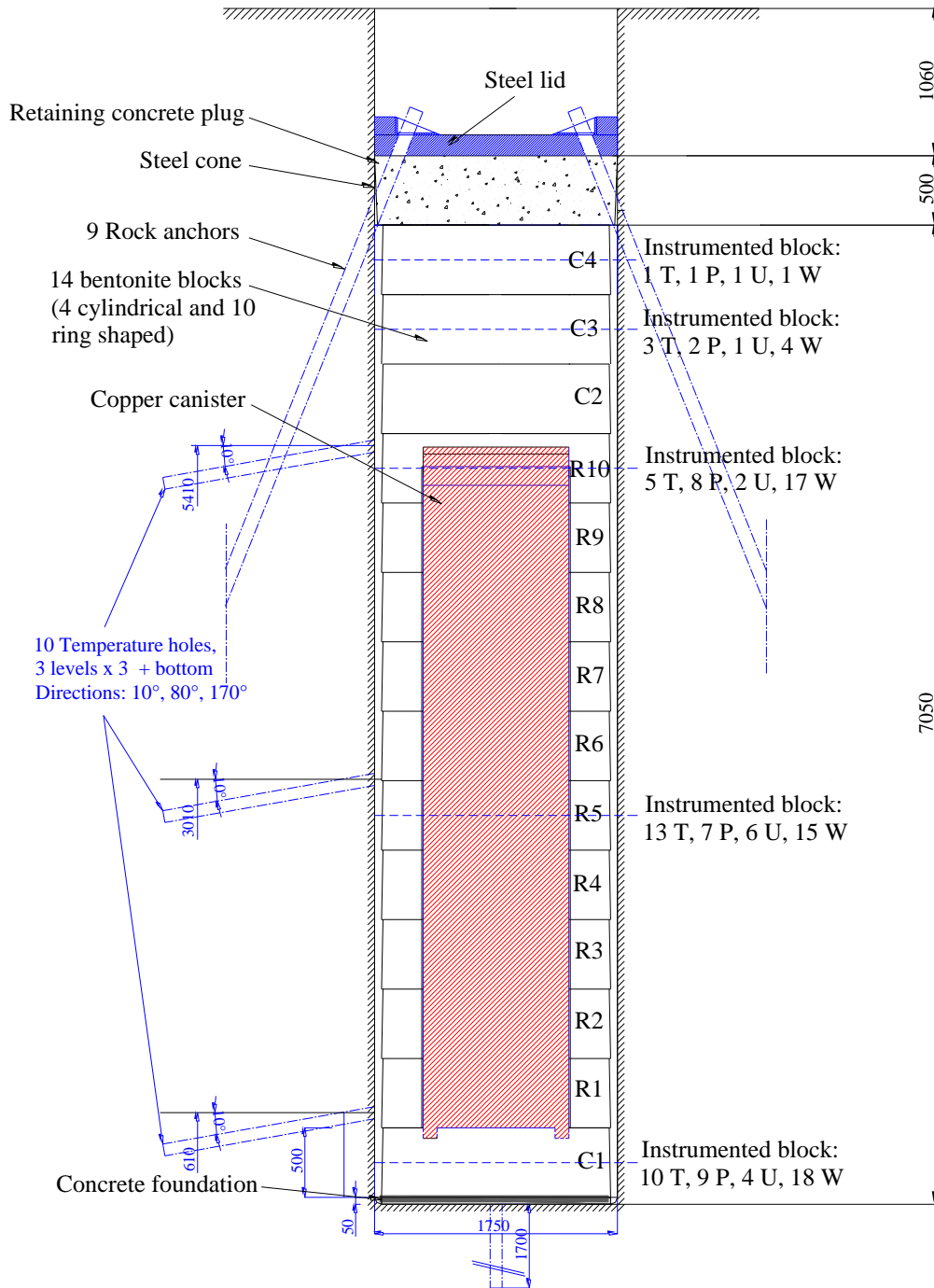


*Figure 4-2 Schematic view showing the experiment layout. Sensors have been placed in five of the bentonite blocks. For each block the number of each sensor type is described. (T=temperature, P=total pressure cell, U=pore pressure cell and W=relative humidity sensor).*

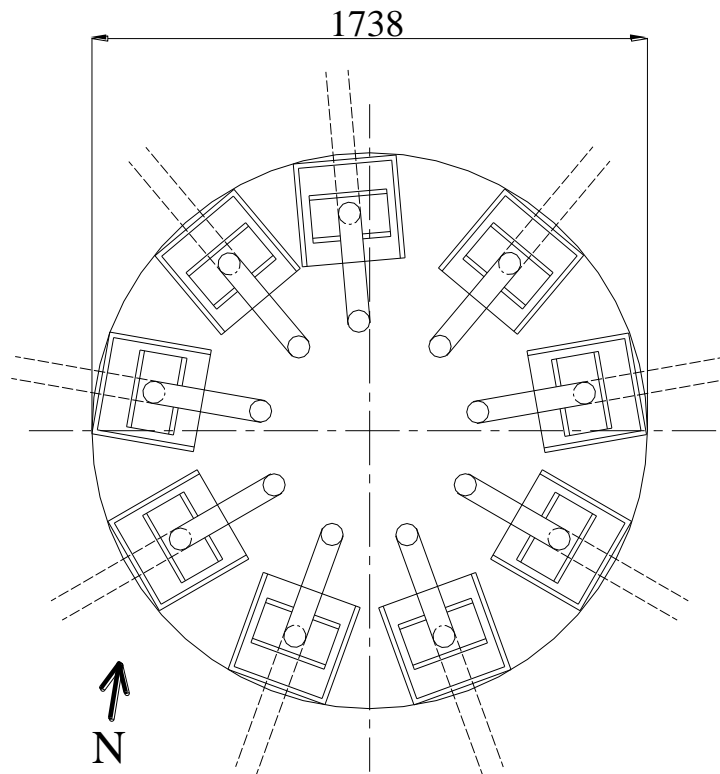


Figure 4-3 Plan of the retaining plug with rock anchors.

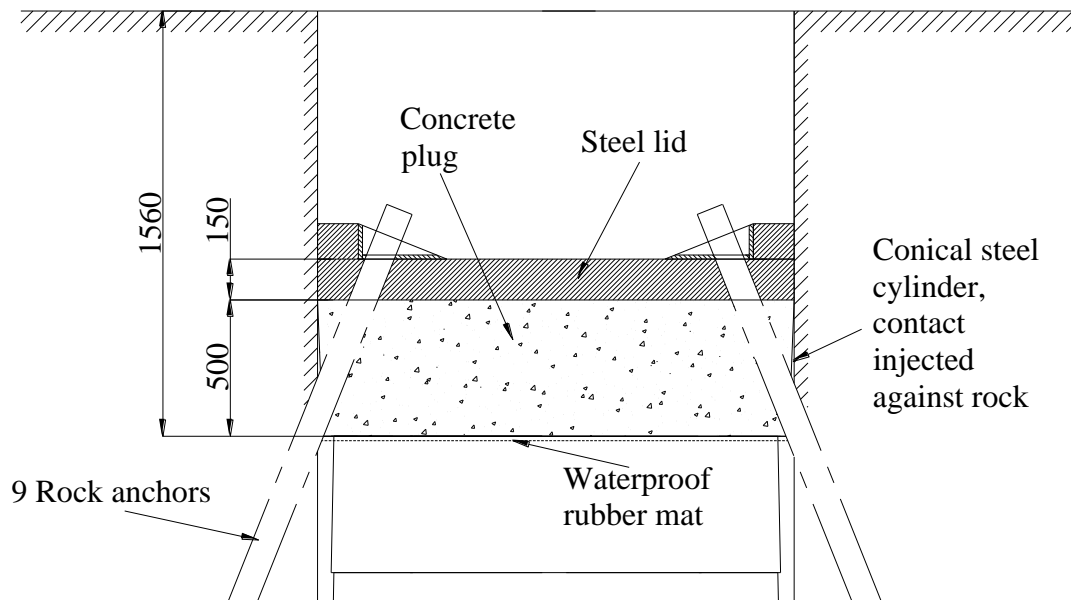


Figure 4-4 Section of retaining plug with rock anchors.

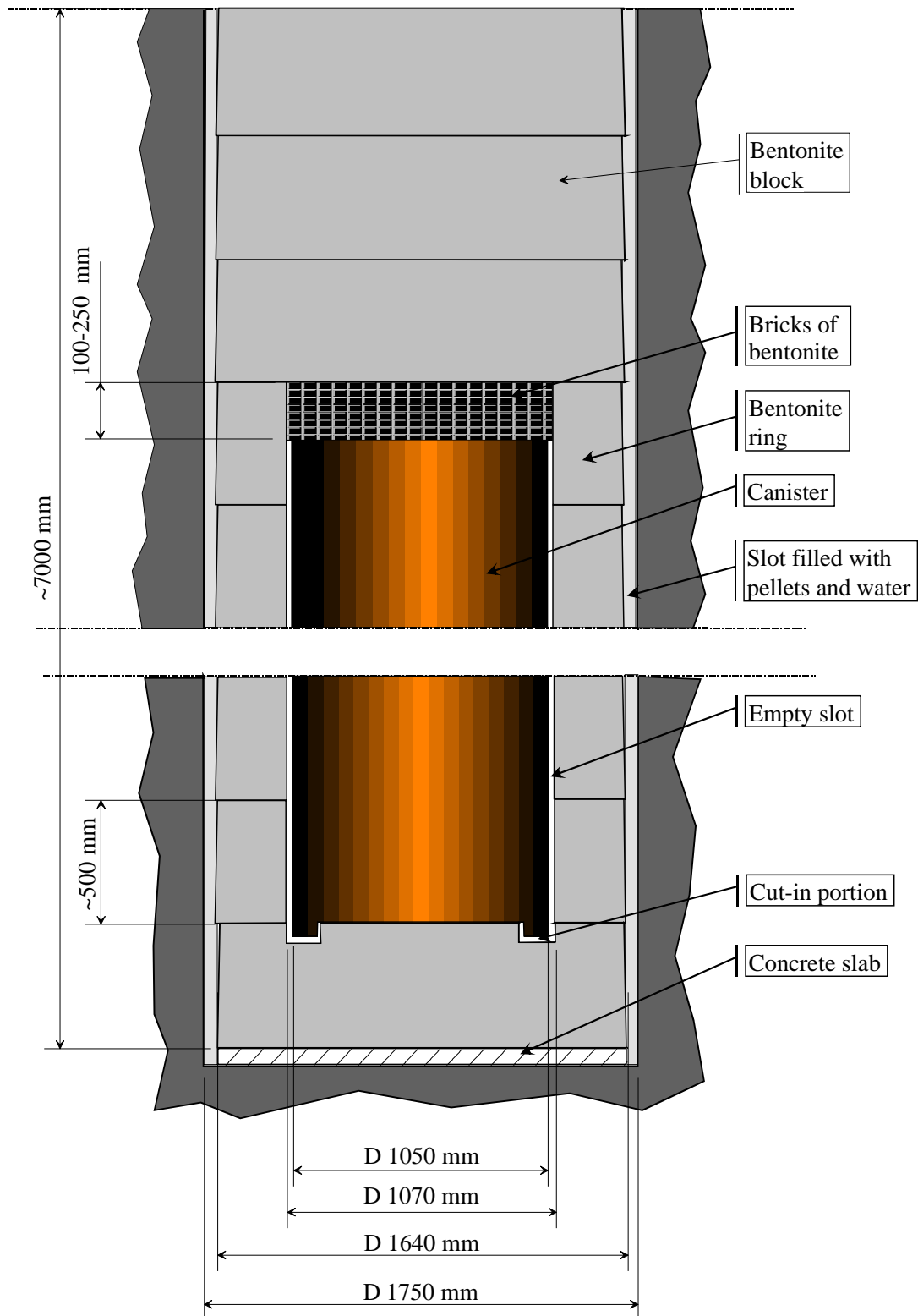


Figure 4-5 Schematic drawing of the canister hole with bentonite blocks with dimensions in mm.



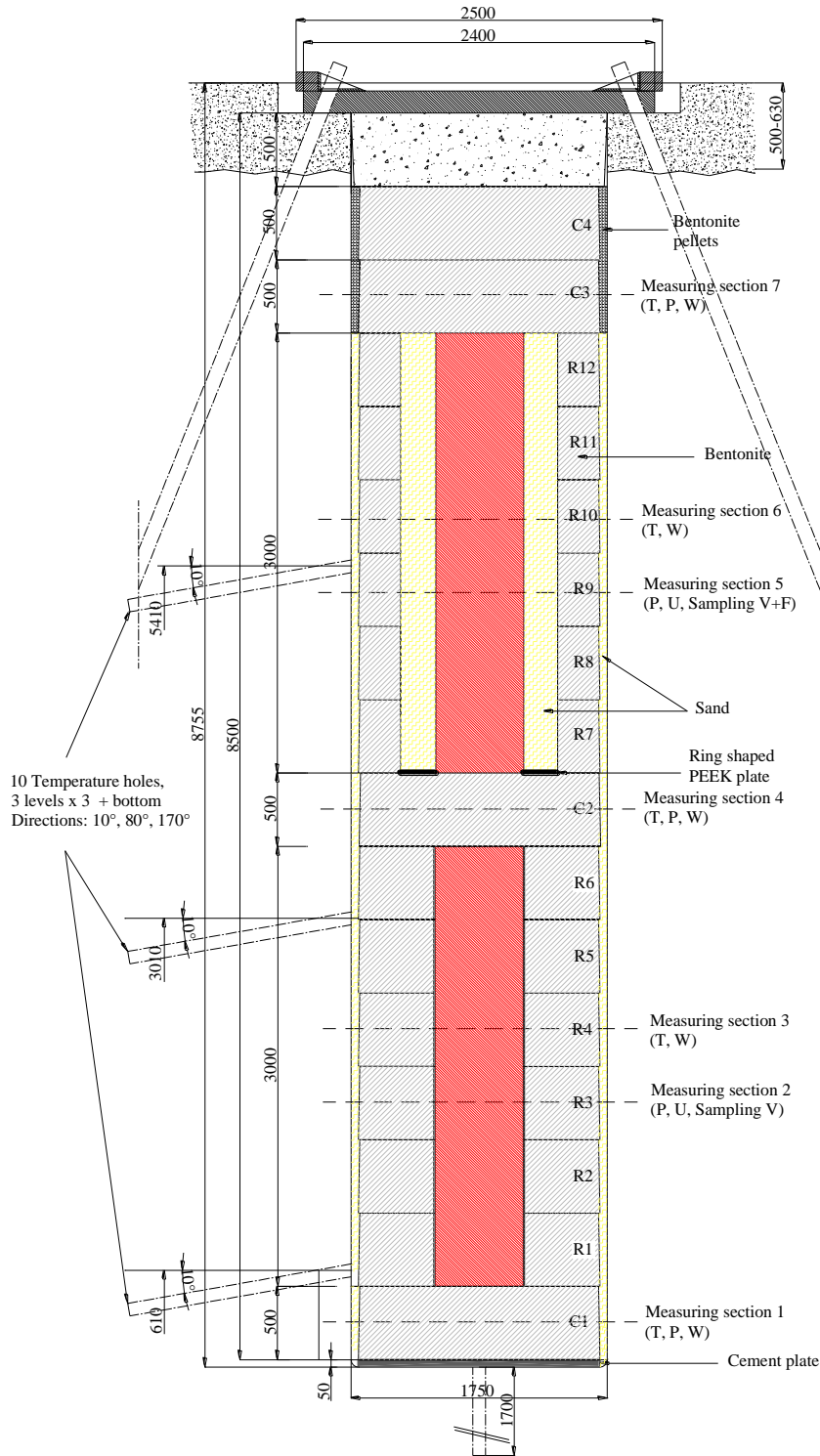


Figure 4-7 TBT geometry.

## 4.2 Summary from installation report

The Canister Retrieval Test was started to demonstrate the capability to retrieve deposited nuclear waste if a better disposal solution is found. The overall objective of the Canister Retrieval Test was to



demonstrate to specialists and to the public that retrieval of canisters is technically feasible at any stage of the operating phase.

The CRT experiment has also been used to carefully record the THM processes in the Swedish KBS-3V deposit technique besides proving the possibility for retrieval of the canisters. This makes it very suitable for modelers to investigate theories, used in their simulations, since the calculated results can be checked against experimental data.

The test was installed in autumn 2000. This report describes the test layout and the installation procedure. The deposition tunnel for the experiment is located on the 420-metre level and is excavated by conventional drill and blast. The centre-to-centre distance between the two deposition holes is 6 metres, which is the spacing being considered for the deep repository, but only one of the holes has been used for this test. A maximum temperature of 100°C on the surface of the canister is aimed at for the Canister Retrieval Test.

The bentonite buffer was installed in form of blocks and rings of bentonite. The blocks have a diameter of 1.65 m and a height of 0.5 m. When the stack of blocks was 6 m high, the canister, equipped with electrical heaters, was lowered down in the centre of the hole and the cables to the heaters and instruments were connected. Additional blocks were emplaced until the hole was filled to a distance of one metre from the tunnel floor. The top of the hole was sealed with a retaining plug made of concrete and a steel plate. The plug was secured against heave caused by the swelling clay with nine cables anchored in the rock. Water was supplied artificially for saturation around the bentonite blocks.

Saturation is predicted to take two-three years in the buffer alongside the canister and 5-10 years in the buffer below and above the canister. The decision on when to start retrieval is dependent on the degree of saturation.

A pilot test, Test of Deposition Process, was performed as a preparatory exercise prior to the Canister Retrieval Test and the Prototype Repository Test. The purpose of the test was to try out and practice with equipment, technique and methods developed for the installation of buffer and canisters.

The deposition hole for the Canister Retrieval Test was bored with a full-face tunnel boring machine modified for boring vertical holes. The deposition hole is 8.55 metres deep and has a diameter of 1.76 metres. The surrounding rock at the upper part of the hole consists mainly of greenstone and the lower part of Äspö diorite.

A 0.15 metre high concrete foundation was built to prevent water leaking from the rock from reaching the bentonite blocks and to reduce the risk of tilting the stack of bentonite rings.

Slots were cut in the rock wall for cables to prevent them from being damaged.

A canister obtained from SKB's Encapsulation Project was used for the Canister Retrieval Test. The outside diameter of the canister is 1,050 mm. The height of the canister is 4.83 m and the weight 21.4 tonnes.

The bentonite used as buffer material is SKB's reference material, named MX-80. The buffer consists of highly compacted bentonite blocks and rings with an initial density of 1,710 and 1,790 kg/m<sup>3</sup>, respectively. The initial water content of the bentonite was 17%.

An artificial pressurised saturation system was built because the supply of water from the rock was judged to be insufficient for saturating the buffer. At the end of the test period, a high water pressure will speed up the saturation process. It will also provide a defined hydraulic boundary. The water is evenly distributed through a number of filter mats attached to the wall of the deposition hole.

A climate control system was used during installation to prevent the bentonite from being damaged by excessively high or low relative humidity.

A retaining structure is used to simulate a real storage situation. The aim of the structure is to prevent the blocks of bentonite from swelling uncontrollably. It consists of a concrete cone plug placed on top of the buffer and a steel lid which is pre-stressed by rock ties.

A large number of instruments are installed to monitor the test as follows:

- Canister – temperature and strain
- Rock mass – temperature and stress



- Retaining system – force and displacement
- Buffer – temperature, relative humidity, pore pressure and total pressure

The data acquisition system consists of a measurement computer and dataloggers. The monitored values are transferred via a serial link from the dataloggers to the measurement computer. The computer is connected to Åspö data network.

Test installation was carried out in the following sequence:

1. Preparations on site – concrete foundation, cutting of slots in the rock wall, drilling for rock anchors and instruments, installation of rock anchors, filter mats for saturation, installation of formwork for plug
2. Emplacement of bentonite blocks and rings including installation of instruments
3. Deposition of canister
4. Continuation of 2.
5. Filling of void between rock and bentonite rings with bentonite pellets and water
6. Casting of concrete plug and placement of steel lid
7. Pre-stressing of retaining system

Heating was started with an initially applied constant power of 700 W on October 27, 2000, one day after casting the plug. The displacements and forces on the plug were carefully checked and followed during the initial phase when the plug was only fixed by three anchors. When the total force exceeded 1500 kN, the remaining anchors were fixed in the prescribed manner. This took place 12-14 December, that is 46-48 days after test start.

### 4.3 Test schedule

The text in **Test start** and **End of the experiment** is copied directly from the installation report and the dismantling report respectively. Information added to the original text is given in italics.

The following sections: **Heater power and filter pressure** and **Rock anchors and heave of the lid**, are compilations of information found in reports concerning the CRT experiment.

#### 4.3.1 Test start

Since pellet filling marks the start of the test, the best description of the launching of the test is a step-by-step description of the procedures from that point in time.

1. Before the pellets were blown into the gap, all preparations described in Chapter 5 (instruments, heaters and wetting system installed) were finished and the tubes for the drainage (pumping) system were removed along with the tubes and transducers for the ventilation system
2. Data collection was started immediately before pellet filling
3. The gap was filled with pellets on **October 26 (2000)**, which thus can be considered the starting date
4. Water was pumped into the gap and the filter mats, and the *(four)* water supply tubes were withdrawn immediately after *(during the)* pellet filling.
5. Measurement of water inflow into the filters started immediately after water filling
6. The rubber mat was placed on top of the upper block



7. The cable slots behind the conical ring were sealed with cement
8. The plug was cast when all preparations had been finished. Not more than 12 hours were allowed to pass between water filling and casting
9. Heating was started with an initially applied constant power of 700 W on October 27, i.e. one day after test start
10. Three prescribed rods were locked on October 31 and the force and displacement transducers installed. *(At the installation the force in the anchors were prescribed to 20 kN /anchor.)*
11. Between test start and locking of the rods (5 days) the plug rose 13 mm due to swelling of the bentonite.
12. The displacements and forces on the plug were carefully monitored
13. When the total force exceeded 1500 kN, the remaining rods were fixed in a prescribed manner. This procedure took place 12-14 December, i.e. 46-48 days after test start. *(When the average force in the three anchors exceeded 500 kN, the six remaining anchors were attached to the lid. The total force where distributed equally between all anchors, i.e. the force was  $\approx 170$  kN/anchor when all nine anchors were installed.)*
14. The canister heating power was raised twice: to 1700 W on November 13 and to 2600 W on February 13.

#### 4.3.2 End of the experiment

*Table 4-1 Events during dismantling of the upper part of the buffer in the Canister Retrieval Test*

Activity	Date	Day	Comments
The power to the canister was switched of.	2005-10-11	1811	The power was switched of about 3 month before the first samples of the buffer were taken
The plug was removed	2006-01-16— 01-18	1908-1910	The rock anchors were removed and the steel lid and concrete plug was lifted up from the deposition hole
Samples were taken from block C4	2006-01-18— 01-23	1910-1915	
Samples were taken from block C3	2006-01-24— 01-30	1916-1922	
Samples were taken from block C2	2006-01-30— 02-02	1922-1925	
Samples were taken from block R10	2006-02-06— 02-10	1929-1933	Samples were taken on both the ring shaped block and the bricks placed on top of the canister lid. The thickness of the filling of bricks was about 220 mm.
Removal of the upper lid of the canister	2006-02-13— 02-14	1936-1937	The upper lid of the canister was removed. Samples were taken on the



filling between the lids of the canister. The power cables were removed from the deposition hole

Samples were taken from block R9	2006-02-14— 02-20	1937-1943
Samples were taken from block R8	2006-02-22— 03-01	1945-1952
Samples were taken from block R7	2006-03-02— 03-09	1953-1960
Samples were taken from block R6	2006-03-13— 03-21	1964-1972

### 4.3.3 Heater power and filter pressure protocols

*Table 4-2 CRT heater power protocol*

Date	Day	Heater power [kW]	Comment
00-10-26	0	0	
00-10-27	1	0.7	
00-11-13	18	1.7	
01-02-13	110	2.6	
01-11-05	375	0	
01-11-06	376	2.6	
02-03-04	494	0	
02-03-11	501	2.6	
02-09-10	684	2.1	
03-12-04	1134	1.6	
05-03-10	1596	1.15	
05-10-11	1811	0	
06-03-28	1979	2	Testing the heaters
06-04-20	2002	0	

*Table 4-3 TBT heater power protocol*

Date	Day	Heater power [kW]
00-10-26	0	0
03-03-26	881	0.9
03-04-03	889	1.2
03-04-10	896	1.5
06-06-09	2052	1.6

**Table 4-4** CRT filter water pressure protocol.

Date	Day	Water pressure [MPa]	Comment
00-10-26	0	0	Started to increase the water pressure gradually.
02-09-05	679	0	
02-10-10	714	0.8	
02-12-05	770	0.1	
03-01-09	805	0.4	
03-01-23	819	0.8	
05-03-12	1598	0	
05-12-16	1877	0	Air flushed

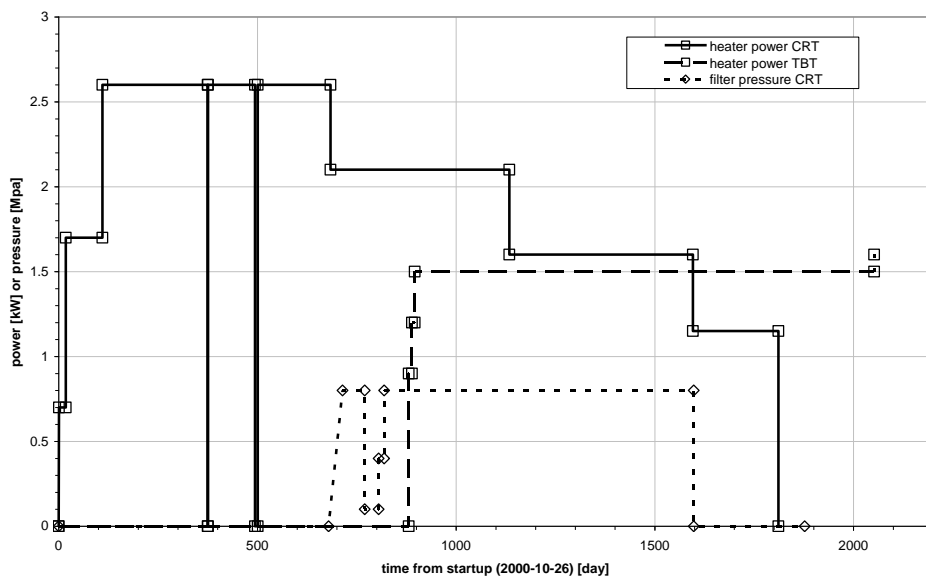


**Figure 4-8** Graph of the power protocols of CRT and TBT and the filter pressure of CRT .

**4.3.4 Rock anchors and heave of the lid**

**Table 4-5** Overview of rock anchor history.

Date	Day	Comment
2000-10-31	5	Three pre-stressed anchors were attached to the lid. The initial force in each anchor was 20 kN.
2002-12-12— 2002-12-14	46 - 48	The remaining six anchors were attached to the lid when the total force exceeded 1.5 MN. The total force was distributed evenly between the anchors, which gives ≈ 170 kN/anchor. The force in three of the anchors has been measured.
2006-01-16— 2006-01-18	1908 - 1910	The rock anchors were removed and the steel lid and concrete plug was lifted up from the deposition hole

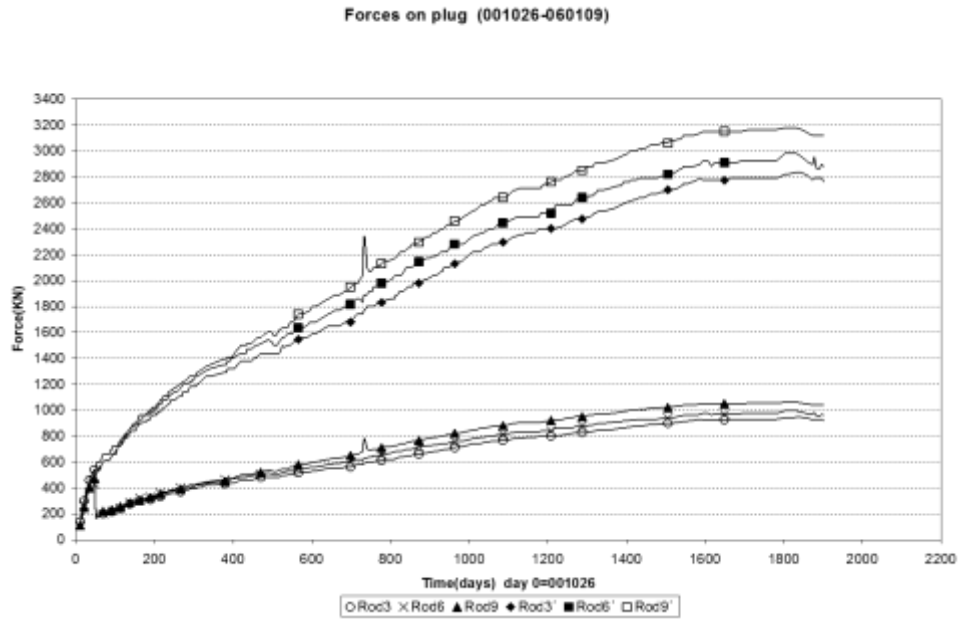


Figure 4-9 Force in rock anchors 3, 6 and 9 (lower three curves).

Table 4-6 Overview of plug displacement.

Date	Day	Comment
00-10-31	5	13 mm heave before attaching the three rock anchors according to late estimate
00-10-31 -	5 -	See measurement called "displacement2". 20.5 mm at the final reading (2006-01-03). Note that 13 mm should be added to "displacement2" in order to obtain the total heave.

Displacement of plug (001026-060501)

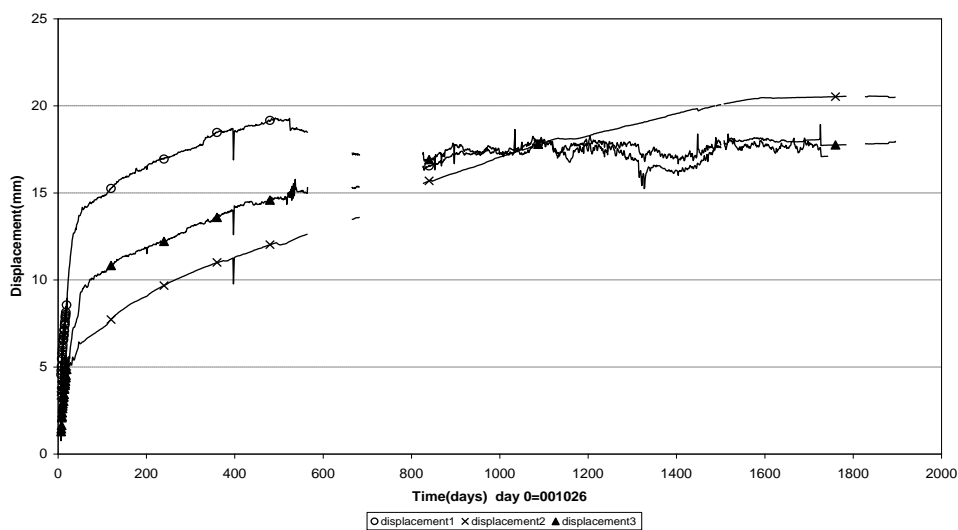


Figure 4-10 Vertical displacement of the plug.



Back calculations of the displacement using the average dry density in each block gives that the total vertical displacement should be  $\approx 40$  mm.

#### 4.3.5 Comments about the installation and operating phase

When water filling the pellet-filled outer slot, the estimated amount of water to fill up the voids between the pellets, 800 l, was exceeded by approximately 150 l. The water is thought to have penetrated through at the interfaces between the bentonite blocks into the inner gap and thereby got access to an additional volume to fill. A calculation of the available volume between the canister and bentonite rings gives 160 l which strengthens the assumption that the inner slot had been water filled.

*The analysis above is quite uncertain.* Both the estimation of the added water volume and the available slot volume are uncertain. Sensor data is however also indicating that the inner slot was filled. The total pressure at the inner surface of R5 shows a peak at the start of the experiment. Both Vaisala sensors (RH) and Wescor sensors (suction) also indicate that there is something happening in the section close to the canister.

The initial conditions of the different sections of the CRT experiment are shown in Table 4-7, where a bentonite compact density of  $2780 \text{ kg/m}^3$  was used when the conditions were calculated.

*Table 4-7 Initial conditions of the CRT experiment.*

Section	Density ( $\text{kg/m}^3$ )	Water ratio	Dry density ( $\text{kg/m}^3$ )	Void ratio	Degr. of saturation
Solid block	1991	0,172	1699	0,636	0,751
Ring shaped block	2087	0,171	1782	0,560	0,849
Bricks	1883	0,165	1616	0,720	0,637
Pellets I	1101	0,100	1001	1,778	0,156
Pellets II	1574	0,572	1001	1,778	0,895

The start date of the experiment (taken as the date when the outer gap was filled with pellets) was 2000-10-26. Schematic protocols of the heater power of CRT and the heater power of TBT is given in Table 4-2 and Table 4-3. The TBT has two heaters with the power-history indicated in Table 4-3.

The TBT experiment has considerable thermal effect upon the CRT experiment since the hole-centers are located with 6 m between them. The thermal effect from the TBT experiment on CRT can clearly be seen in Figure 4-11 where rock temperatures at canister mid-height are shown. At approximately 900 days after the startup of CRT the rock temperatures increase suddenly due to the start of the TBT experiment.

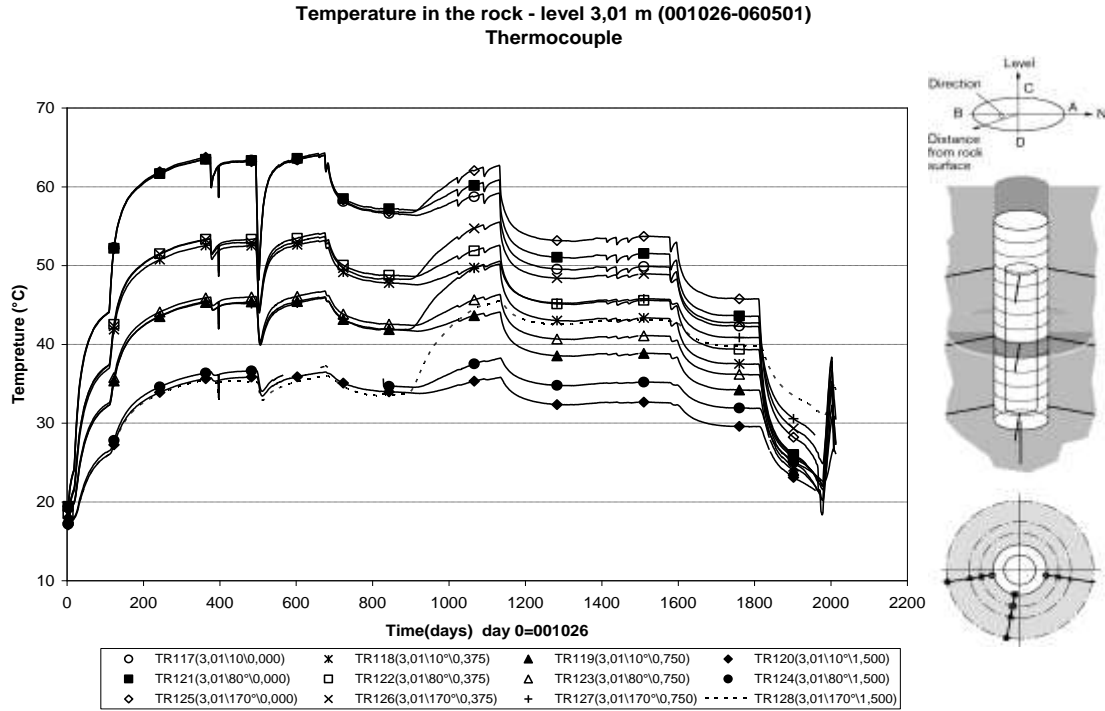


**Figure 4-11** Rock temperatures in the CRT experiment.

The protocol of the water pressure in the filter is given in

Table 4-4 below. Note that the pressure additional to the atmosphere pressure is shown. The measured inflow of water into the filter is given in Figure 4-12 below. In Figure 4-8 a graphical overview of the heater power and filter pressure protocols is given.

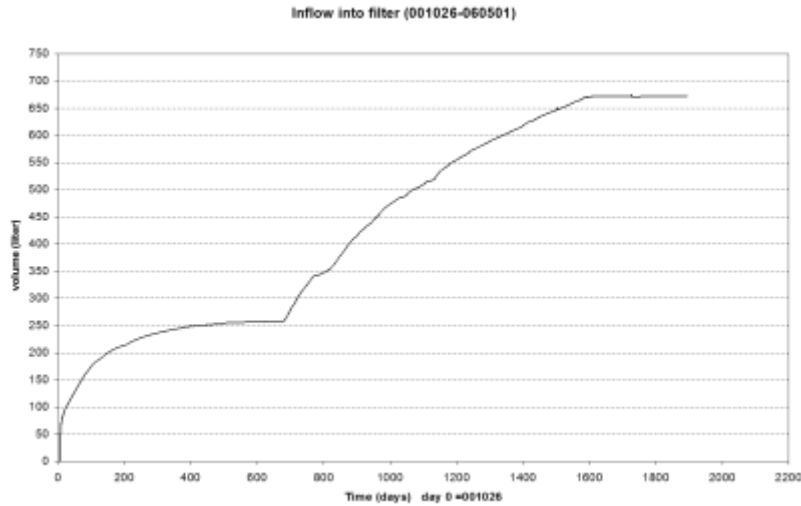


**Figure 4-12** Measured water inflow.

2000-10-31, five days after the test start, three pre-stressed rock anchors were attached to the lid. At this time the heave of the plug was 13 mm due to swelling of the bentonite, according to late estimates which are somewhat uncertain. Day 46-48 the remaining six, also pre-stressed, rock anchors were fixed since the total force had exceeded 1.5 MN. The forces in the rock anchors can be seen in Figure 4-9 and the displacement of the plug is shown in Figure 4-10.



In Figure 4-9 both the actual measurement and this multiplied with three are shown for anchor 3,6 and 9 since only these three of the anchors were instrumented. An estimate of the total force in all the anchors can thus be obtained by adding the  $\times 3$  values.

The measured vertical displacement of the plug is not entirely reliable. The curve called “displacement2” in Figure 4-10 is considered to be the most accurate. Back calculations of the displacement using the average dry density in each block gives that the total vertical displacement should be  $\approx 40$  mm instead of  $\approx 20$  mm, as the measurements show. In Figure 4-13 the calculated accumulated swelling is shown at different height from the hole bottom and in

**Table 4-8** the average dry density at installation and dismantling, the calculated vertical swelling and the absorbed water are shown for each bentonite block section.

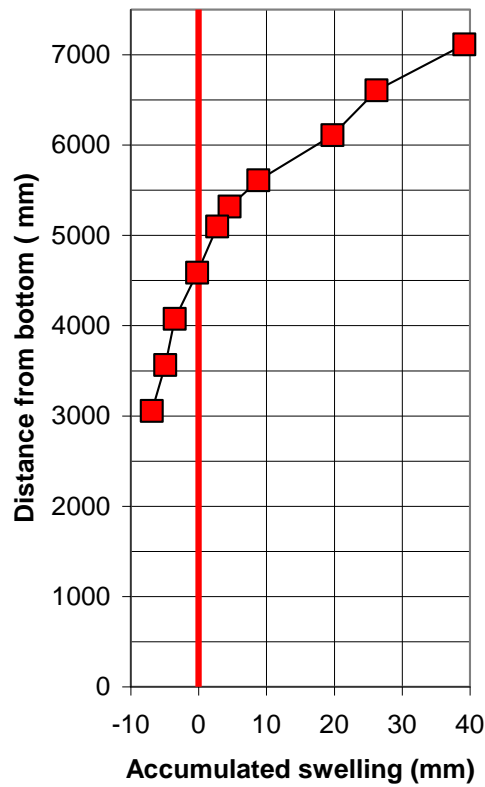


*Figure 4-13* Calculated accumulated swelling at different height from the hole bottom.



**Table 4-8** *The average dry density at installation and at dismantling at different sections of the buffer together with the calculated vertical displacement and absorbed amount of water. The absorbed water for rings R5-R1 are assumed to be the average absorbed water of rings R6-R9, block C1 is assumed to be the same as block C2.*

Block No	Average dry density at installation. (kg/m <sup>3</sup> )	Average dry density at dismantling (kg/m <sup>3</sup> )	Calculated vertical swelling (mm)	Absorbed water (kg)
C4	1598	1558	12.9	79.7
C3	1598	1578	6.5	89.6
C2	1598	1563	10.9	83.6
R10 <sup>*)</sup>	1608	1578	4.2	47.7
R10 <sup>**)</sup>	1569	1559	1.8	35.7
R9	1569	1560	2.9	61.0
R8	1569	1580	-3.3	53.7
R7	1569	1574	-1.4	50.4
R6	1569	1575	-2.0	56.6
R5 <sup>***)</sup>	1569		0	55.4
R4 <sup>***)</sup>	1569		0	55.4
R3 <sup>***)</sup>	1569		0	55.4
R2 <sup>***)</sup>	1569		0	55.4
R1 <sup>***)</sup>	1569		0	55.4
C1 <sup>***)</sup>	1598		0	83.6
$\Sigma$			39.1	918.2

<sup>\*)</sup> Above the canister top    <sup>\*\*) Underneath the canister top    <sup>\*\*\*)</sup> Estimated</sup>

If the displacement of 13 mm, reported during the first five days, is added to the measured displacements a total of 33 mm is obtained. The remaining displacement up to the back calculated estimate 40 mm could origin from elastic deformations in the buffer occurring after unloading when the experiment was dismantled. Note also that the 13 mm of vertical swelling at day 5 is only a late estimate.

## 4.4 Sensor position

The simulated processes should be compared with the specified sensor data in the notes. Below the exact position of the sensors is described.

### 4.4.1 Strategy for describing the position of each device

Every instrument is named with a short unique name consisting of 1-2 letters describing the type of measurement and 3 figures numbering the device. Every instrument position in the buffer and rock is described with three coordinates according to Figure 4-14.

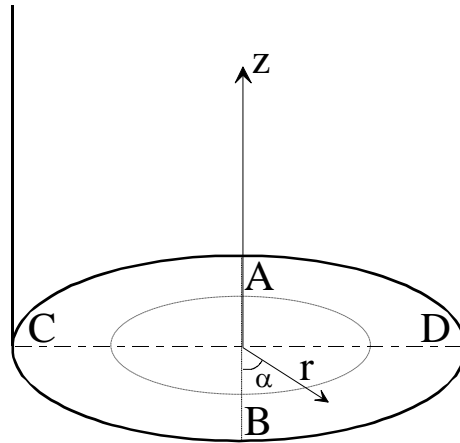


**Figure 4-14** The instrument planes (A-D) and the coordinate system used when describing the instrument positions.

The r-coordinate is the horizontal distance from the center of the hole and the z-coordinate is the height from the bottom of the hole (the block height is set to 500 mm). The  $\alpha$ -coordinate is the angle from the vertical direction B (almost south).

The short description of the positions in the diagrams differs between the buffer and the rock.

**Buffer:** Three positions with the following meaning: (bentonite block or cylinder number counted from the bottom \ direction A, B, C, or D \ radius in mm from center line)

**Rock:** Three positions with the following meaning: (distance in meters from the bottom \  $\alpha$  according to Fig 3-1 \ distance in meters from the hole surface)

The bentonite blocks are called cylinders and rings. The cylinders are numbered C1-C4 and the rings R1-R10 respectively (Figure 4-15).

#### 4.4.2 Position of each instrument in the bentonite

Measurements are done in four vertical sections A, B, C and D according to Figure 4-14. Direction A and B are placed in the tunnels axial direction.

An overview of the positions of the instruments is shown in Figure 4-15. Exact positions are described in Table 4-9, Table 4-12

The instruments are located in two main levels in the blocks, 50 mm and 160 mm, from the upper surface. The thermocouples have mostly placed in the 50mm level and the other gauges in the 160 mm level.

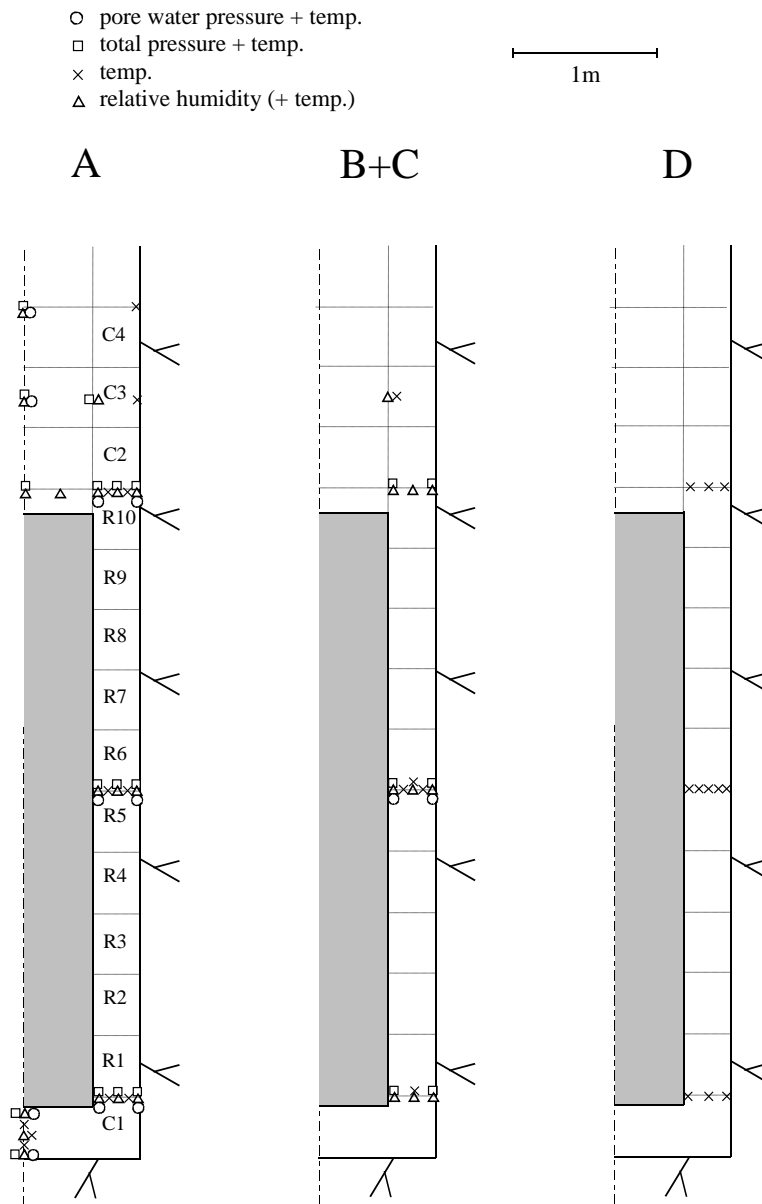


*Figure 4-15 Schematic view over the instruments in four vertical sections and the block designation.*



**Table 4-9** *Numbering and position of instruments for measuring temperature (T)*

Type and number	Block	Instrument position in block				Cable pos.		Fabricate	Remark
		Direction	$\alpha$	r	Z	$\alpha$			
T101	Cyl. 1	Center	90	50	50	242	BICC		
T102	Cyl. 1	Center	90	50	250	238	BICC		
T103	Cyl. 1	Center	90	50	450	230	BICC		
T104	Cyl. 1	A	180	635	450	206	BICC		
T105	Cyl. 1	A	180	735	450	202	BICC		
T106	Cyl. 1	B	365	685	450	38	BICC		
T107	Cyl. 1	C	275	685	450	274	BICC		
T108	Cyl. 1	D	90	585	450	96	BICC		
T109	Cyl. 1	D	90	685	450	94	BICC		
T110	Cyl. 1	D	90	785	450	92	BICC		
T111	Ring 5	A	180	635	2950	224	BICC		
T112	Ring 5	A	180	735	2950	218	BICC		
T113	Ring 5	B	360	610	2950	318	BICC		
T114	Ring 5	B	360	685	2950	322	BICC		
T115	Ring 5	B	360	735	2950	324	BICC		
T116	Ring 5	C	270	610	2950	258	BICC		
T117	Ring 5	C	270	685	2950	260	BICC		
T118	Ring 5	C	270	735	2950	262	BICC		
T119	Ring 5	D	90	585	2950	44	BICC		
T120	Ring 5	D	90	635	2950	46	BICC		
T121	Ring 5	D	90	685	2950	48	BICC		
T122	Ring 5	D	90	735	2950	50	BICC		
T123	Ring 5	D	90	785	2950	52	BICC		
T124	Ring 10	A	180	635	5450	200	BICC		
T125	Ring 10	A	180	735	5450	194	BICC		
T126	Ring 10	D	90	585	5450	54	BICC		
T127	Ring 10	D	90	685	5450	56	BICC		
T128	Ring 10	D	90	785	5450	58	BICC		
T129	Cyl. 3	A	180	785	6250	166	BICC		
T130	Cyl. 3	B	365	585	6250	358	BICC		
T131	Cyl. 3	C	275	585	6250	280	BICC		
T132	Cyl. 4	A	180	785	6950	66	BICC		



**Table 4-10** *Numbering and position of instruments for measuring total pressure (P)*

Type and number	Block	Instrument position in block			Z(mm)	Cable pos.		Remark
		Direction	$\alpha$	r(mm)		$\alpha$	Fabricate	
P101	Cyl. 1	Center	180	50	0	244	Kulite	
P102	Cyl. 1	Center	180	50	450	232	Kulite	
P103	Cyl. 1	A	185	585	340	208	Geokon	
P104	Cyl. 1	A	185	685	340	204	Geokon	
P105	Cyl. 1	A	185	785	340	186	Geokon	
P106	Cyl. 1	B	365	585	340	40	Geokon	
P107	Cyl. 1	B	365	785	340	2	Geokon	
P108	Cyl. 1	C	275	585	340	278	Geokon	
P109	Cyl. 1	C	275	785	340	270	Geokon	
P110	Ring 5	A	185	585	2840	228	Geokon	
P111	Ring 5	A	185	685	2840	222	Geokon	
P112	Ring 5	A	185	785	2840	188	Geokon	
P113	Ring 5	B	365	535	2840	36	Geokon	
P114	Ring 5	B	365	825	2840	16	Geokon	
P115	Ring 5	C	275	585	2840	296	Geokon	
P116	Ring 5	C	275	785	2840	290	Geokon	
P117	Ring 10	Center	180	50	5340	24	Kulite	
P118	Ring 10	A	180	585	5340	216	Geokon	
P119	Ring 10	A	180	685	5340	198	Geokon	
P120	Ring 10	A	180	785	5340	192	Geokon	
P121	Ring 10	B	365	585	5340	20	Kulite	
P122	Ring 10	B	365	785	5340	18	Kulite	
P123	Ring 10	C	275	585	5340	286	Kulite	
P124	Ring 10	C	275	785	5340	284	Kulite	
P125	Cyl. 3	Center	180	50	6250	158	Geokon	
P126	Cyl. 3	A	180	585	6250	162	Geokon	
P127	Cyl. 4	Center	180	50	6840	64	Kulite	

**Table 4-11** *Numbering and position of instruments for measuring pore water pressure (U)*

Type and number	Block	Instrument position in block			Z(mm)	Cable pos.		Remark
		Direction	$\alpha$	r(mm)		$\alpha$	Fabricate	
U101	Cyl. 1	Center	270	50	50	246	Geokon	
U102	Cyl. 1	Center	270	50	450	236	Geokon	Horizontal
U103	Cyl. 1	A	175	585	340	126	Geokon	
U104	Cyl. 1	A	175	785	340	178	Geokon	
U105	Ring 5	A	175	585	2840	138	Geokon	
U106	Ring 5	A	175	785	2840	180	Geokon	
U107	Ring 5	B	355	535	2840	314	Geokon	In the slot
U108	Ring 5	B	355	825	2840	348	Geokon	In the slot
U109	Ring 5	C	265	585	2840	256	Geokon	
U110	Ring 5	C	265	825	2840	264	Geokon	In the slot
U111	Ring 10	A	175	585	5340	146	Geokon	
U112	Ring 10	A	175	785	5340	152	Geokon	
U113	Cyl. 3	Center	270	50	6250	156	Geokon	
U114	Cyl. 4	Center	270	50	6950	62	Kulite	



**Table 4-12**      *Numbering and position of instruments for measuring water content (W)*

Type and number	Block	Instrument position in block				Cable pos.		Fabricate	Remark
		Direction	$\alpha$	r	Z	$\alpha$			
W101	Cyl. 1	Center	360	50	50	248	Vaisala		
W102	Cyl. 1	Center	360	400	160	240	Vaisala		
W103	Cyl. 1	Center	360	50	450	234	Vaisala	Horizontal	
W104	Cyl. 1	A	180	585	340	128	Vaisala		
W105	Cyl. 1	A	180	685	340	132	Vaisala		
W106	Cyl. 1	A	180	785	340	184	Vaisala		
W107	Cyl. 1	A	170	585	340	124	Wescor		
W108	Cyl. 1	A	170	685	340	130	Wescor		
W109	Cyl. 1	A	170	785	340	134	Wescor		
W110	Cyl. 1	B	360	585	340	304	Vaisala		
W111	Cyl. 1	B	360	785	340	360	Vaisala		
W112	Cyl. 1	B	360	685	340	308	Vaisala		
W113	Cyl. 1	B	355	585	340	302	Wescor		
W114	Cyl. 1	B	355	685	340	306	Wescor		
W115	Cyl. 1	B	355	785	340	310	Wescor		
W116	Cyl. 1	C	270	585	340	250	Wescor		
W117	Cyl. 1	C	270	685	340	252	Wescor		
W118	Cyl. 1	C	270	785	340	254	Vaisala		
W119	Ring 5	A	180	585	2840	226	Vaisala		
W120	Ring 5	A	180	685	2840	220	Vaisala		
W121	Ring 5	A	180	785	2840	182	Vaisala		
W122	Ring 5	A	170	585	2840	136	Wescor		
W123	Ring 5	A	170	685	2840	140	Wescor		
W124	Ring 5	A	170	785	2840	142	Wescor		
W125	Ring 5	B	360	535	2840	316	Vaisala	In the slot	
W126	Ring 5	B	360	685	2840	34	Vaisala		
W127	Ring 5	B	360	785	2840	350	Vaisala		
W128	Ring 5	B	350	535	2840	312	Wescor	In the slot	
W129	Ring 5	B	350	685	2840	320	Wescor		
W130	Ring 5	B	350	785	2840	346	Wescor		
W131	Ring 5	C	270	585	2840	294	Wescor	In the slot	
W132	Ring 5	C	275	685	2840	292	Wescor		
W133	Ring 5	C	270	785	2840	288	Wescor		
W134	Ring 10	Center	360	50	5340	22	Vaisala		
W135	Ring 10	A	180	262	5340	26	Vaisala		
W136	Ring 10	A	180	585	5340	214	Vaisala		
W137	Ring 10	A	180	685	5340	196	Vaisala		
W138	Ring 10	A	180	785	5340	190	Vaisala		
W139	Ring 10	A	170	585	5340	144	Wescor		
W140	Ring 10	A	170	685	5340	148	Wescor		
W141	Ring 10	A	170	785	5340	150	Wescor		
W142	Ring 10	B	360	585	5340	328	Vaisala		
W143	Ring 10	B	360	685	5340	332	Vaisala		
W144	Ring 10	B	360	785	5340	336	Vaisala		
W145	Ring 10	B	355	585	5340	326	Wescor		
W146	Ring 10	B	355	685	5340	330	Wescor		
W147	Ring 10	B	355	785	5340	334	Wescor		
W148	Ring 10	C	270	585	5340	266	Wescor		
W149	Ring 10	C	270	685	5340	268	Wescor		
W150	Ring 10	C	270	785	5340	272	Vaisala		
W151	Cyl. 3	Center	360	50	6250	154	Vaisala		
W152	Cyl. 3	A	180	585	6250	160	Vaisala		
W153	Cyl. 3	B	360	585	6250	356	Vaisala		
W154	Cyl. 3	C	270	585	6250	276	Wescor		
W155	Cyl. 4	Center	360	50	6840	60	Vaisala		



### 4.4.3 Instruments in the rock

The position of the thermocouples in the rock is shown in Table 4-13.

*Table 4-13 Numbering and positions of thermocouples in the rock*

Type and number	Level	Direction	Distance from rock surface	Cable pos.		Remark
				$\alpha$	Fabricate	
TR101	0	Center	0.000	70°-90°	BICC	
TR102	0	Center	0.375	70°-90°	BICC	
TR103	0	Center	0.750	70°-90°	BICC	
TR104	0	Center	1.500	70°-90°	BICC	
TR105	0.61	10°	0.000	4°-14°	BICC	
TR106	0.61	10°	0.375	4°-14°	BICC	
TR107	0.61	10°	0.750	4°-14°	BICC	
TR108	0.61	10°	1.500	4°-14°	BICC	
TR109	0.61	80°	0.000	70°-90°	BICC	
TR110	0.61	80°	0.375	70°-90°	BICC	
TR111	0.61	80°	0.750	70°-90°	BICC	
TR112	0.61	80°	1.500	70°-90°	BICC	
TR113	0.61	170°	0.000	168°-176°	BICC	
TR114	0.61	170°	0.375	168°-176°	BICC	
TR115	0.61	170°	0.750	168°-176°	BICC	
TR116	0.61	170°	1.500	168°-176°	BICC	
TR117	3.01	10°	0.000	4°-14°	BICC	
TR118	3.01	10°	0.375	4°-14°	BICC	
TR119	3.01	10°	0.750	4°-14°	BICC	
TR120	3.01	10°	1.500	4°-14°	BICC	
TR121	3.01	80°	0.000	70°-90°	BICC	
TR122	3.01	80°	0.375	70°-90°	BICC	
TR123	3.01	80°	0.750	70°-90°	BICC	
TR124	3.01	80°	1.500	70°-90°	BICC	
TR125	3.01	170°	0.000	168°-176°	BICC	
TR126	3.01	170°	0.375	168°-176°	BICC	
TR127	3.01	170°	0.750	168°-176°	BICC	
TR128	3.01	170°	1.500	168°-176°	BICC	
TR129	5.41	10°	0.000	4°-14°	BICC	
TR130	5.41	10°	0.375	4°-14°	BICC	
TR131	5.41	10°	0.750	4°-14°	BICC	
TR132	5.41	10°	1.500	4°-14°	BICC	
TR133	5.41	80°	0.000	70°-90°	BICC	
TR134	5.41	80°	0.375	70°-90°	BICC	
TR135	5.41	80°	0.750	70°-90°	BICC	
TR136	5.41	80°	1.500	70°-90°	BICC	
TR137	5.41	170°	0.000	168°-176°	BICC	
TR138	5.41	170°	0.375	168°-176°	BICC	
TR139	5.41	170°	0.750	168°-176°	BICC	
TR140	5.41	170°	1.500	168°-176°	BICC	

## 4.5 Proposed cases for CRT

The cases proposed in this document have been developed under the EBS task force framework (Börgesson and al., 2017). Within the Beacon project, the objective is to show the capacity for the model to reproduce the observations and measurements but also to evaluate the role of heterogeneities in the observations. In particular, it will be interesting to have a focus on the zone where pellets are installed at the interface with blocks and the consequences on final properties of this zone after dismantling. An interesting point is that in CRT can be found the application at large scale of situation explored during the first task of Beacon WP5.1 (verification test cases). This means hydration of blocks, pellets and mixt situation pellets+blocks.



As a reference case, it is proposed to model the entire engineered buffer with most of its complexity. This means a 3D representation of the experiment with a coupling between thermal, hydraulic and mechanical processes. Due to limitation of some tools or models used by the partners, a second case is proposed as an alternative case. The 2D geometry make it able to model by most of the partners involved in Beacon.

## 4.6 Reference case: Thermo-hydro-mechanical simulation of the entire engineered buffer in CRT

### 4.6.1 Loads, boundary conditions and initial conditions

#### Load

The thermal load (canister power) can be obtained from the protocol given in Table 4-2 or the experimentally measurement given in Goudarzi et al., 2006.

#### Boundary conditions

Table 4-14 is an attempt to structure the conditions that should be considered in the same manner as is done in the former task. The conditions are, however, defined in a more “fuzzy” fashion. The modellers are in this way given more freedom when it comes to designing the models in this task.

Table 4-14 Suggested conditions

Type of process		
Thermal	Hydraulic	Mechanical
Tunnel air temperature. $T = 15\text{ °C}$ .	Water pressure from filter protocol.	The effect from the rock anchors should be modeled.  The steel lid and concrete plug are allowed to move in the vertical direction.

To facilitate the control of the simulated thermal process the measured rock temperatures are shown in Goudarzi et al., 2006.

#### Initial conditions

Also here the initial conditions, shown in Table 4-15, have been obtained from Johannesson, 2007

Table 4-15 Initial conditions

Constituent	Type of process		
	Thermal	Hydraulic	Mechanical
Bentonite blocks			
- Cylinder-shaped	$T = 20\text{ °C}$	$S_r = 0.751$	$\sigma = 0\text{ MPa}, n = 0.39$
- Ring-shaped	$T = 20\text{ °C}$	$S_r = 0.859$	$\sigma = 0\text{ MPa}, n = 0.36$
Pellet-filled gap	$T = 20\text{ °C}$	$S_r = 0.895$	$\sigma = 0\text{ MPa}, n = 0.64$
Bentonite bricks	$T = 20\text{ °C}$	$S_r = 0.637$	$\sigma = 0\text{ MPa}, n = 0.42$

### 4.6.2 Material properties

The properties of the materials are given in the appendix.



### 4.6.3 Results to present

The results that the teams should present are 1) variable histories at specified points and 2) variable profiles at specified times. Some of the selected results can be compared with experimental measurements. The experimental data to compare with, provided in the form of excel-files, are listed in the next chapter "Sensor data to compare with". The sensor names, positions and issues of the sensors can also be found in the next section.

For Ring 5 (at canister mid-height, 2.84 m from the hole bottom) all the results specified for the previous task should also be presented for this task, where the entire buffer is considered. In addition to this the history of variables belonging to points in Ring 10 (at the top of the canister, 5.34 m from the hole bottom) and Cylinder 3 (the second ring from the top, 6.25 m from the hole bottom) should be shown. Also profiles of variables at R10 and C3 should be presented at the specified times. Also iso-maps of variables at the given times should be shown. Finally the heave of the lid and the force on the plug also should be presented.

Below follows a list of the results that should be presented. As before the point position will change according to the deformation of the material, the definition is given in the undeformed configuration. In the list the points (radial position) where sensor data is available are indicated using a bold font.

C5: see the previous task.

Temperature histories at the radial distances [mm] (in the initial configuration):

- R10: 50, 585, **685**, 785, 847.5
- C3: 50, 585, 685, **785**, 847.5

Water saturation histories at the radial distances [mm]:

- R10: **50**, 585, **685**, 785, 847.5
- C3: **50**, 585, **685**, 785, 847.5

Total vertical (axial) stress histories at the radial distances [mm]:

- R10: 50, 585, **685**, 785, 875
- C3: **50**, 585, 685, 785, 875

Total horizontal (radial) stress histories at the radial distances [mm]:

- R10: 50, 585, 685, 785, 875
- C3: 50, 585, 685, 785, 875

Dry density histories at the radial distances [mm]:

- R10: 50, 585, 685, 785, 847.5
- C3: 50, 585, 685, 785, 847.5

Profiles of Temperature, Water saturation and Dry density in the buffer at day:

- R10: 670, 1400, 1800, 1910
- C3: 670, 1400, 1800, 1910

Iso-maps (contour plots) of Temperature, Water saturation and Dry density in the buffer at day: 670, 1400, 1800, 1910

The history of the plug displacement

The history of the force acting on the plug

#### 4.6.4 Sensor data to compare with

For R5 the sensors defined for the previous task should be used. Below the sensors that should be used for R10 and C3 are given.

The sensors have been selected as consequent as possible with respect to position. The positions are given according to the definitions in Figure 4-16 where the direction A ( $\alpha = 180^\circ$ ) is closest to the north (located at  $\alpha \approx 170^\circ$ ).

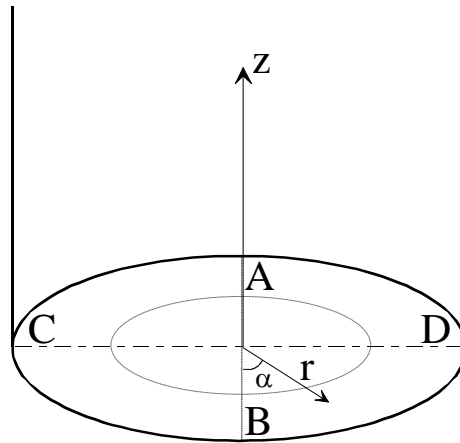


*Figure 4-16 The instrument planes (A-D) and the coordinate system used when describing the instrument positions.*

For the indicated block (R10 or C3) the sensor names are followed by the radial position in mm and the direction name (A, B, C and D). The type (Wescor or Vaisala) of the “hydraulic” sensors is also indicated. The profile data is also indicated where available. The data are also shown in the appendix.

#### **Thermal**

R10: T127(685) D

C3: T129(785) A

Hydraulic

R10:

- Vaisala: W134(50) center, W142(585) B, W137(685) A
- Wescor: W140(685) A
- $S_r$  profile for R10

C3:

- Vaisala: W153(685) C, W151(50) center
- Wescor: W154(685) C
- $S_r$  profile for C3

Contour plot of the water saturation obtained after dismantling the test is available for the upper part (from C4 to R6) of the buffer.

#### **Mechanical**

R10:

- P119(685) A
- Dry density profile for R10

C3:

- P125(50) center,
- Dry density profile for C3

Contour plot of the dry density obtained after dismantling the test is available for the upper part (from C4 to R6) of the buffer.

Here also the vertical displacement of the plug and the total force on the plug should be compared with experimental measurements.

## 4.7 Alternative case: Thermo-hydro-mechanical simulation of the engineered buffer at canister mid-height

### 4.7.1 Geometry

This task is focused on the mid-section of the buffer. A disc of the engineered buffer is to be modeled, rotational symmetry can be assumed, see Figure 4-17.



Figure 4-17 A schematic drawing of the CRT geometry and a blow up of a disc at the mid-section.

A radially symmetric model can be used, where the model should contain:

- the inner gap (0.01 m width)
- the ring shaped bentonite block
- the outer gap filled with bentonite pellets (0.055 m width)

Figure 4-18 shows the geometry of the considered mid-section.

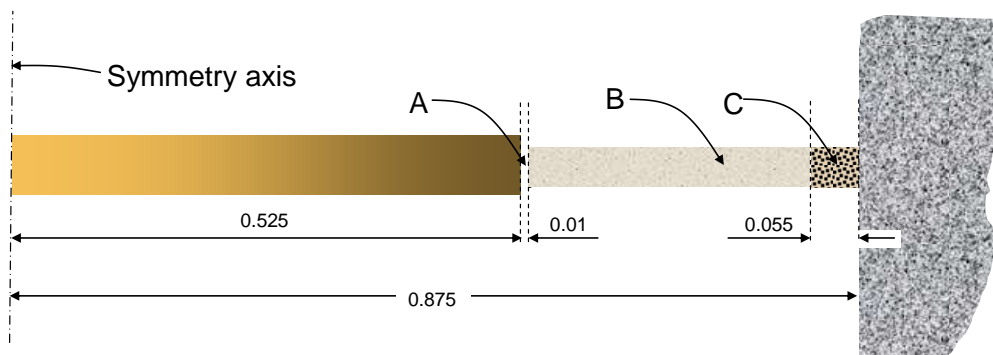


Figure 4-18 Geometry of the mid-section.



#### 4.7.2 Boundary conditions and initial conditions

##### **Boundary conditions**

Suggested boundary conditions of the selected disk of the engineered buffer are given in Table 4-16. When present, the names of the sensors, providing data for input as boundary conditions, are given. The sensor data is given in the appendix. The canister temperature data is however incomplete since the sensors broke down after approximately 1000 days. Therefore the simulated temperature and heat flux are also available.

**Table 4-16** Suggested boundary conditions

Boundary	Type of process		
	Thermal	Hydraulic	Mechanical
Canister	Temperature from experimental data. Sensor P12	Zero water flux	Roller conditions
Horizontal	Zero thermal flux	Zero water flux	Roller conditions
Hole wall	Experimental data. Sensor TR125	Water pressure from filter pressure protocol.	Roller conditions

##### **Initial conditions**

The initial conditions are given in terms of the temperature,  $T$ , the water saturation,  $S_r$ , the total stress tensor,  $\sigma$ , and the porosity,  $n$ . The water saturation is defined as  $S_r = dV_w/dV_p$  and the porosity  $n = dV_p/dV$ .

In both the definitions given above we make use of an additive split of a volume element,  $dV$ , in a solid volume element,  $dV_s$ , and a pore volume element,  $dV_p$ . Furthermore the pore volume element is additively split into a water volume element,  $dV_w$ , and an air volume element,  $dV_a$ .

The initial conditions are given in Table 4-17. The estimation of the initial values of the  $S_r$  and  $n$  parameters is based on the values given in /Johannesson, 2007/. The pellet-filled slot has here been considered as a homogenized material, i.e. the individual pellets interaction with each other and with the surroundings is not considered in detail.

**Table 4-17** Initial conditions.

Section	Type of process		
	Thermal	Hydraulic	Mechanical
A. Inner gap	$T = 20 \text{ }^\circ\text{C}$	$S_r = 0-1$ ? (is it filled)	$\sigma = 0 \text{ MPa}$ , $n = 1$
B. Bentonite block	$T = 20 \text{ }^\circ\text{C}$	$S_r = 0.859$	$\sigma = 0 \text{ MPa}$ , $n = 0.36$
C. Pellet-filled gap	$T = 20 \text{ }^\circ\text{C}$	$S_r = 0.895$	$\sigma = 0 \text{ MPa}$ , $n = 0.64$

#### 4.7.3 Material properties

The material characteristics are shown in appendix.

#### 4.7.4 Results to present

The results that the teams should present are 1) variable histories at specified points and 2) variable profiles at specified times. Some of the selected results can be compared with experimental measurements. The experimental data to compare with, provided in the form of excel-files, are listed in the next chapter “Sensor data to compare with”. The sensor names, positions and issues of the sensors can also be found in the next section.

The entire set of points, defined as a position of a material particle in the initial (undeformed) configuration, that is selected is shown schematically in Figure 4-19 below. The point position will thus change according to the deformation of the material. Note that all variables should not be shown for all points. See the list below for the correct variable – point selection. In the list the points (radial position) where sensor data is available are indicated using a bold font.

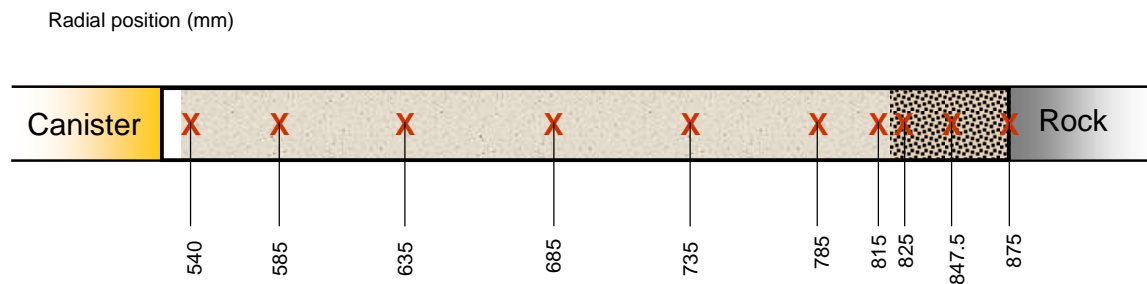


**Figure 4-19** Schematic drawing of the points where variable histories should be presented. The radial distances are given in the initial (undeformed) configuration.

Temperature histories at the radial distances [mm] (in the initial configuration):

540, **585**, 635, **685**, 735, 785, 815, 825, 847.5

Water saturation histories at the radial distances [mm]:

540, **585**, 635, **685**, 735, 785, 815, 825, 847.5

Total vertical (axial) stress histories at the radial distances [mm]:

540, **585**, **685**, **785**, 815, 825, 847.5, 875

Total horizontal (radial) stress histories at the radial distances [mm]:

540, 585, 685, 785, 815, 825, 847.5, 875

Dry density histories at the radial distances [mm]:

540, 585, 635, 685, 735, 785, 815, 825, 847.5

Displacement histories at the radial distances [mm]:

540, 585, 635, 685, 735, 785, 815, 825, 847.5

Profiles of Temperature, Water saturation and Dry density in the buffer at day:

670, 1400, 1800, 1910

#### 4.7.5 Sensor data to compare with

This model is considered to mimic the behavior of the buffer at canister mid-height (ring 5) in the direction towards the TBT experiment (direction A or  $\alpha = 180^\circ$  in the nomenclature used in the sensors data report (Goudarzi et al., 2006).

The model can be compared with sensor data obtained during the experiment, (see Goudarzi et al., 2006), and with data obtained after dismantling and sampling the buffer, (see Johannesson, 2007). The



sensor names below are in some cases given together with the radial position given in mm (bracketed after the sensor name), e.g. T111(635) means sensor T111 at the radial position 635 mm from the hole center. The experimental data are shown in the appendix.

The results obtained from the simulation are to be presented together with the corresponding experimental data at least for the sensor names and profiles obtained by sampling after dismantling the experiment that are given below.

### ***Thermal***

Temperatures in the buffer can be checked against the temperatures measured by Vaisala sensors (which are RH sensors also able to measure temperature), but these broke down after  $\approx 600$  days. There are also thermocouples that can be used in this direction that worked during the entire experiment.

Vaisala: W119T(585), W120T(685), W121T(785)

Thermocouples: T111(635), T112(735)

### ***Hydraulic***

The wetting evolution can be checked comparing with RH-data and/or suction-data. The CRT-experiment has been equipped with two complimentary sensors measuring the moisture in the buffer.

The Vaisala sensor measures relative humidity. These sensors functions well below  $\approx 95$  % RH, but give scattered results in the region above this limit. They also tend to break down when sudden drops in temperature occurs (decrease in canister power) depending on the resulting peak in RH.

The Wescore psychrometer measures the suction. These sensors work well above  $\approx 96$  % RH, and give more steady measurements as compared to Vaisala in this region. Below  $\approx 96$  % RH they do not give correct measurements since they can only record suctions less than 5 MPa.

Dependent on the behavior of the hydraulic sensors described above, the best overview of the saturation evolution is probably obtained if the sensors are used as a complement of each other, using Vaisala to begin with, when RH < 95 %, and Wescore later on, when RH > 95% or the suction < 5 MPa.

Vaisala: W119(585), W120(685), W121(785)

Wescore: W122(585), W123(685), W124(785)

From the samples taken in ring 6 and ring 7 (ring 5 was not sampled) after dismantling the experiment the corresponding water saturation profiles have been calculated. The profiles obtained at the end of the simulation can thus be compared with these experimental results.

### ***Mechanical***

Two different mechanical parameters, the axial stress and the dry density profile at the end of the test, are used as an indication of how well the model mimics the mechanical processes in the experiment.

In the experiment Geokon total pressure sensors were installed. The measured total pressure is in some cases found to be lower as compared to the expected total pressure at the given block density. The Geokon sensors have a cigar-shape where the pressure is measured at the tip of the sensor. When the sensors were installed, holes were drilled in the right position and the sensors were placed in the holes together with bentonite powder used to back fill the holes. At the tip where the pressure is measured there could therefore be a cavity, or lower density as compared to the block density, that might be responsible for the obtained low values of total pressure.

The total axial (vertical) stress  $\sigma_a$  in ring 5 is given by the selected sensors.

P110(585), P111(685), U106(785) (The sensor name U106 indicates that this sensor should measure pore pressure, but it was changed later on to measure total pressure.)

The dry density profile in ring 6 and ring 7 at end of test is also available. Comparison of the simulated profiles and the measured indicates whether the homogenization has been correctly captured or not.



## References

### EB

**Mayor J.-C., García-Siñeriz J.-L., Alonso E., Alheid H.-J., Blümling P., 2005** - Engineered barrier emplacement experiment in Opalinus Clay for the disposal of radioactive waste in underground repositories, EUR 21920

**Bossart P., Trick T., Meier P., Mayor J.-C., 2004** - Structural and hydrogeological characterisation of the excavation-disturbed zone in the Opalinus Clay (Mont Terri Project, Switzerland) Applied Clay Science 26 (2004) 429- 448

**Bossart P., Thury, M., 2008** -. Mont Terri Rock Laboratory Project, programme 1996 to 2007 and results. Wabern: Reports of the Swiss Geological Survey no. 3 Characteristics of the Opalinus Clay at Mont Terri.

**Palacios B., Rey M., García-Siñeriz J.L., 2013** - Engineered Barrier Emplacement Experiment in Opalinus Clay: "EB" Experiment AS-BUILT OF DISMANTLING OPERATION – PEBS deliverable D2.1-4

Hoffmann 2007

### FEBEX

**Martínez V., Abós H., García-Siñeriz J.L. 2016** - FEBEXe: Final Sensor Data Report (FEBEX "in situ" Experiment). AITEMIN. NAGRA Arbeitsbericht NAB16-19.

**Amiguet J.-L., 1985** - Grimsel Test Site. Felskennwerte von intaktem Granit. Zusammenstellung felsmechanischer Laborresultate diverser granitischer Gesteine. NAGRA, NIB 85-08, Sep. 1985.

**ENRESA, 2000** - FEBEX project. Full-scale engineered barriers experiment for a deep geological repository for high level radioactive waste in crystalline host rock. Final report. ENRESA, Madrid.

**ENRESA, 2004** - FEBEX II Project Final report on thermo-hydro-mechanical laboratory tests. ENRESA, Madrid.

**Guimerà J., Carrera J., Martínez L., Vázquez E., Ortuño F., Fierz T., Bülher C., Vives L., Meier P., Medina A., Saaltink M., Ruiz B. and Pardillo J., 1998** - FEBEX Hydrological characterization and modelling. UPC, 70-UPC-M-0-1001, Jan. 1998.

**Keusen H.R., Ganguin J., Schuler P. and Buletta M., 1989** - Grimsel Test Site. Geology. NAGRA, NTB 87-14E, Feb. 1989.

**Pardillo J. and Campos R., 1996** - FEBEX - Grimsel Test Site (Switzerland) Considerations respect to the fracture distribution. CIEMAT, 70-IMA-L-2-05, Mar. 1996.

**Pardillo J., Campos R. and Gimerà J., 1997** - Caracterización geológica de la zona de ensayo FEBEX (Grimsel - Suiza). CIEMAT, 70-IMA-M-2-01, May 1997.

**Pintado X. and Lloret A., 1997** - THM laboratory tests in FEBEX Phase 3. UPC, 70-UPC-L-3-01, Dec. 1997.

**Schneebeli M., Flühler H., Gimmi T., Wydler H. and Läser H.-P., 1995** - Measurements of water potential and water content in unsaturated crystalline rock. Water Resour. Res., 31(8), 1837-1843, 1995.

**Alonso E., Alcoverro J., 2005** - DECOVALEX III PROJECT, Modelling of FEBEX In-Situ Test, SKI Report 2005:2

### CRT

**Börgesson L, Åkesson M., Kristensson O., Dueck A., 2007** - EBS TF – THM modelling BM 2 – Large scale field tests SKB, TR-13-07

**Kristensson O., Börgesson L, 2015** - Canister Retrieval Test, Final report, SKB TR-14-19



**Dueck A.; Johannesson, L-E., 2008.-** Tests and analyses of bentonite reference material and field exposed material from the CRT test at Äspö. SKB IPR-08-17,

**Goudarzi R., Börgesson L., Röshoff K. and Edelman M., 2006 -** Sensors data report (Period: 001026-060501) Canister retrieval test, Report no. 12., SKB IPR-06-35

**Johannesson L-E., 2007 -**, Canister Retrieval Test, Dismantling and sampling of the buffer and determination of density and water ratio, SKB IPR-07-16.

**Thorsager P., Börgesson L., Johannesson L-E and Sandén T., 2002 -** Canister retrieval test, Report on installation, International progress report 02-30



## Appendix

### 1 THE FEBEX BENTONITE

In order to characterize the T-H-M behaviour of the FEBEX bentonite, besides the determination of identification properties, two types of tests have been carried out, namely: tests for direct parameter determination and tests for calibration of models. The first type of tests yields values of standard parameters or functions generally required by a mathematical T-H-M model. The second type of tests may be used with back analysis techniques in order to infer the values of the parameters or functions required by particular mathematical models and to improve the accuracy of parameter determination. The design of these tests, especially the tests for calibration of models, has been guided by the FEBEX “mock-up” and the FEBEX “in-situ” tests. The tests have been carried out mainly by CIEMAT and UPC and the description of the tests and the results obtained have been summarized in two reports. These reports are written in Spanish and in this Section we will try to make them more accessible to the participants. Throughout this Section we will refer to specific Sections of the report by CIEMAT (Villar, 2000) using “CIEMAT-Section” and to specific Sections of the report by UPC (Pintado, 2000) using “UPC-Section”.

In the tests carried out by CIEMAT, two types of samples of FEBEX bentonite have been used: unmixed and homogenized. The first type refers to samples taken from one of the bags into which the bentonite was packed. The second type refers to samples taken from the homogeneous mixture of all samples of the first type made by CIEMAT. Results obtained using any of these samples are considered to be representative of the characteristics of the FEBEX bentonite. In the tests that require addition of water, three types of water have been used: distilled water (used by convention and as a reference), granitic water (commercial water representative of the water that will saturate an engineered bentonite barrier) and saline water (water prepared with a chemical composition representative of the pore water inside the bentonite barrier). The chemical composition of the granitic water and of the saline water is given in Table 1-1.

*Table 1-1 Chemical composition of the water used in the tests (in mg/l), and pH*

dissolved ions and pH	granitic	saline
Cl <sup>-</sup>	13.1	3550.0
SO <sub>4</sub> <sup>2-</sup>	14.4	1440.0
Br <sup>-</sup>	0.1	—
NO <sub>3</sub> <sup>-</sup>	4.8	—
HCO <sub>3</sub> <sup>-</sup>	144.0	—
SiO <sub>2</sub> (aq)	22.2	—
Mg <sup>2+</sup>	9.4	360.0
Ca <sup>2+</sup>	44.9	400.8
Na <sup>+</sup>	11.0	253.9
K <sup>+</sup>	1.0	—
Sr <sup>2+</sup>	0.09	—
pH	8.3	7.0

In the tests carried out by UPC, the FEBEX bentonite taken from the homogenized sample was always used. Samples were prepared at the water content in equilibrium with the laboratory, which is of  $w = 13.3 \pm 1.3\%$ . Distilled water was used in infiltration tests and for preparing samples with a water content higher than the hygroscopic.

#### 1.1 Origin and general properties

##### 1.1.1 Origin and general aspects

The FEBEX bentonite (also called “Serrata” clay in some FEBEX reports) has been extracted from the Cortijo de Archidona deposit, exploited by Minas de Gádor, S. A., in the zone of Serrata de Níjar



(Almería, Spain). This deposit was selected in the ENRESA R&D plans previous to the FEBEX project as the most suitable material for the backfilling and sealing of a HLW repository. Reasons for this selection were its very high content of montmorillonite, large swelling pressure, low permeability, acceptable thermal conductivity, good retention properties and ease of compaction for the fabrication of blocks.

Over several years prior to FEBEX, and following the selection of this deposit as the reference bentonite (called bentonite S-2 in reports and publications), numerous characterization and behavior (thermal, hydraulic, mechanical, and geochemical) studies were performed. As a result, there is an extensive database on the properties of this bentonite. These data were used in the preliminary modelling for the design of the two large-scale tests of the FEBEX project.

Approximately 300 tons of suitably homogenized and conditioned bentonite were stocked for FEBEX. Based on the experience acquired in the aforementioned studies, the selected raw bentonite was required to meet the following specifications:

- Fraction of particles of more than 5 mm, less than 5%, and fraction of particles smaller than 74  $\mu\text{m}$ , greater than 85%.
- Liquid limit greater than 90%.
- Swelling pressure ranging between 3 MPa and 7 MPa, for a dry density of 1.60 g/cm<sup>3</sup>.
- Water content, after conditioning, between 12.5% and 15.5%.

The conditioning of the bentonite in the quarry, and later in the factory, was strictly mechanical (homogenization, rock fragment removal, drying, crumbling of clods, and sieving) to obtain a granulated material with the specified characteristics of grain-size distribution and water content. A quality assurance (QA) program was applied to the conditioning process. The conditioned material was packaged in large waterproof bags (about 1300 kg each). During the packaging, a sample of 8 to 10 kg was taken every 2.5 tons of bentonite, for laboratory testing.

However homogeneous it might be, a bentonite deposit has both horizontal and vertical spatial variations. For a research project such as FEBEX, a material as homogeneous as possible must be used and, furthermore, its properties must be determined by specific tests on samples of the same material. Homogenization reduces the uncertainties in modelling, in laboratory results and in the final interpretation of the entire test. For performance assessment (PA) purposes, however, knowledge of the range of variations in the relevant properties of a massive source of bentonite supply is needed. Thus, it is important to compare the properties of clays (known as S-2 bentonite in the earlier studies and FEBEX bentonite in this test) obtained from the same deposit but in two study phases separated by more than five years.

Comparison of the results of the two sets of characterization tests –S-2 bentonite and FEBEX bentonite– indicates that the deposit is very homogeneous. Consequently, it was possible to use certain parameters from the tests on S-2 bentonite for the purposes of the FEBEX test.

In the following sections, several general conclusions on the properties of the bentonite from this deposit are summarized.

### **1.1.2 Identification properties**

The data presented in Table 1-2 are the so-called identification properties (according to the terminology of geotechnical engineering). They provide an initial idea of the type of physico-chemical behavior to be expected in the clay buffers.

It is interesting to notice that the values of the liquid limit for the S-2 and FEBEX bentonites are very similar in the tests performed by CIEMAT, in contrast to those obtained by UPC-DIT for the FEBEX bentonite, which are somewhat lower. In any case, whichever laboratory is considered, the measured values seem to be low for a bentonite with such a high content of montmorillonite and which also has a relatively high concentration of sodium as exchangeable cation.

Regarding differences in the grain-size distributions between the S-2 and FEBEX bentonites, it should be noted that the results obtained from CIEMAT and UPC-DIT differ considerably as regards the content of the < 2  $\mu\text{m}$  fraction (clay size). The proportion of the clay size fraction obtained depends on the previous treatment of the bentonite for the determination of its grain-size distribution. The differences



may be explained by the fact that a very strong dispersion procedure, including ultrasounds, was used by CIEMAT, while UPC-DIT employed standard geotechnical techniques.

**Table 1-2 Identification properties (ENRESA, 2000)**

Property	Bentonite S-2		FEBEX Bentonite		
	CSIC-Zaidín	CIEMAT	CSIC-Zaidín	CIEMAT	UPC-DIT
Water content in equilibrium with the air in the laboratory, in %	—	10 to 13	—	13.7 ± 1.3	13.3 ± 1.3
Liquid limit, in %	—	105 ± 10	—	102 ± 4	93 ± 1
Plastic limit, in %	—	—	—	53 ± 3	47 ± 2
Plasticity index	—	—	—	49 ± 4	46 ± 2
Specific weight	—	2.78	—	2.70 ± 0.04	—
Grain-size distribution, in %					
Fraction less than 74 µm	93 ± 3	86	—	92 ± 1	87
Fraction less than 2 µm	82 ± 6	65 ± 1	—	68 ± 2	45
Specific surface, in m <sup>2</sup> /g					
Total	614 ± 74 <sup>(1)</sup>	516 ± 37 <sup>(2)</sup>	649 ± 5 <sup>(1)</sup>	725 ± 47 <sup>(1)</sup>	—
External, BET	—	37	—	32 ± 3	—

<sup>(1)</sup> Determined by the Keeling hygroscopicity method

<sup>(2)</sup> Determined by the methylene blue method

The value obtained for the external specific surface (BET) is somewhat lower than the average values for smectites (as found in the scientific literature).

The low content of the < 2 µm fraction had already been noticed in the first studies performed on the S-2 bentonite. It was proposed at that time that the smaller particles were agglutinated or cemented with colloidal silica (during alteration of the original volcanic material). This would make dispersion of the clay, and consequently separation of the < 2 µm fraction, more difficult. This argument is supported since the most of the silt-sized material, and some of the sand-sized, is formed by “pseudomorphs” of volcanic grains transformed into smectite. The “pseudomorphs” are relatively stable and would moderate the physical behavior of the bentonite: they are identified as smectite from a chemical point of view, but do not have the physical effects of the bentonite. This interpretation may also explain the relatively low values of liquid limit found in tests.

### 1.1.3 Porosity

The pore size distribution has been measured using a mercury injection porosimeter with a range of injection pressure from 7 kPa to 210 MPa that allows to measure pore diameters between 200 µm and 0.006 µm. Before placing the samples in the porosimeter, water was eliminated by liophilization, in order to minimize microstructural changes. 45 samples were taken from 15 of the bentonite blocks fabricated for the FEBEX “mock-up” test. These blocks were made using bentonite with a water content of 14.1±1.0 % and uniaxially compacted at pressures of 40-45 MPa which produced a dry density  $\rho_d = 1.78 \pm 0.03$  g/cm<sup>3</sup>. The samples tested had a dry density of  $\rho_d = 1.58$ -1.80 g/cm<sup>3</sup>. The result of these porosimetric tests (see Figure 1-1) did not show any significant difference between different positions in a given bentonite block nor between different block types.

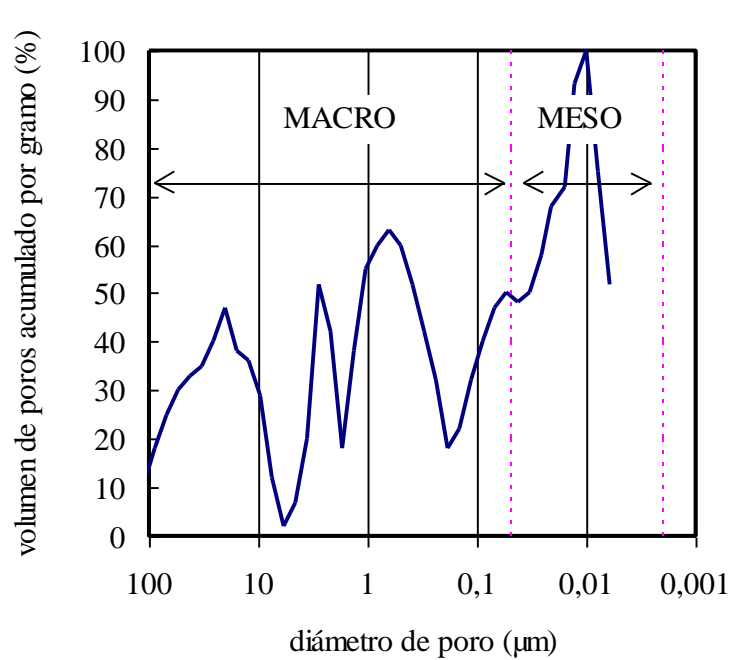


*Figure 1-1 Typical pore size distribution of a sample of compacted FEBEX bentonite (cumulative pore volume per gram in % as a function of pore diameter in µm)*

## 1.2 Parameter determination tests

### 1.2.1 Mechanical properties

In order to characterize the mechanical behaviour of the bentonite, strength tests, compressibility tests, swelling pressure tests, swelling under load tests and resonant column tests were made.

#### **Strength-unconfined compression and triaxial tests**

In the years previous to FEBEX, strength had been determined only on samples of the bentonite S-2. Some of these data are presented herein for informative purposes.

The unconfined compressive strength is 2.5 MPa for samples prepared with a water content at equilibrium with the air in the laboratory (laboratory conditions) and at a density of 1.70 g/cm<sup>3</sup>. It was found that unconfined compressive strength increases exponentially with dry density.

Various types of triaxial tests were performed, with saturated and unsaturated samples. The results from the unsaturated samples, prepared at different dry densities with the water content at equilibrium with the laboratory conditions, are presented in Table 1-3.

*Table 1-3 Strength parameters obtained in triaxial tests on unsaturated specimens of bentonite S-2 prepared with a water content in equilibrium with the laboratory conditions and at different initial dry densities (ENRESA, 2000)*

$\rho_a$ g/cm <sup>3</sup>	initial Sr %	range of $\sigma_3$ MPa	cohesion MPa	friction angle degrees
1.6	41 – 47	0.5 – 3.0	0.7	25
1.6	41 – 47	3.0 – 10.0	2.8	14
1.6	41 – 47	10.0 – 30.0	4.4	14
1.7	49 – 60	0.5 – 3.0	0.8	30
1.7	49 – 60	3.0 – 10.0	1.0	26
1.7	49 – 60	10.0 – 30.0	3.5	16
1.8	53 – 59	3.0 – 10.0	4.3	16
1.8	53 – 59	10.0 – 30.0	3.6	18
1.9	65 – 79	3.0 – 10.0	4.5	19

**Compressibility-oedometric tests**

Oedometric tests have been performed on samples of the bentonite S-2 for initial dry densities of 1.40 g/cm<sup>3</sup> and 1.60 g/cm<sup>3</sup>. Table 1-4 shows the parameters resulting from these tests.

**Table 1-4** Oedometer parameters (*C<sub>c</sub>* = compression index of the virgin compression line, with stress in decimal log scale; *C<sub>s</sub>* = unloading-reloading compression index, with stress in decimal log scale; *a<sub>v</sub>* = virgin confined compression index, with stress in natural scale; *m<sub>v</sub>* = *a<sub>v</sub>* / (1 + *e*<sub>0</sub>), where *e*<sub>0</sub> is the initial void ratio; and *k* = saturated permeability) (ENRESA, 2000)

$\rho_d$ g/cm <sup>3</sup>	$C_c$	$C_s$	$a_v$ m <sup>2</sup> /kN	$m_v$ m <sup>2</sup> /kN	$k$ m/s
1.4	0.38	0.20	$2.5 \cdot 10^{-5}$	$1.7 \cdot 10^{-5}$	$4.7 \cdot 10^{-12}$
1.6	0.38	0.33	$2.3 \cdot 10^{-5}$	$1.4 \cdot 10^{-5}$	$1.3 \cdot 10^{-13}$

**Swelling pressure**

Swelling pressure tests were performed using conventional oedometers on samples saturated with distilled water. A regression curve was developed as a function of dry density for the swelling pressure of the FEBEX bentonite, as shown on Figure 1-2, and expressed by the equation

$$P_s = \exp(6.0\rho_d - 9.07) \tag{1.1}$$

where  $P_s$  is the swelling pressure in MPa and  $\rho_d$  is the dry density in g/cm<sup>3</sup>. The deviation of the experimental values with respect to this fitting may be as high as 25 %. The dispersion observed in the values is larger for higher dry densities, this probably being due to technical limitations, as the load capacity of the oedometers is almost exceeded by the swelling pressure. The swelling pressure values and the regression curve for the bentonite S-2 are also shown in Figure 1-2. The difference in the swelling pressures of the S-2 and the FEBEX bentonites, may be considered negligible for practical purposes.

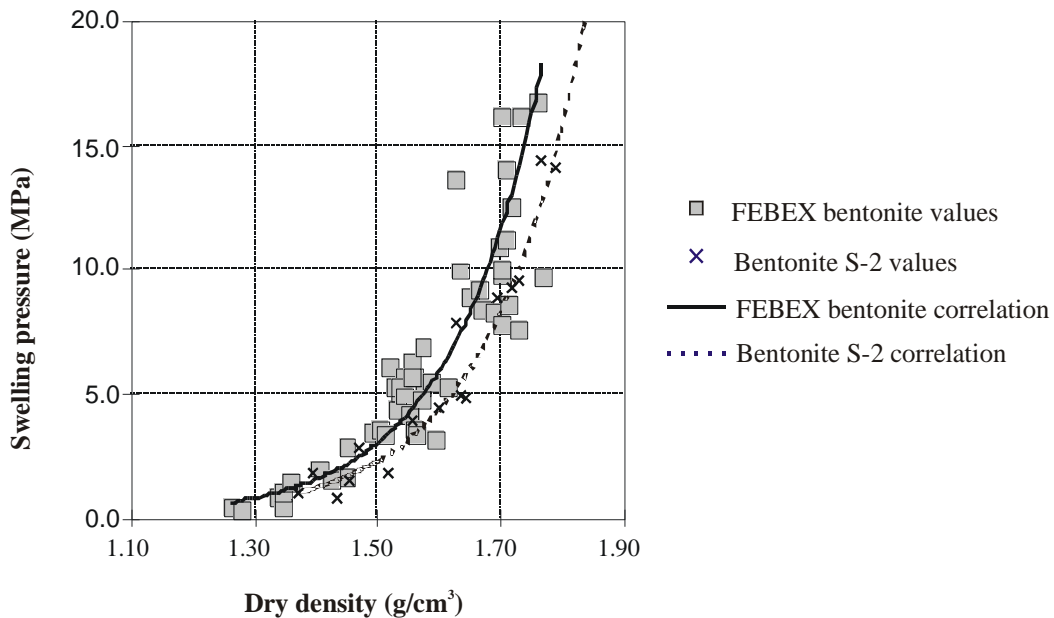


**Figure 1-2** Swelling pressure as a function of dry density (ENRESA, 2000)



**Swelling under load**

These tests were performed using conventional oedometers on samples of the FEBEX bentonite. During the pre-operational stage, CIEMAT carried out tests with distilled water on specimens with a nominal dry density of 1.60 g/cm<sup>3</sup>. Four of these tests were performed under a load of 0.5 MPa and the other three under a load of 0.9 MPa. Subsequently, several series of swelling under load tests were performed, in which samples having a nominal dry density of 1.60 g/cm<sup>3</sup> were subjected to different loads ranging between 0.1 and 3.0 MPa. Both granitic and saline water were used to saturate the sample. A commercial granitic water was used. The saline water is a synthetic product having a chemical composition similar to that of the bentonite interstitial water, but simplified to include only the major elements. The chemical composition of both waters is shown in Table 1-5.

**Table 1-5** Chemical composition of the water used in the tests (in mg/l), and pH

dissolved ions and pH	granitic	saline
Cl <sup>-</sup>	13.1	3550.0
SO <sub>4</sub> <sup>2-</sup>	14.4	1440.0
Br <sup>-</sup>	0.1	—
NO <sub>3</sub> <sup>-</sup>	4.8	—
HCO <sub>3</sub> <sup>-</sup>	144.0	—
SiO <sub>2</sub> (aq)	22.2	—
Mg <sup>2+</sup>	9.4	360.0
Ca <sup>2+</sup>	44.9	400.8
Na <sup>+</sup>	11.0	253.9
K <sup>+</sup>	1.0	—
Sr <sup>2+</sup>	0.09	—
pH	8.3	7.0

In addition, some tests have been performed with specimens compacted to nominal dry densities of 1.70 and 1.50 g/cm<sup>3</sup> saturated with granitic water, and some others with specimens compacted to nominal dry densities of 1.70 g/cm<sup>3</sup> and saturated with saline water.

As expected, the specimens compacted to a dry density of 1.50 g/cm<sup>3</sup> undergo strain, on saturation with granitic water, somewhat lower than in the case of specimens compacted to a dry density of 1.60 g/cm<sup>3</sup>. Specimens compacted to a dry density of 1.70 g/cm<sup>3</sup> experienced higher swelling strains under the same load, in tests with both saline and granitic water.

Figure 1-3 shows the final swelling strain of the clay in the tests performed with samples compacted to nominal dry densities of 1.60 g/cm<sup>3</sup> and saturated with different kinds of water, along with the fitting for the tests performed with both granitic and saline water. The final values of strain do not seem to be particularly dependent on the kind of water, although in the tests performed with saline water they are somewhat higher than in those performed with granitic water, the values for distilled water being the highest.

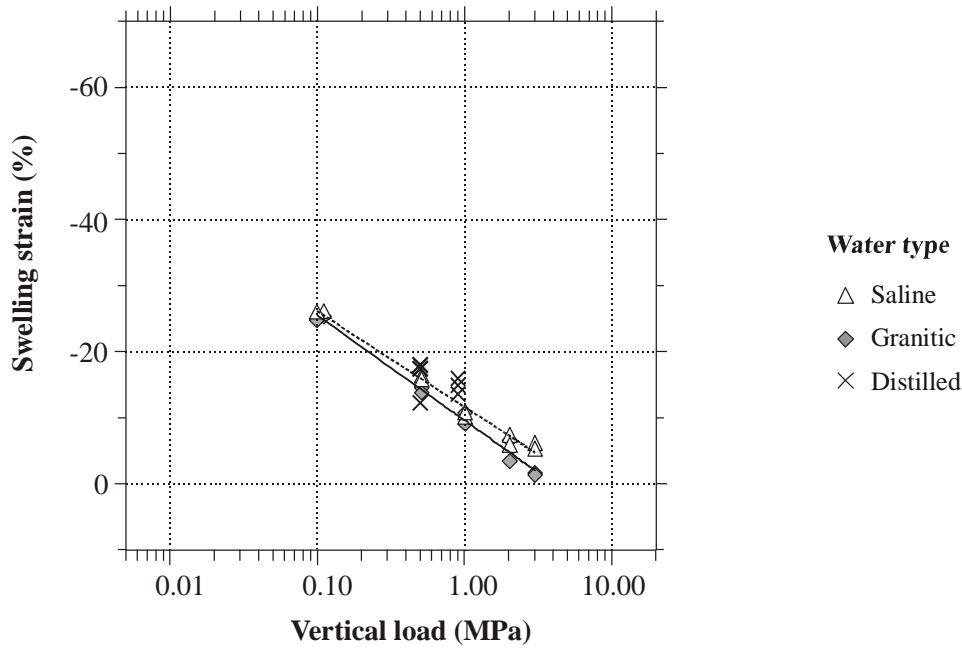


**Figure 1-3** Swelling strain of specimens compacted to dry density 1.60 g/cm<sup>3</sup> on saturation under vertical load with different kinds of water (ENRESA, 2000)

Strain ( $\varepsilon$ , %) as a function of vertical load ( $\sigma$ , MPa) may be approximately expressed by the following equations:

$$\varepsilon = \begin{cases} -9.4 + 15.9 \log \sigma & \text{for granitic water} \\ -11.4 + 14.4 \log \sigma & \text{for saline water} \end{cases} \quad (1.2)$$

UPC performed 21 flooding-under-load tests on specimens prepared at various dry densities varying between 1.57 g/cm<sup>3</sup> and 1.87 g/cm<sup>3</sup>, with an initial water content of 11.7% (water content at equilibrium with laboratory conditions). The specimens were saturated with distilled water while being subjected to a constant load ranging between 0.01 MPa and 10.00 MPa.

The strain ( $\varepsilon$ , %) induced after saturation is shown in Figure 1-4 and may be approximately expressed by the equation

$$\varepsilon = -46.9 - 19.4 \log \sigma + 36.6 \rho_d \quad (1.3)$$

where  $\sigma$  is the vertical load in MPa and  $\rho_d$  is the initial dry density in g/cm<sup>3</sup>.

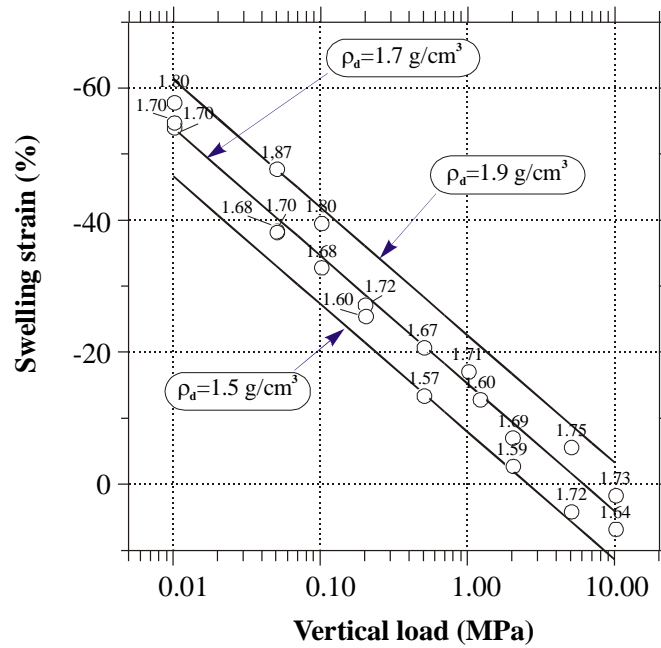


Figure 1-4 Swelling strain for different applied vertical loads with the value of initial dry density, in  $\text{g/cm}^3$ , indicated for each point (ENRESA, 2000)

The strain values obtained with this equation for a dry density of  $1.60 \text{ g/cm}^3$  are slightly higher than those obtained with the fitting used by CIEMAT for tests performed with granitic water. The discrepancy is more marked for low loads, with a maximum difference of 5 percentage points. This would confirm that swelling under saturation with distilled water is somewhat higher than the swelling expected when saturation takes place with granitic water.

**Elastic shear modulus, G**

UPC-DIT determined the elastic shear modulus, G, at small deformations ( $10^{-6} \leq \gamma \leq 10^{-4}$ ) for the FEBEX bentonite. The tests were performed in a resonant column on 10 specimens compacted at various dry densities and degrees of saturation. The results are shown in Table 1-6 and in Figure 1-5

Table 1-6 Elastic shear modulus obtained in resonant column tests (ENRESA, 2000)

dry density $\text{g/cm}^3$	water content %	degree of saturation %	void ratio	elastic shear modulus, G, in MPa				
				$\sigma_3 = 0.01$ MPa	$\sigma_3 = 0.1$ MPa	$\sigma_3 = 0.2$ MPa	$\sigma_3 = 0.4$ MPa	$\sigma_3 = 0.8$ MPa
1.58	14.7	54	0.757	140	207	245	300	370
1.66	13.6	57	0.668	211	223	270	—	—
1.54	3.4	12	0.802	78	106	174	208	326
1.56	2.8	10	0.777	89	106	138	—	—
1.62	24.6	95	0.717	240	270	—	331	336
1.66	21.3	87	0.677	252	296	370	429	502
1.65	4.7	19	0.685	74	90	137	190	310
1.72	10.4	47	0.615	200	219	293	381	429
1.68	3.7	16	0.652	61	89	141	200	290
1.62	12.7	50	0.713	122	180	240	299	387

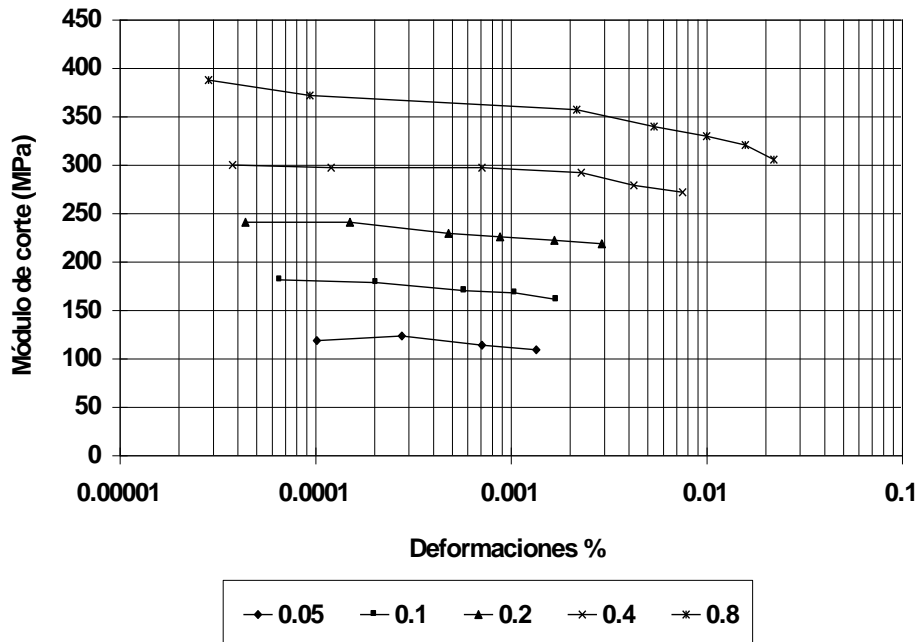


Figure 1-5 Shear modulus  $G$  as a function of the deformation at a degree of saturation of 0.5 and various confining pressures

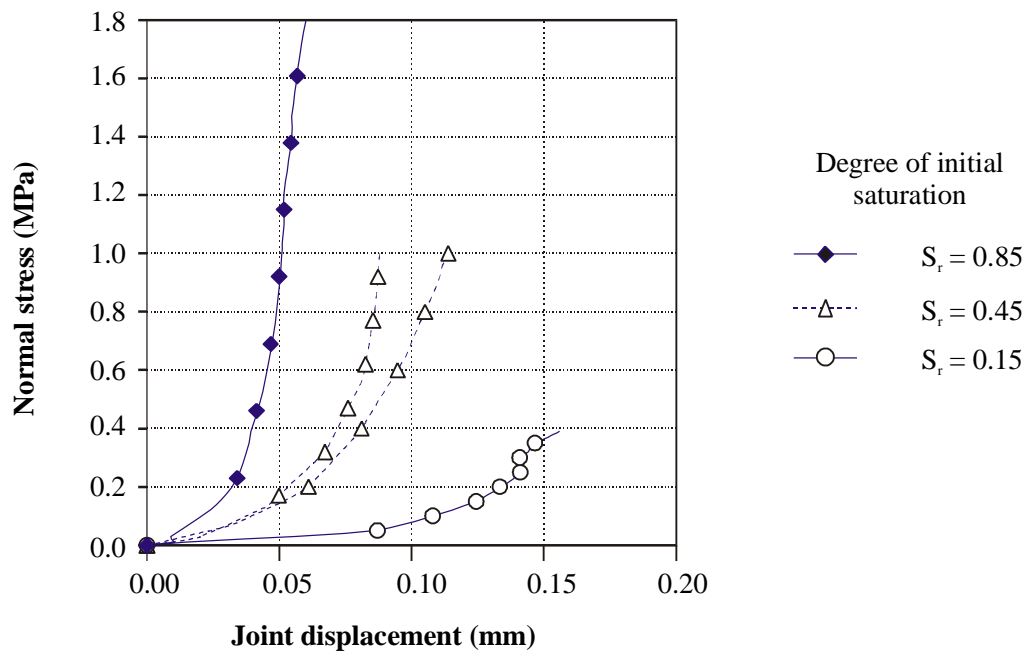


Figure 1-6 Displacement between joint surfaces for different degrees of saturation (ENRESA, 2000)

### 1.1.1.1 Compressibility of joints

UPC-DIT performed unconfined compression tests on specimens of the FEBEX bentonite to obtain the relationship between normal stress and displacement in the joints between blocks. The joint displacements were calculated by comparing the average deformations in two specimens for the same level of load: one was a continuous specimen with a height of 7.8 cm and the other was formed by two pieces, each 3.9 cm in height, placed one on top of the other. Each specimen was tested with three



different degrees of initial saturation. Figure 1-6 shows the value of the decrease in distance between the joint surfaces of two blocks as a function of the normal load applied, for different degrees of saturation.

### 1.2.2 Hydraulic properties

#### **Saturated hydraulic conductivity**

An empirical relationship has been obtained, using saturated specimens, for the coefficient of permeability of the FEBEX bentonite as a function of dry density. It was expressed by the following equations

$$\log k = \begin{cases} -6.00\rho_d - 4.09 & 1.30 \leq \rho_d \leq 1.47 \quad (r^2 = 0.97, 8 \text{ points}) \\ -2.96\rho_d - 8.57 & 1.47 \leq \rho_d \leq 1.84 \quad (r^2 = 0.70, 26 \text{ points}) \end{cases} \quad (1.4)$$

where  $k$  is the coefficient of permeability for distilled water, in m/s, and  $\rho_d$  is the dry density, in g/cm<sup>3</sup>. The variation of the values actually obtained with respect to these fittings is of the order of 30 %.

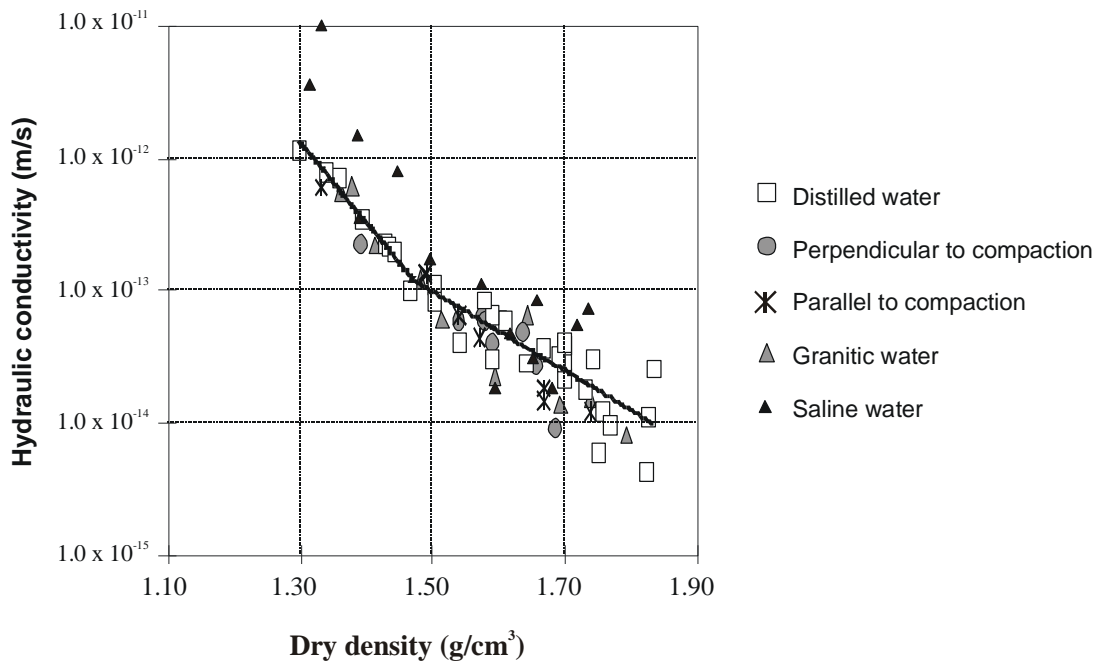


**Figure 1-7** Saturated hydraulic conductivity as a function of dry density (ENRESA, 2000)

Figure 1-7 shows the regression lines for the coefficient of permeability of FEBEX bentonite shown above and the points obtained in different determinations. The influence of the water used as permeant has been tested, as well as the influence of the direction of the measurement, parallel or perpendicular to the compaction effort, in the value of the coefficient of permeability. None of these aspects seems to be relevant, with the exception of the use of saline water, that yields a higher hydraulic conductivity. The data indicate that the FEBEX bentonite is less permeable than the bentonite S-2. However, differences are small: in some cases it is even less than the scattering shown in the same set of tests.

#### **Relative permeability**

Unsaturated hydraulic conductivity is highly dependent on the degree of saturation  $S_r$  and may be expressed as the product of relative permeability  $k_r$  times the saturated hydraulic conductivity. The

dependence on the degree of saturation is usually expressed by means of a potential law for the relative permeability:

$$k_r = S_r^n \quad (1.5)$$

The water infiltration tests carried out by CIEMAT in small teflon cells (see Figure 1-8) provide data allowing unsaturated hydraulic conductivity and its dependence on the degree of saturation to be obtained. In the tests, water content throughout the specimen was measured at different times after initiation of the infiltration process. By means of parameter identification techniques similar to those used in groundwater engineering and geophysics, intrinsic permeability and the exponent of the law used to obtain the relative permeability may be estimated. The values obtained were  $K = 2.95 \cdot 10^{-21} \text{ m}^2$  (for a porosity of 0.4) and  $n = 4.64$  respectively, in the case of samples with an initial dry density of  $1.75 \text{ g/cm}^3$ .

Similar infiltration tests have been carried out at UPC-DIT. In this case, in order to study the possibility of desaturation of the surrounding rock at the interface between the bentonite and the granite, a hydraulic gradient was prescribed across a specimen of granite in contact with another specimen of bentonite. The test was carried out in a triaxial cell with a confinement pressure of 0.8 MPa (see Figure 1-9). Specimens were initially compacted at a dry density of  $1.76 \text{ g/cm}^3$  and a water content of 13%. No change in the water content of the granite was detected during the test. However, the measurements of water content in the bentonite allow a new value to be estimated for the exponent in the relative permeability law. Figure 1-10 shows how good agreement is achieved between the measurements and numerical model computations, with the parameters derived from the identification process.

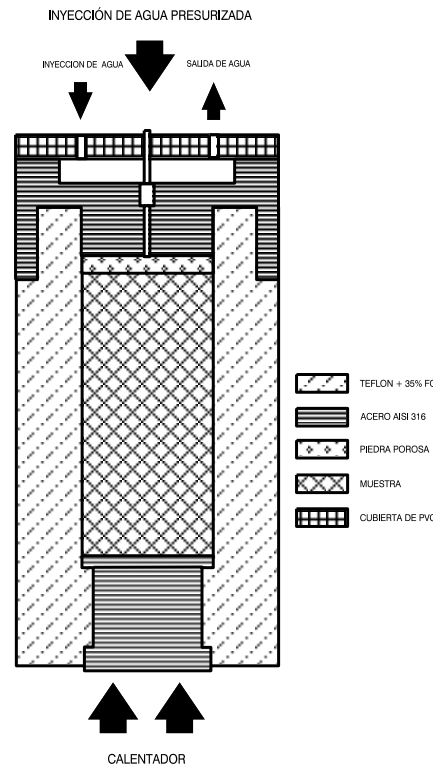


**Figure 1-8** Scheme of the Teflon cell. The lateral walls of the cell are made of Teflon. Water may be enter or leave the cylindrical sample through a porous stone placed on the top of the sample. The openings in the upper steel cap allow the flow of water to or from the porous stone. The lower steel cap allows the heating of the bottom of the sample

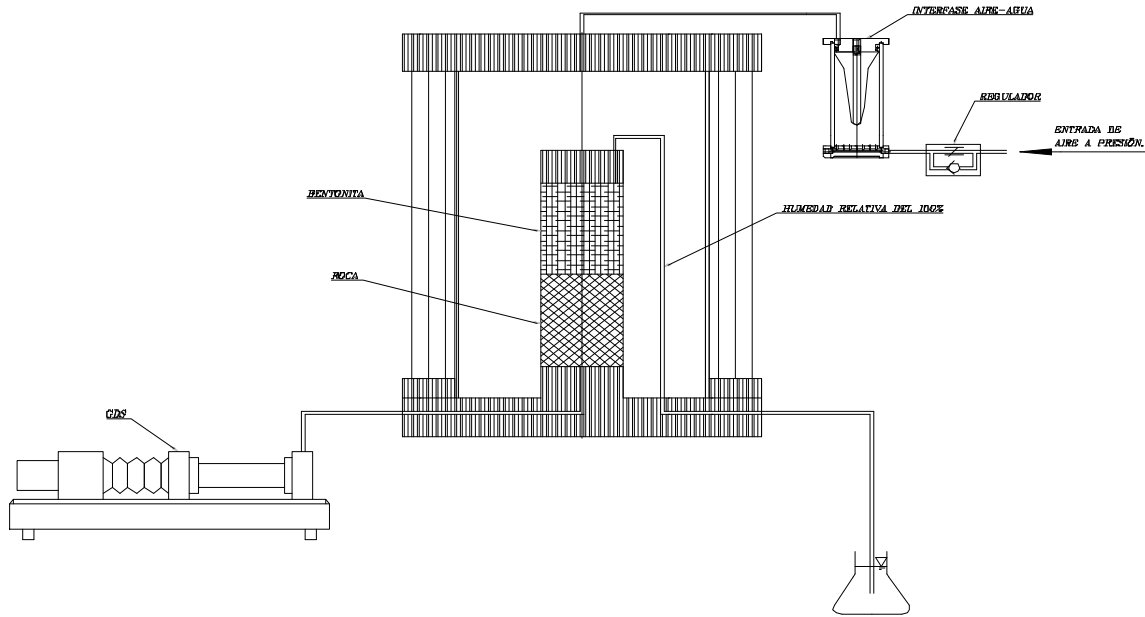


Figure 1-9 Scheme of the set up used in the infiltration tests

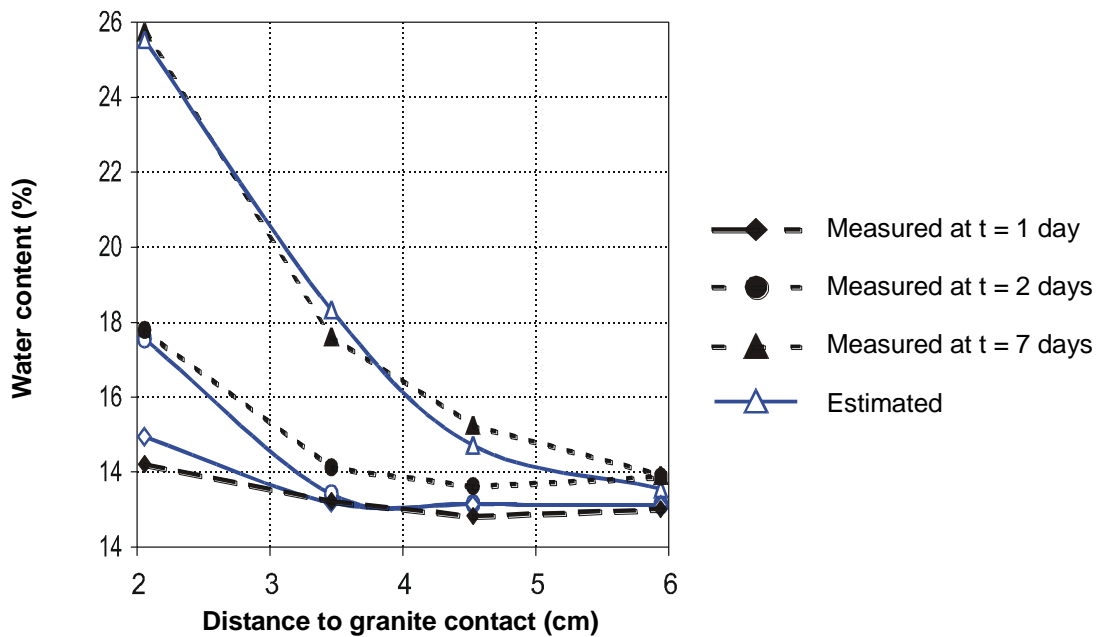


Figure 1-10 Measured and computed water content in infiltration tests (ENRESA, 2000)

In addition, the unsaturated water conductivity may be estimated in thermo-hydraulic experiments with prescribed heat and water flows. The summary of values obtained for the parameter  $n$  in the relative permeability law in Table 1-7.

**Table 1-7** Exponent  $n$  in relative permeability law (1.5) from different test types (ENRESA, 2000)

Test	$n$
Water infiltration in small teflon cells	4.64
Water infiltration in bentonite in contact with granite	3.50
Heat and water flow experiment 1	3.06
Heat and water flow experiment 2	1.10
Heat and water flow experiment 3	1.68

**Suction–water content relationship at 20 °C**

**Tests on unconfined samples**

CIEMAT has carried out suction–water content tests for the FEBEX bentonite, both in compacted samples and in samples trimmed from blocks. The relationship between suction and water content was initially determined in compacted samples for three different suction values and, subsequently following wetting and drying–wetting paths. UPC tested specimens at various temperatures and suctions between 3 MPa and 700 MPa following similar wetting and drying paths. Figure 1-11 shows the tests results grouped according to initial dry density ( $\rho_{d0}$ ). Tests with a dry density of 1.67 and 1.75 g/cm<sup>3</sup> were performed by CIEMAT and tests with a dry density of 1.64 g/cm<sup>3</sup> were performed by UPC. The relationship between suction  $s$  in MPa and the water content  $w$  in %, may be fitted by means of the following equation:

$$w = (45.1\rho_{d0} - 39.2) - (18.8\rho_{d0} - 20.34) \log s \tag{1.6}$$

where  $\rho_{d0}$  is the initial density in g/cm<sup>3</sup>.

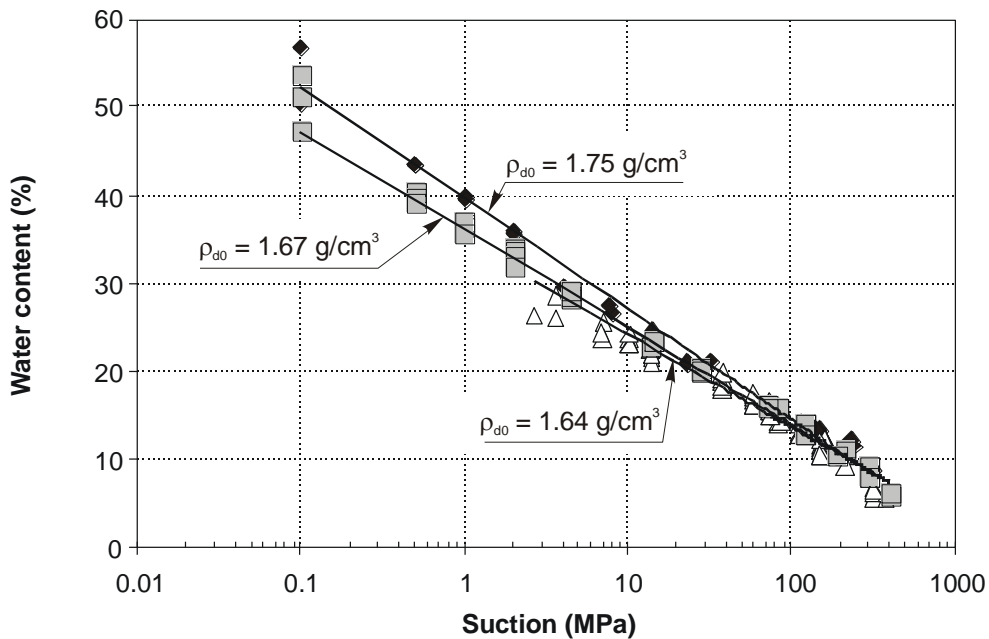


**Figure 1-11** Suction/water content relationship in tests on unconfined samples, for FEBEX bentonite (ENRESA, 2000)

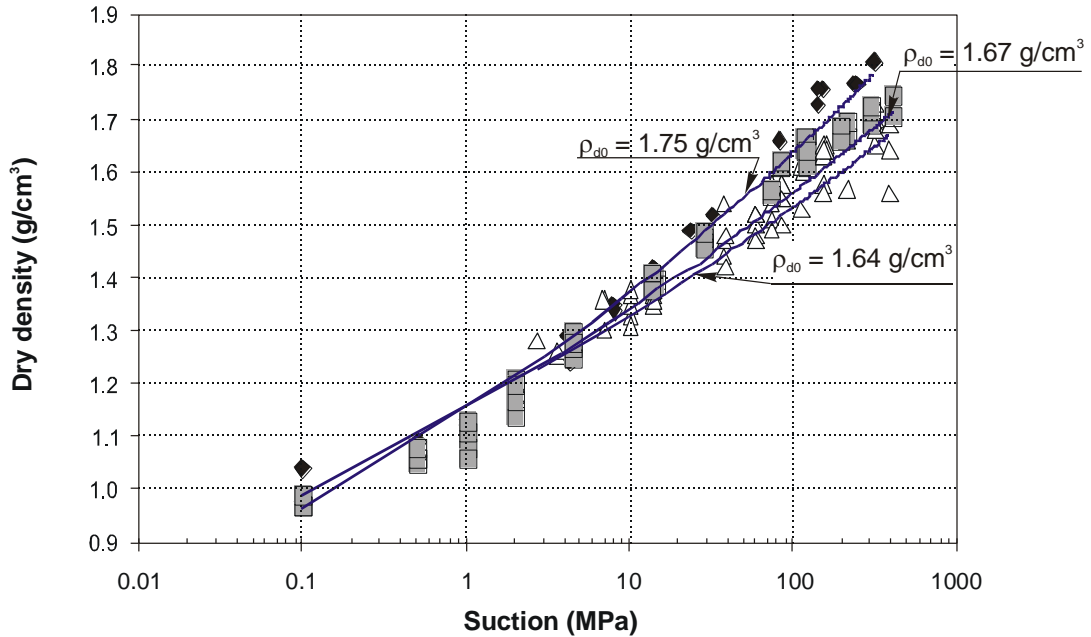


**Figure 1-12** Relationship between dry density and suction in tests on unconfined samples, for FEBEX bentonite (ENRESA, 2000)

The volume variations observed with changing suction are important. Figure 1-12 shows the relationship between the dry density and the change in suction for the different samples tested, grouped according to their initial dry densities. The dry density for values of suction ranging from 400 to 0.1 MPa may be obtained through the following expression:

$$\rho_d = 1.15 s^{0.13 \rho_{d0} - 0.15} \quad (1.7)$$

where  $\rho_{d0}$  is the initial dry density in  $\text{g/cm}^3$  and  $s$  is the suction in MPa.

For suctions varying between 2.0 MPa and 385.0 MPa, an empirical equation relating water content and suction was determined for the bentonite S-2

$$w = 36.1 - 12.0 \log s \quad (r^2 = 0.94, 191 \text{ points}) \quad (1.8)$$

which does not depend on initial dry density. In this equation,  $w$  is the water content in %, and  $s$  the suction in MPa. Figure 1-13 shows the regression curves for the bentonites (S-2 and FEBEX) and the points obtained by CIEMAT and UPC for each bentonite.

As may be seen, the differences between the two curves are very small, one or two percentage points in the water content, depending on the suction value. Nevertheless, it may be said that there exists a difference that is reflected in the water content in equilibrium with the laboratory conditions, as was indicated in Table 1-1. For all practical purposes, the differences between the two bentonites are very small.

In the low range of suction, water contents determined at a temperature of 72°C are higher than those determined at 20°C. However, the results are limited and more tests are required to quantify the effect of temperature on suction/water content relationship.

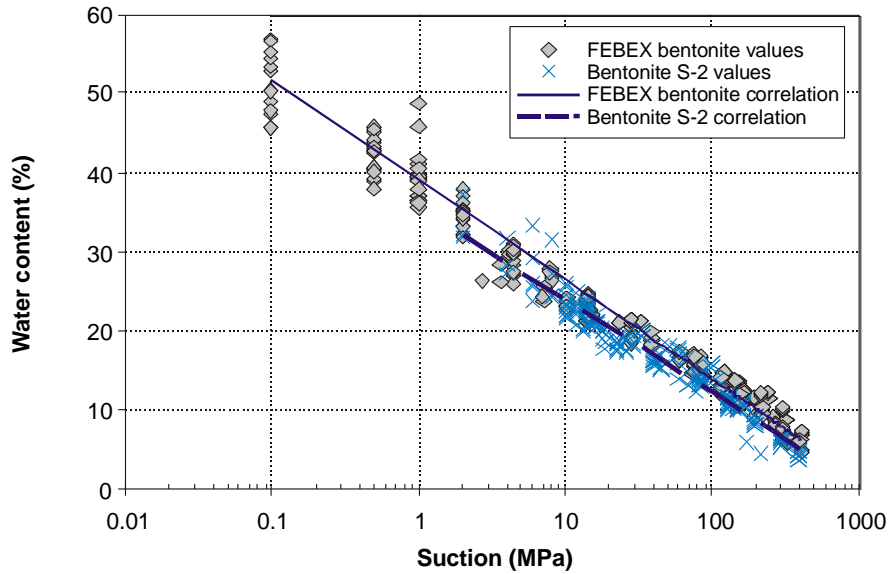


**Figure 1-13** Suction/water content relationship in tests on unconfined samples, for S-2 and FEBEX bentonites (ENRESA, 2000)

**Tests on confined samples**

In unconfined tests, the dry density and structure of the bentonite undergo important changes during the hydration process. However, volume changes are small in a bentonite barrier, and knowledge of the relationship between suction/water content at constant dry density (characteristic or water retention curve) is essential.

To determine the retention curve, two kinds of tests have been performed. CIEMAT used suction controlled oedometers to hinder swelling of the clay, by adding the appropriate loads. UPC designed containers made from sintered metal to fix the volume of the sample, while the water vapor in the clay changes with the atmosphere in which the capsule is placed. In both cases, minor volume changes have occurred.

The retention curves determined may be fitted by means of the Van Genuchten expression:

$$S_r = S_{r_0} + (S_{r_{max}} - S_{r_0}) \left[ 1 + (s/P_0)^{1/(1-\lambda)} \right]^{-\lambda} \tag{1.9}$$

or to a modification of this expression that is more suitable for higher values of suction:

$$S_r = S_{r_0} + (S_{r_{max}} - S_{r_0}) \left[ 1 + (s/P_0)^{1/(1-\lambda)} \right]^{-\lambda} \left[ 1 - s/P_s \right]^{\lambda_s} \tag{1.10}$$

where  $S_{r_0}$  and  $S_{r_{max}}$  are the residual and maximum degree of saturation and  $P_0$  is the air entry value and  $\lambda$ ,  $P_s$  and  $\lambda_s$  are material parameters. Table 1-8 shows the parameters fitted for the wetting paths, that are plotted together with the experimental points in Figure 1-14. Table 1-9 shows the parameters fitted for the wetting paths, that are plotted together with the experimental points Figure 1-15.

**Table 1-8** Parameters of the retention curves (ENRESA, 2000)

$\rho_d$ range g/cm <sup>3</sup>	type of equation	$P_0$ MPa	$\lambda$	$S_{r_0}$	$S_{r_{max}}$	$P_s$ MPa	$\lambda_s$
1.70 – 1.75	Van Genuchten (1)	90	0.45	0.00	1.00	—	—
1.70 – 1.75	modified van Genuchten (2)	100	0.45	0.01	1.00	1500	0.05

1.60 – 1.65	Van Genuchten (3)	30	0.32	0.10	1.00	—	—
1.60 – 1.65	modified van Genuchten (4)	35	0.30	0.01	1.00	4000	1.5
1.58 – 1.59	Van Genuchten (5)	4.5	0.17	0.00	1.00	—	—
1.58 – 1.59	modified van Genuchten (6)	2.0	0.10	0.01	0.99	1000	1.3

**Table 1-9** Parameters for fitting of the drying paths after saturation (ENRESA, 2000)

$\rho_d$ range g/cm <sup>3</sup>	type of equation	$P_0$ MPa	$\lambda$	$S_{r0}$	$S_{rmax}$	$P_s$ MPa	$\lambda_s$
1.70 – 1.75 drying	Van Genuchten (1)	180	0.62	0.0	1.0	—	—
1.70 – 1.75 wetting	modified van Genuchten (2)	100	0.45	0.01	1.0	1500	0.05
1.58 – 1.59 drying	Van Genuchten (3)	30.0	0.15	0.0	1.0	—	—
1.58 – 1.59 wetting	modified van Genuchten (4)	2.0	0.10	0.01	0.99	1000	1.3

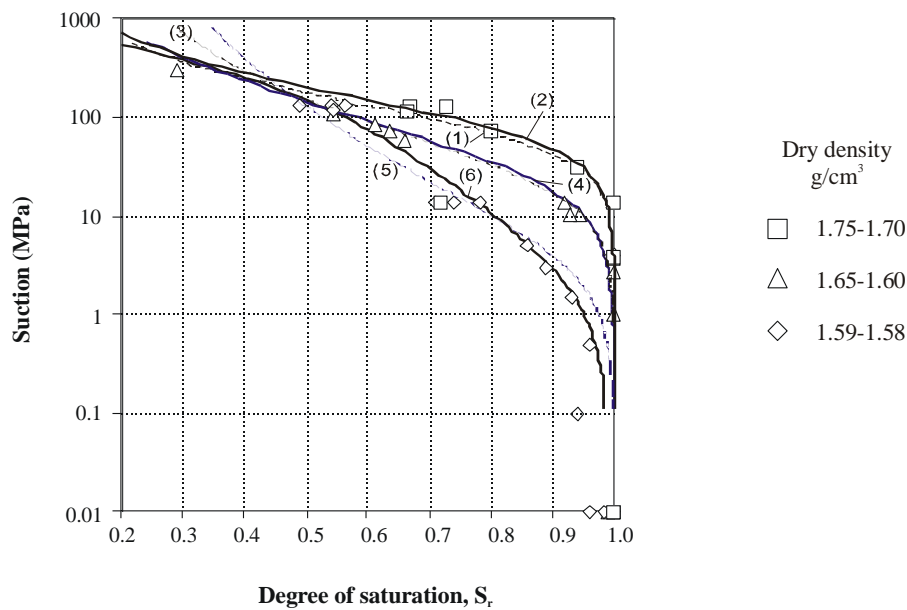


**Figure 1-14** Measured and fitted retention curves in wetting paths performed on confined samples. In parentheses, the number of the equation used in Table 1-8 is shown (ENRESA, 2000)

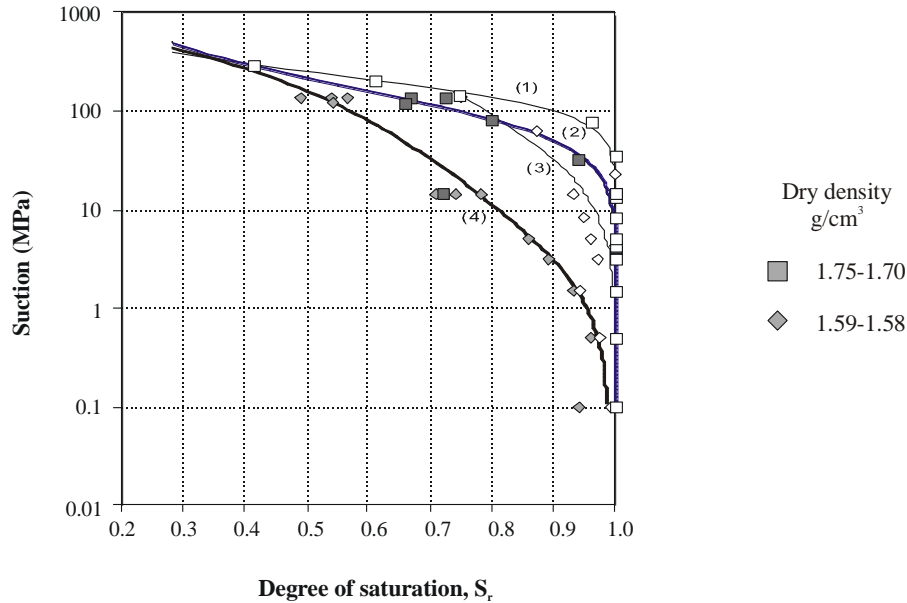


**Figure 1-15** Hysteresis effect on the wetting-drying paths under confined conditions. Bold symbols correspond to wetting paths. In parentheses the numbers of the curves indicated in Table 1-9 (ENRESA, 2000)

### Gas permeability

The gas permeability of the compacted clay has been determined using nitrogen gas as a fluid, injected at a low pressure. Specimens of nominal dry densities ranging from 1.50 to 1.70 g/cm<sup>3</sup> and with different water contents have been tested. The values obtained are plotted in Figure 1-16 together with the fitting obtained (valid only for the degree of saturation between 25 and 80 %):

$$K_g = 3.164 \cdot 10^{-6} [e(1 - S_r)]^{4.3} \quad (r^2 = 0.82, 39 \text{ points}) \quad (1.11)$$

where  $K_g$  (m/s) is the gas permeability,  $e$  the void ratio and  $S_r$  the degree of saturation.

The gas permeability for the same degree of saturation is a function of dry density and decreases with the degree of saturation, for the same dry density. In tests performed with the bentonite equilibrium water content compacted to different dry densities it was observed that gas permeability decreases logarithmically with increasing dry density.

In all of the tests performed, the values of intrinsic permeability obtained (which ranges between 10<sup>-16</sup> and 10<sup>-12</sup> m/s) are higher than those obtained when intrinsic permeability is calculated from hydraulic conductivity tests conducted with the clay under saturated conditions (Figure 1-17). This is due to the different structural disposition of the saturated and unsaturated specimens, caused by swelling of the clay as it hydrates. In water flow tests performed under saturated and confined conditions, the bentonite tries to swell and fill the interaggregate pores. Under these conditions, mean pore diameter is close to intra-aggregate pore size (about 0.01 μm). In the case of gas flow under dry conditions, this flow takes place through interaggregate pores with a diameter of more than 1 μm. This difference in accessible pore size may explain the different values of intrinsic permeability that have been derived from water and gas flow.

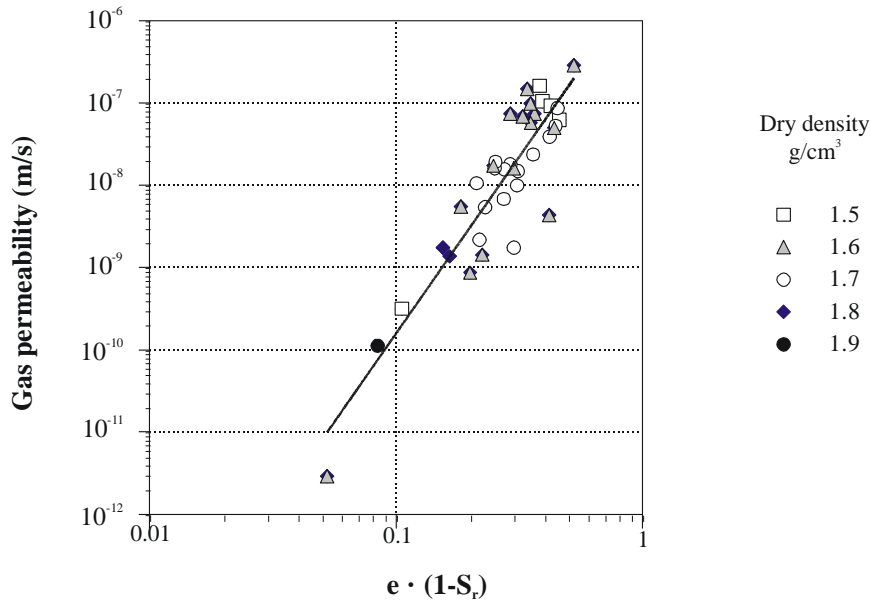


**Figure 1-16** Gas permeability measured in specimens of FEBEX bentonite compacted to different dry densities and with varying water content (ENRESA, 2000)

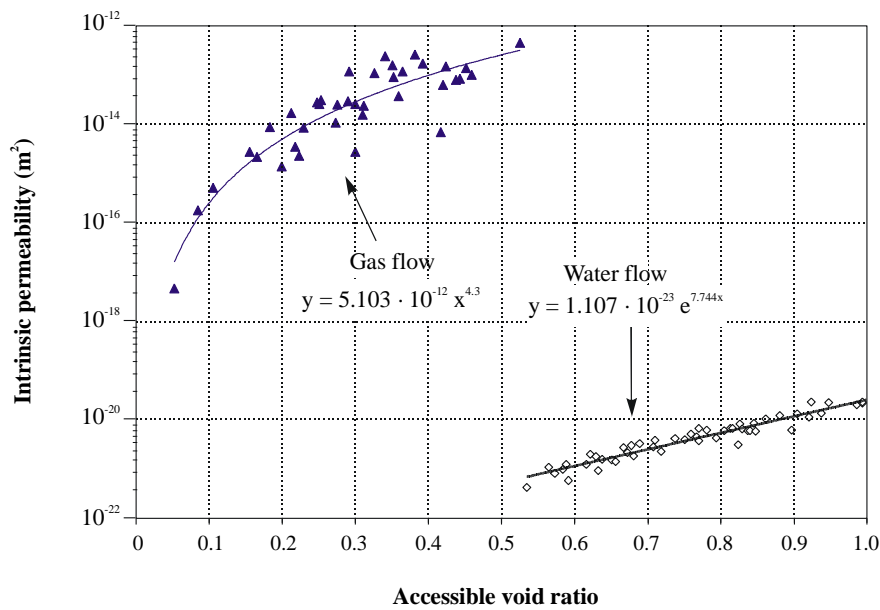


**Figure 1-17** Intrinsic permeability of the compacted clay obtained from saturated water flow and from unsaturated gas flow tests. In gas flow tests, the accessible void ratio indicates the ratio between gas accessible pore volume and particle volume ( $e(1-S_r)$ ) (ENRESA, 2000)

### 1.2.3 Thermal properties

#### Specific heat

Specific heat has been determined only for bentonite S-2. The relationship between specific heat and temperature fit the following equation, in a range of temperatures of between 45°C and 150°C:

$$c_s = 1.38T + 732.5 \tag{1.12}$$

where  $c_s$  is the specific heat, in J/kg°C, and  $T$  is the temperature, in °C.

**Thermal conductivity**

The superficial thermal conductivity of the FEBEX bentonite has been determined in compacted specimens at various nominal dry densities and with different water contents.

Figure 1-18 shows the regression curves of the values of superficial thermal conductivity as a function of the degree of saturation, for bentonites S-2 and FEBEX. A good correlation of the sigmoidal type (Boltzmann) was obtained for the two bentonites by means of the following equation:

$$\lambda = A_2 + \frac{A_1 - A_2}{1 + e^{(S_r - x_0)/d_x}} \tag{1.13}$$

where  $\lambda$  is the thermal conductivity, in W/m<sup>2</sup>·K,  $S_r$  is the degree of saturation,  $A_1$  is the value of  $\lambda$  for  $S_r = 0$ ,  $A_2$  is the value of  $\lambda$  for  $S_r = 1$ ,  $x_0$  is the degree of saturation for which the thermal conductivity is the average value between the extreme values, and  $d_x$  is a parameter. Table 1-10 shows the parameters obtained in the fitting of the curves.

There is a difference between the values measured for FEBEX and S-2 bentonite (see Figure 1-18). This difference is more noticeable for lower values of the degree of saturation. No clear evaluation of the differences is possible, because thermal conductivity increases not only with the water content but also with dry density. In addition, for the bentonite S-2, there are only two points for the lower degrees of saturation. However, taking into account all the experimented points, differences between the two bentonites seem to be small.

**Table 1-10** Parameters for fitting of the drying paths after saturation (ENRESA, 2000)

parameter	bentonite S-2	FEBEX bentonite
$A_1$	0.39 ± 0.08	0.57 ± 0.02
$A_2$	1.34 ± 0.06	1.28 ± 0.03
$x_0$	0.54 ± 0.03	0.65 ± 0.01
$d_x$	0.15 ± 0.03	0.10 ± 0.02

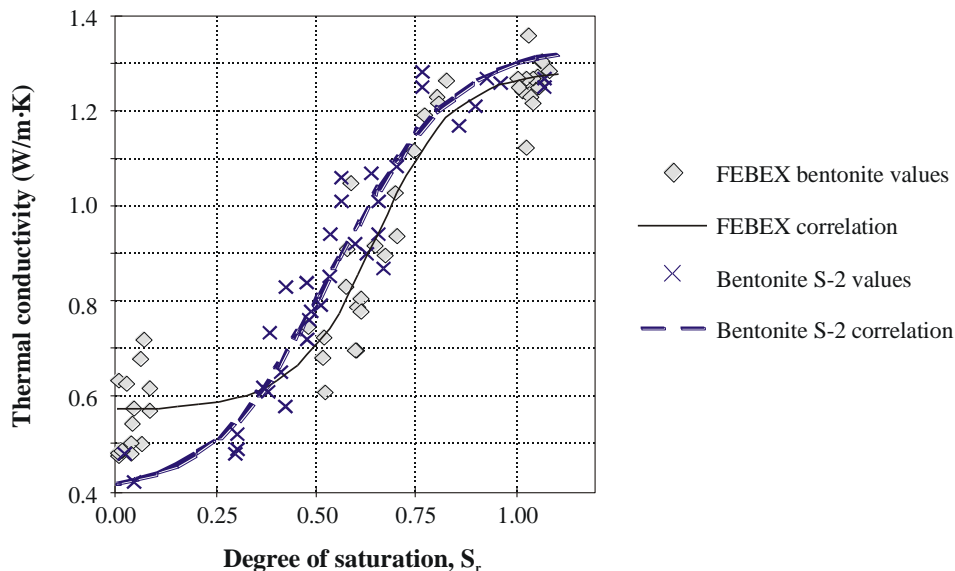


**Figure 1-18** Thermal conductivity as a function of degree of saturation (ENRESA, 2000)

**Coefficient of linear thermal expansion**

Measurements of thermal expansion have been carried out on 12 samples of compacted bentonite for initial dry densities ranging between 1.57 and 1.72 g/cm<sup>3</sup> and a water content varying between 12.5 and 25.1 %. The specimens (38 mm in diameter, 76 mm in height) were placed in an isothermal bath with controlled temperature. A latex membrane keeps the overall water content of the soil constant throughout the heating and cooling processes. Temperature varies between 25 and 70 °C. In each test, several cycles of heating and cooling are applied to the sample.

The vertical strains in the first heating path are higher than the strains measured during the second and subsequent cycles. In addition, in each cycle the strains measured during the heating process are higher than those observed throughout the cooling path and, as a result, an accumulation of irreversible strains is observed. The slope of the relationship between temperature and strain is shown in Figure 1-19. This slope increases slightly with temperature. The following correlations for the linear thermal expansion coefficient have been obtained from this figure:

$$\Delta \varepsilon_z / \Delta T = \begin{cases} -0.118 \times 10^{-4} + 6.5 \times 10^{-6} T & \text{(first heating paths)} \\ -1.265 \times 10^{-4} + 6.5 \times 10^{-6} T & \text{(subsequent heating paths)} \\ -1.538 \times 10^{-4} + 6.5 \times 10^{-6} T & \text{(cooling paths)} \end{cases} \quad (1.14)$$

where  $\varepsilon_z$  is the linear strain and  $T$  the temperature in °C. At temperatures higher than 55°C, an increase in the dispersion of the results is observed. This dispersion is due to experimental difficulties, such as equipment calibration and specimen sealing.

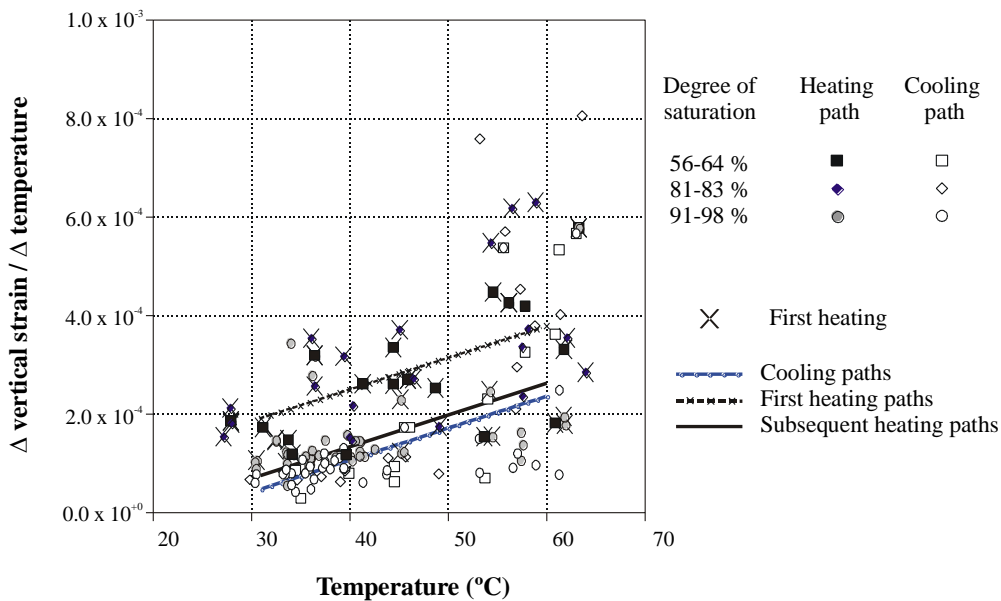


Figure 1-19 Linear thermal expansion as a function of temperature (ENRESA, 2000)

**1.3 Thermo-hydro-mechanical tests**

**1.3.1 Tests for calibration of models by backanalyses. Thermohydraulic cell.**

A general methodology has been developed for the performance of systematic backanalysis of laboratory tests involving the thermohydraulic behaviour of bentonite. The procedure is based on a maximum likelihood approach, which defines a probabilistic framework in which error measurements and the reliability of the parameters identified can be estimated. With a view to identifying the model parameters, an objective function incorporating the differences between measured data and model computations is minimized. The method is applied to the identification of certain thermal and

hydraulic properties of a bentonite specimen, using temperature and water content measurements as input data. The finite element code “CODE BRIGHT” (V2.0) has been used to model the thermohydraulic behaviour of clay. Although the code allows the mechanical behaviour of soils to be studied in a coupled manner, only the thermal and water flow capacities of the code have been used.

A new testing device has been developed to obtain the data required for the identification of certain thermohydraulic parameters. A controlled heat flux is applied at one end of a cylindrical specimen (38 mm in diameter, 76 mm long) and the other end is maintained at constant temperature. A latex membrane, that allows deformation and keeps overall water content constant, and a 5.5 cm thick heat insulating deformable foam surrounds the specimen. In order to ensure knowledge of the heat flux crossing the sample, two specimens symmetrically placed with respect to the heater are used in the tests. The heater is a copper cylinder (38 mm diameter, 50 mm long) with five small electrical resistances inside. A constant power of 2.6 W has been used in the tests, allowing steady temperatures in the range of 70-80 °C to be reached at the hotter end of the specimen. At the cold end, a constant temperature of 30°C is maintained by flowing water in a stainless steel head in contact with the soil. Figure 1-20 shows a scheme of the thermohydraulic cell.

Axisymmetric analyses performed with CODE BRIGHT allowed the effect of lateral loss of heat to be evaluated. It was estimated as 60% of total heater power. This indicates the importance of performing a 2D analysis of the experiment.

During the tests, the temperatures at both ends of the specimen, and at three internal points located at regular intervals, are monitored. At the end of the tests, changes in diameter were measured at some points of the specimen, with an accuracy of up to 0.01 mm. Finally, the soil samples were cut in six small cylinders and the water content of each slice was determined.

Three specimens of bentonite compacted at a dry density of 1.68 g/cm<sup>3</sup> and with water contents of 15.3, 16.9 and 17.1 % were tested. The temperatures measured during the heating period for one of the specimens are shown in Figure 1-21. Temperature reaches a quasi-steady regime 10 hours after the start of the test.

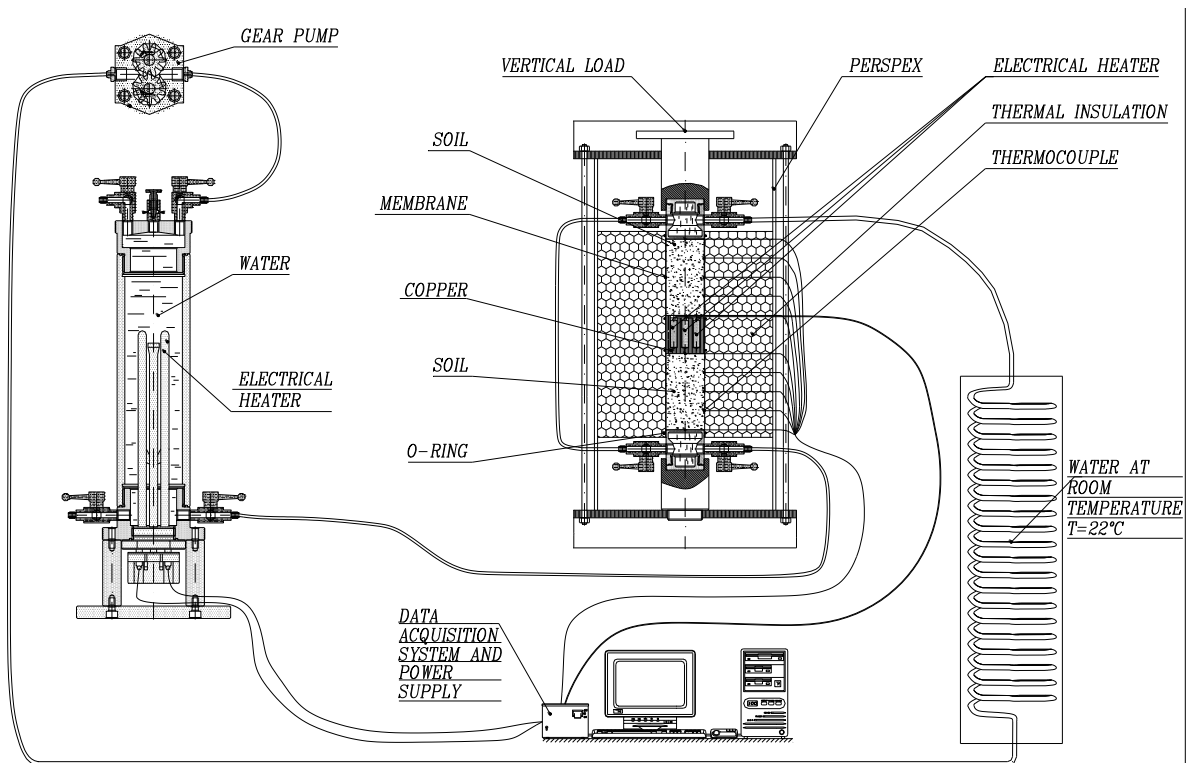
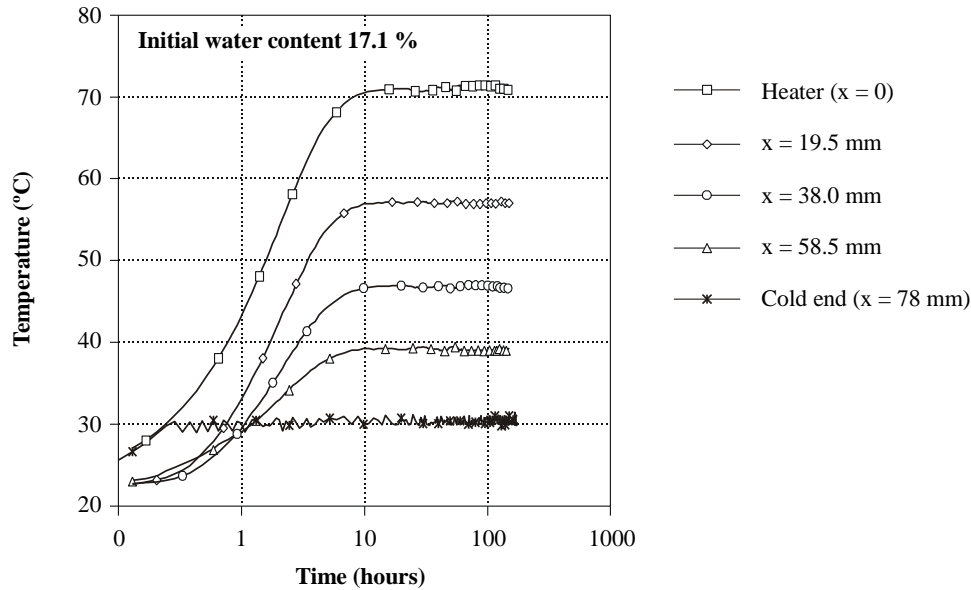


Figure 1-20 Scheme of the thermohydraulic cell



**Figure 1-21** Evolution of temperature in a prescribed heat flow test (ENRESA, 2000)

A fully coupled thermo-hydraulic model has been used to simulate the experiment. The temperatures obtained under steady-state conditions and the water content measured at the end of the test have been considered as input data. In each test, three parameters have been identified: the conductivity of bentonite under saturated conditions,  $\lambda_{sat}$ , needed to obtain unsaturated thermal conductivity ( $\lambda = (\lambda_{sat})^{S_r}$  ( $\lambda_{dry})^{(1-S_r)}$ ); the tortuosity,  $\tau$  (a parameter of the diffusion constant) and the exponent “n” for the unsaturated (relative) permeability law ( $k_r = S_r^n$ ). The thermal conductivity under dry conditions ( $\lambda_{dry}$ ) is fixed at 0.47 W/m°C. The parameters obtained during the identification process are similar but not identical in the three tests, as shown in Table 1-11. The values are within the normal range of these parameters. In addition, the identification technique provides a systematic and consistent procedure allowing the parameters that best reproduce the measurements for the selected model to be found. The method also gives an insight into the model structure, and allows the dependence and coupling between parameters to be detected. In the present type of test, analysis of the model structure shows that the values of the parameter “n” that has been obtained entail a higher degree of uncertainty than the values of the other parameters. This is in accordance with the relative influence of water flow in liquid and vapour phases.

**Table 1-11** Exponent n in relative permeability law, tortuosity factor  $\tau$  and saturated thermal conductivity  $\lambda_{sat}$  obtained from different thermal flow tests (ENRESA, 2000)

test	water content	n	$\tau$	$\lambda_{sat}$ W/m°C
1	15.5	3.06	0.56	1.19
2	16.9	1.10	0.74	1.31
3	17.1	1.08	0.90	1.18

The optimization procedure showed that there are a few combinations of parameters that give similar result in terms of the objective function. This is reasonable, as measured water content is a global quantity, and it is difficult to distinguish between water transported by liquid flow (controlled by “n”) and by vapour diffusion (controlled by  $\tau$ ).

Figure 1-22 shows the objective function in terms of the tortuosity factor  $\tau$  and the exponent “n” for the relative permeability law, for one of the controlled heat flow tests. In order to give the same importance to the sets of measurements for temperature and water content, a weighting procedure has been used

to define the objective function. Contours are isolines of the objective function with different combinations of the parameters. The parameter values obtained by backanalysis are located at the minimum of the objective function. The same figure includes points representing the values of the parameters obtained in the other backanalyzed tests. In the case of the hydraulic tests described in Section 0 only the exponent “n” is known. In all cases, the representative points are located in the same area of the objective function, with similar values of error. A set of optimum parameters and laws (see Table 1-12) may be selected taking all the tests into account.

**Table 1-12** Values for the saturated hydraulic conductivity  $k_{sat}$ , the relative permeability  $k_r$ , the tortuosity factor  $\tau$  and the thermal conductivity  $\lambda$  (ENRESA, 2000)

parameter	Value
$k_{sat}(\text{porosity} = 0.4)$	$2 \cdot 10^{-21} \text{ m}^2$
$k_r$	$S_r^3$
$\tau$	0.8
$\lambda(\text{W/m}^\circ\text{C})$	$0.47^{1-S_r} 1.15^{S_r}$

This set of parameters has been used to solve the direct problem and to simulate some water infiltration and heat flow tests. Figure 1-23 to Figure 1-26 show that the agreement between the measurements and the model computations is satisfactory.

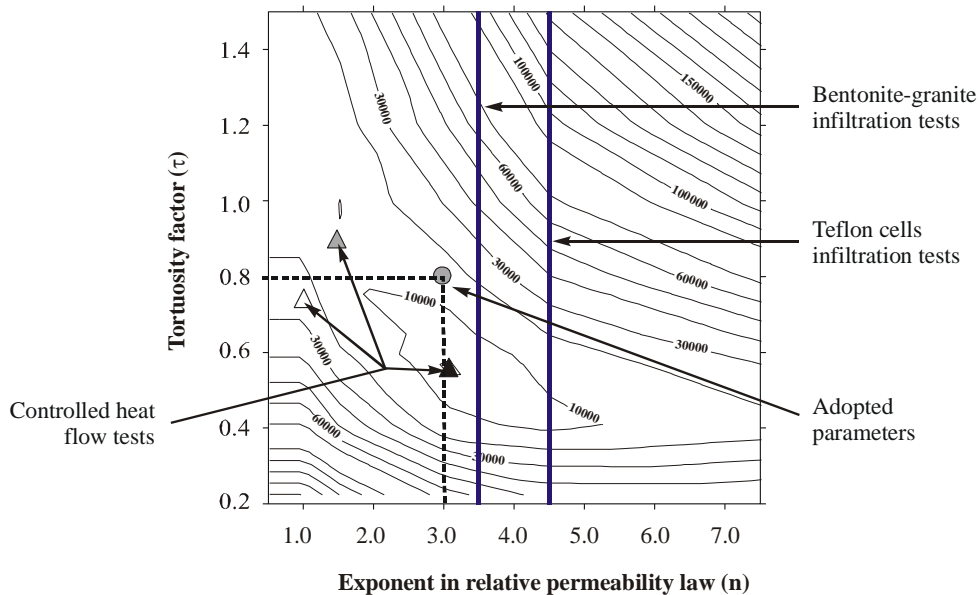


**Figure 1-22** Contour map of objective function in the case of thermal flow test 1. The same graph shows the parameter values obtained by backanalyzing different tests (ENRESA, 2000)

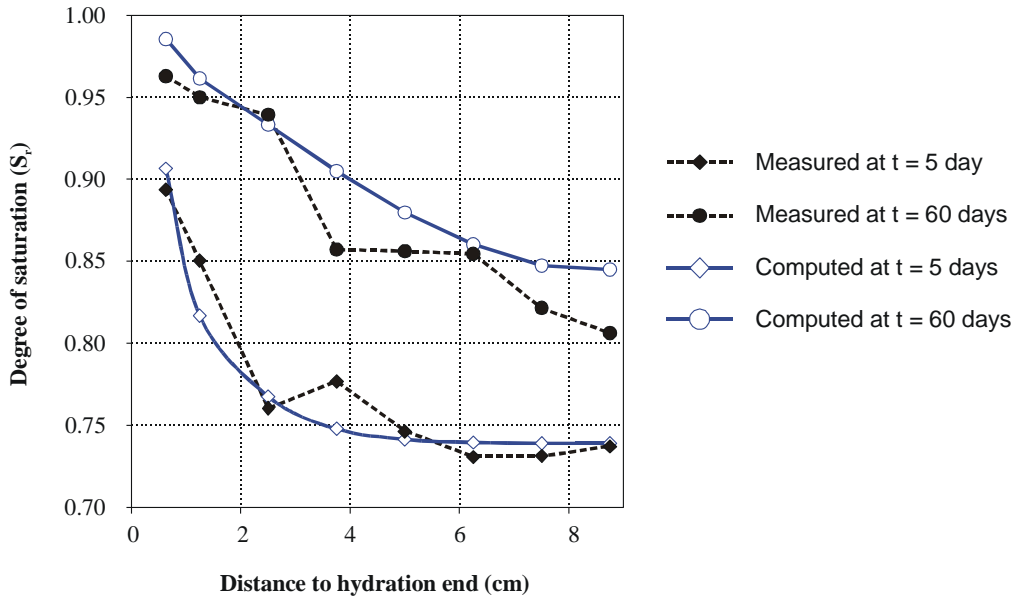


**Figure 1-23** Measured and computed degree of saturation in small cell infiltration tests carried out in CIEMAT, using the final selected parameters (ENRESA, 2000)

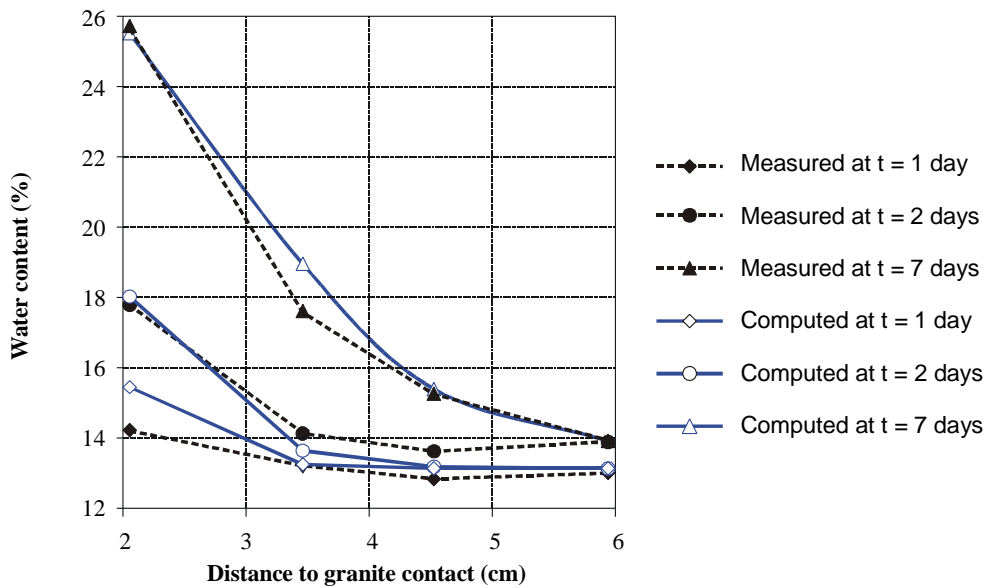


**Figure 1-24** Measured and computed water content in bentonite-granite infiltration tests carried out at UPC, using the final selected parameters (ENRESA, 2000)

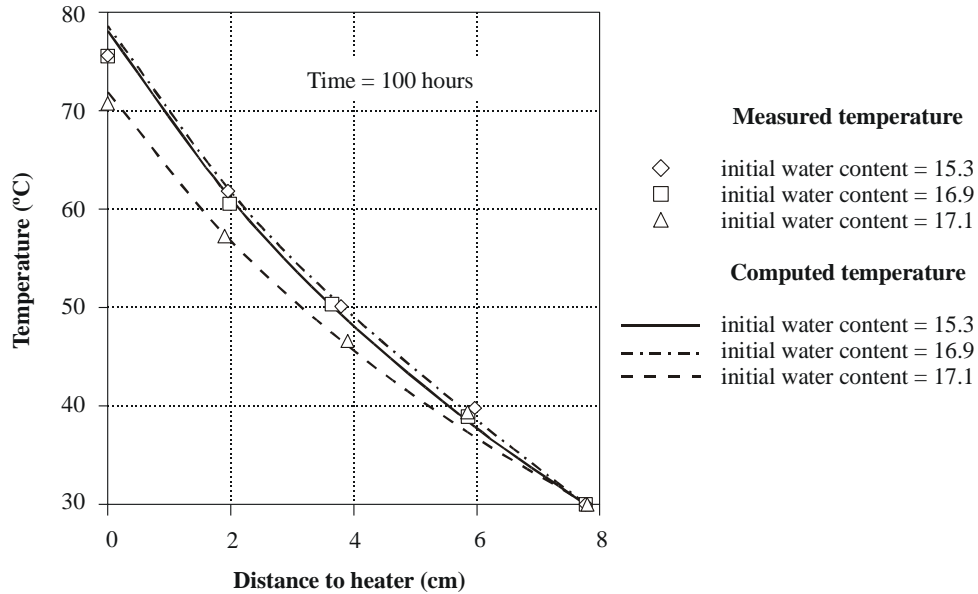


**Figure 1-25** Measured and computed temperature in prescribed heat flow tests, using the final selected parameters (ENRESA, 2000)

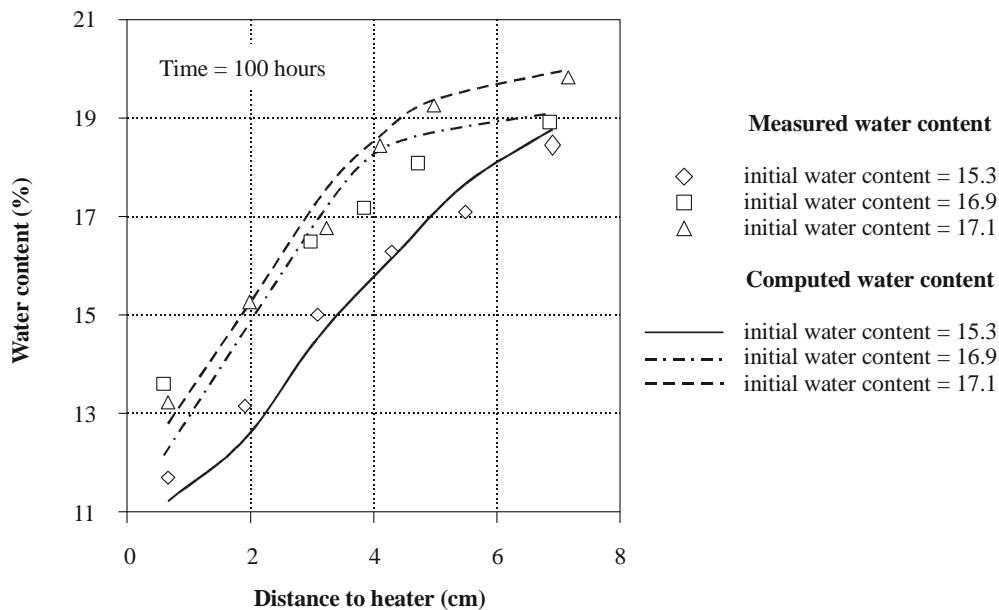


**Figure 1-26** Measured and computed water content in prescribed heat flow tests, using the final selected parameters (ENRESA, 2000)

### 1.3.2 Mechanical properties: oedometer tests with controlled suction

Suction controlled oedometer tests have been performed at CIEMAT (24 tests) and UPC (5 tests) on compacted bentonite with a water content in equilibrium with the laboratory conditions, and at dry densities of 1.7 and 1.65 g/cm<sup>3</sup> respectively. Three types of paths have been followed. In the first type, simulating the behaviour of a point near the heater, an initial drying process is followed by a loading path, and finally the bentonite is saturated. In the second type, simulating a point near the external boundary, an initial path of suction decrease is followed by an increase in load. In the third case, aimed at reproducing a swelling pressure test, an attempt was made to maintain the height of the sample constant during a suction reduction path by applying increments of vertical load. Suction is applied,

with the relative humidity of the air on the sample being controlled by means of sulphuric acid or salt solutions in the high suction range, and by the axis translation technique in the case of suctions ranging from 0 to 14 MPa.

Figure 1-27, reproduces the results of two of the tests carried out at CIEMAT (EDS3\_9 and EDS5\_5). The volume changes measured reflect the typical behaviour of compacted clay. It may be observed that for a small value of vertical load the vertical strains on saturation are higher than when a high load is applied. At the same time, the strain under the loading path is higher when the soil is in saturated conditions after reaching important swelling strains. Figure 1-28 and Figure 1-29 show the experimental results in the case of suction decrease paths with different values of applied vertical load and load increase paths with different values of applied suction.

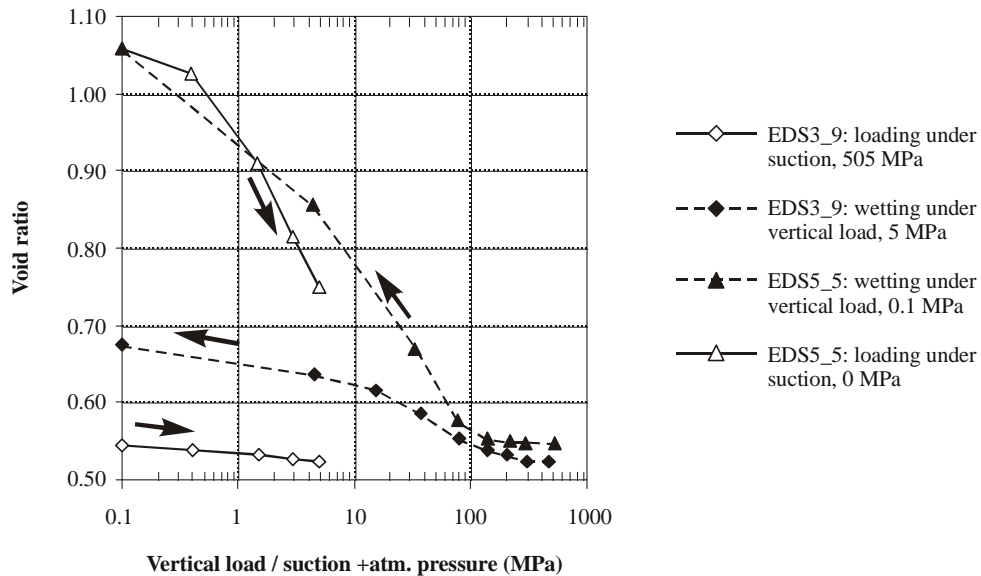


**Figure 1-27** Typical results in two suction controlled oedometer tests on compacted bentonite with an initial density of  $1.7 \text{ g/cm}^3$  (ENRESA, 2000)

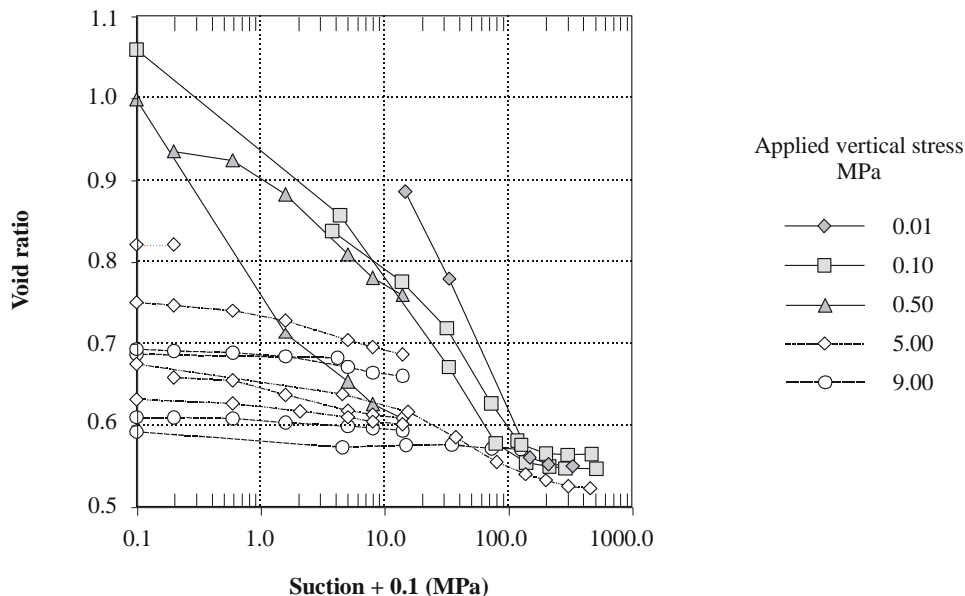


**Figure 1-28** Volume changes measured in suction controlled oedometer tests, in wetting paths under different loads. Initial dry density  $1.7 \text{ g/cm}^3$  (ENRESA, 2000)

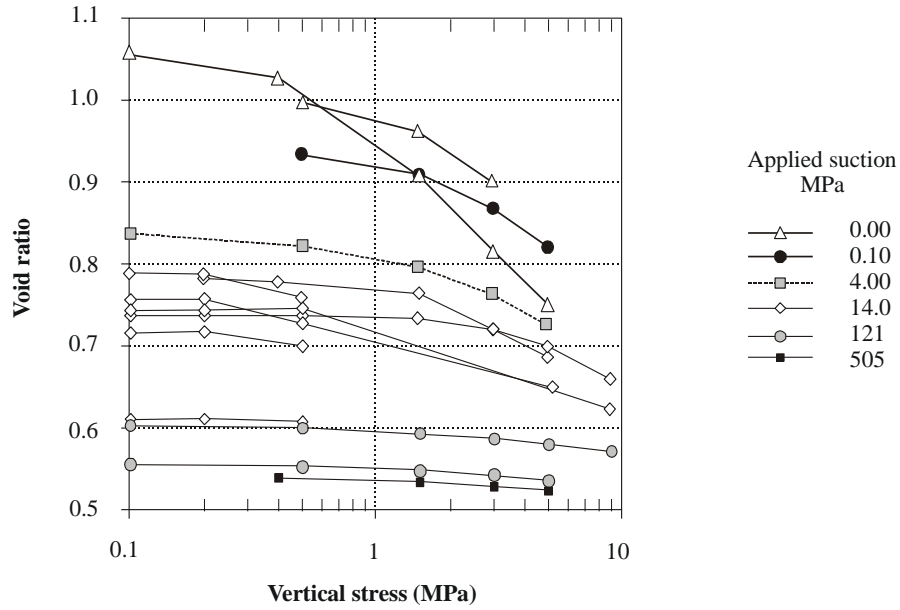


**Figure 1-29** Volume changes measured in suction controlled oedometer tests, in loading paths under different suctions. Initial dry density  $1.7 \text{ g/cm}^3$  (ENRESA, 2000)

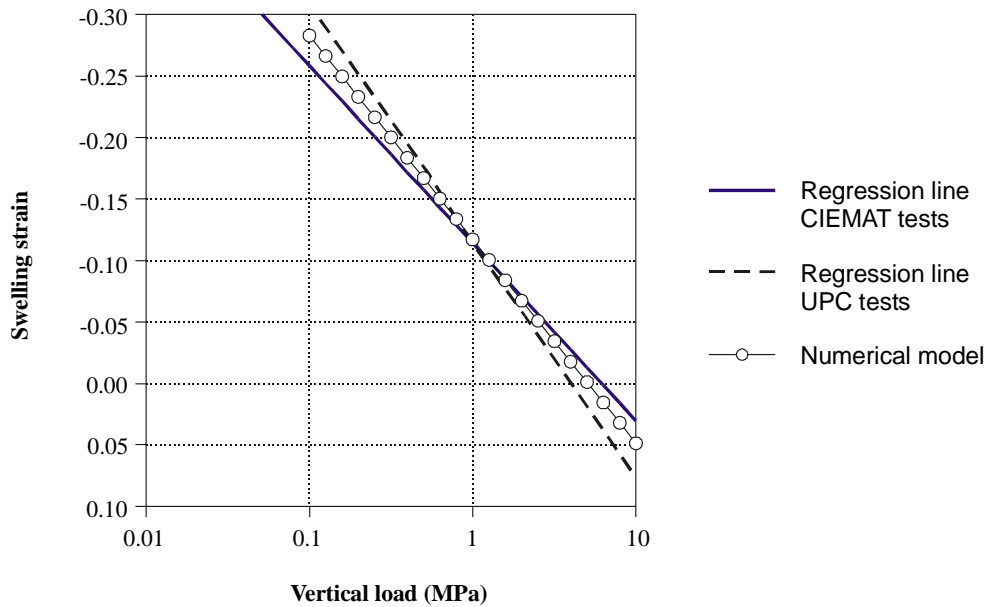


**Figure 1-30** Comparison between swelling strains measured at the CIEMAT and UPC laboratories and computed strains obtained from constitutive equations used in numerical modelling (initial dry density  $1.60 \text{ g/cm}^3$ ) (ENRESA, 2000)

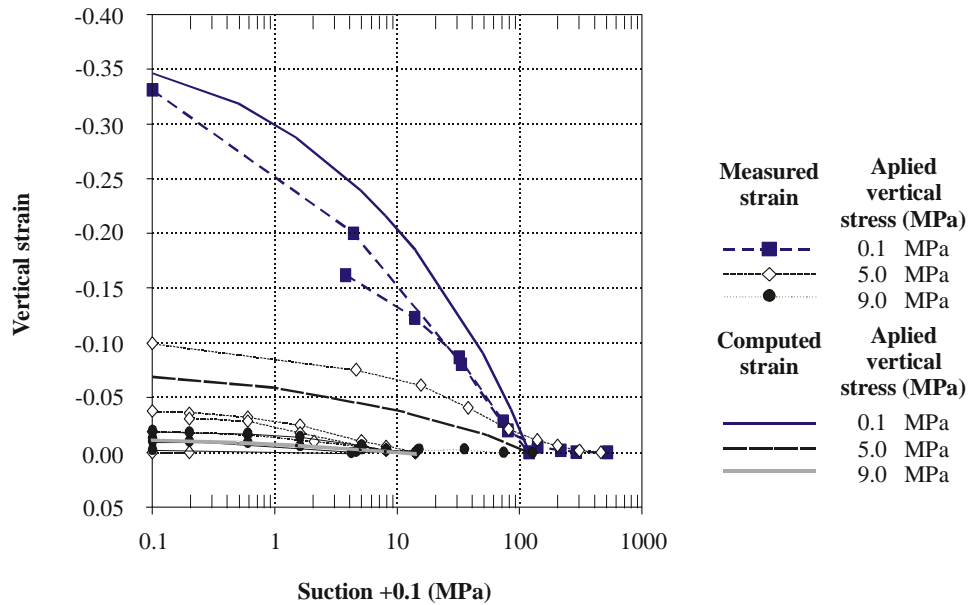


**Figure 1-31** Comparison between swelling strains measured in suction controlled oedometer tests performed by CIEMAT and computed strains obtained from constitutive equations used in numerical modelling (ENRESA, 2000)

In order to find the hydromechanical parameters of the constitutive model of the bentonite, tests were simulated by means of a numerical tool (CODE BRIGHT). A trial and error technique was used to reproduce the results of both the swelling pressure and swelling under load tests described in Appendix Section 1.2.1 (pages 82 and 83, paragraphs “Swelling pressure” and “Swelling under load”). Figure 1-30 shows a comparison between the numerical model output and the swelling strains measured at the CIEMAT and UPC laboratories.

Using the parameters obtained from the swelling tests, the suction controlled oedometer tests may be modelled as a boundary value problem, using CODE BRIGHT. Figure 1-31 shows the results of both experimental and numerical model results in the case of wetting paths under different values of applied vertical stresses.

Some general comments may be made concerning the behaviour of the clay when subjected to different stress paths:

- As a result of equipment limitations, the compaction load of the specimens (about 20 MPa) has been higher than the highest external load applied in the oedometers (9 MPa). Furthermore, the samples have shown minor collapse (with suction decreasing to values of between 15 and 5 MPa) only when a high vertical load (9 MPa) is applied.
- High swelling strains have been measured in suction reduction paths in response to minor vertical stresses. The hydration process opens the bentonite structure (pore volume increases) developing irreversible swelling strains, and subsequently an important decrease in stiffness is measured when a vertical load is applied. In these cases, a yield point in the loading paths may be observed at relatively small vertical loads (Figure 1-29).
- Drying of the sample beyond suctions of 120 MPa, does not imply a significant decrease in volume. Furthermore, under suctions higher than this value the external load does not produce any important consolidation of the sample, which remains very stiff. After a drying/wetting cycle the swelling pressure of the clay remains almost unchanged, in keeping with the fact that plastic strains are small in suction increase paths.

### 1.3.3 Tests to advance knowledge of the THM behaviour of expansive clays

#### Hydraulic tests on joints

Hydraulic tests were performed on specimens in which joints were present, to gain insight into the influence of the joints of the clay barrier on its hydraulic behaviour. The analysis included mainly the

influence of joints on hydration rate, their sealing capacity (see Figure 1-32) and the modification that they induce on hydraulic conductivity. Different cylindrical cells with water inlet/outlet were used. The specimens were made from four compacted bentonite slices (with final dry densities ranging between 1.61 and 1.23 g/cm<sup>3</sup> and initial water content ranging between 15.0 and 11.7%), some with vertical joints.

The main conclusions of this study are as follows:

- When hydration occurs under a given injection pressure, even if it is low, the volume of water taken up and its distribution inside the clay is controlled by the existence of joints (fissures), their volume and their configuration.
- The clay of the specimens takes the water both from the direct hydration surface and from the block joints. Figure 1-33 shows the final distribution of water content in two hydrated tests, in which four half-sectioned specimens were piled and hydrated from the top, illustrating this observation.
- The volume of water initially taken up depends on hydration pressure.
- Once the joints have been filled with water, the rate of water intake appears not to depend on injection pressure but on the dry density of the clay.
- The sealing of a joint, attained after hydration for 24 hours, is effective against hydraulic pressures of up to 5 MPa.
- Before sealing of the joints is attained, the strain experienced by every slice on saturation is the strain which corresponds to its initial dry density.



*Figure 1-32 Perspex cell used in joint sealing tests*

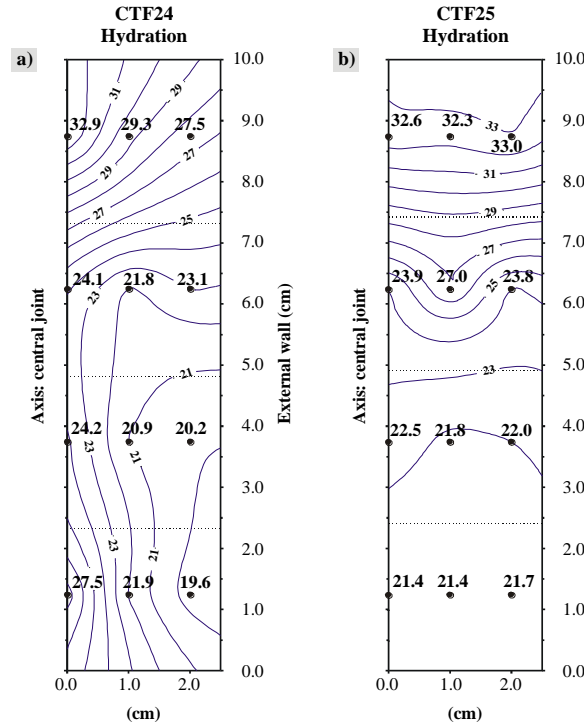


Figure 1-33 Water content distribution of the clay after two sealing tests (piling of four slices) performed under a hydration pressure of 0.5 MPa and lasting a) 1 day, b) 7 days (half section) (ENRESA, 2000)

**Suction and temperature controlled oedometer tests**

Four oedometer tests including suction decrease and increasing vertical load paths have been performed by CIEMAT at temperatures of 40 and 60 °C on bentonite compacted at a water content in equilibrium with laboratory conditions and at dry densities of 1.7 and 1.6 g/cm<sup>3</sup>. Figure 1-34 shows the evolution of the void ratio during wetting paths starting at a low range of suction (14 MPa), under a vertical stress of 5MPa, and at a high range of suction (120-450 MPa), under a vertical load of 0.1 MPa. Figure 1-35 shows the comparison curves measured at different combinations of suction and temperature, which were maintained constant during the test.

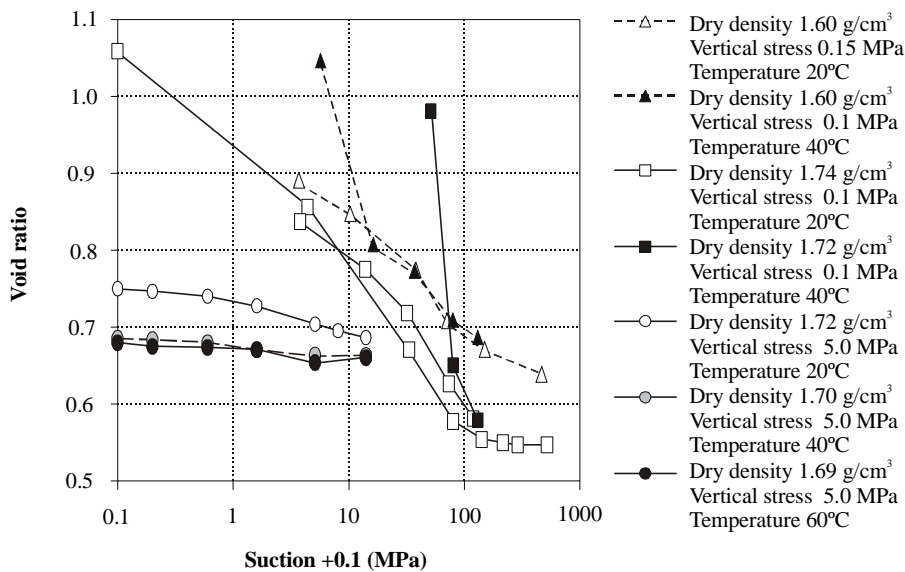


Figure 1-34 Wetting paths in suction controlled oedometer tests carried out at different temperatures (ENRESA, 2000)

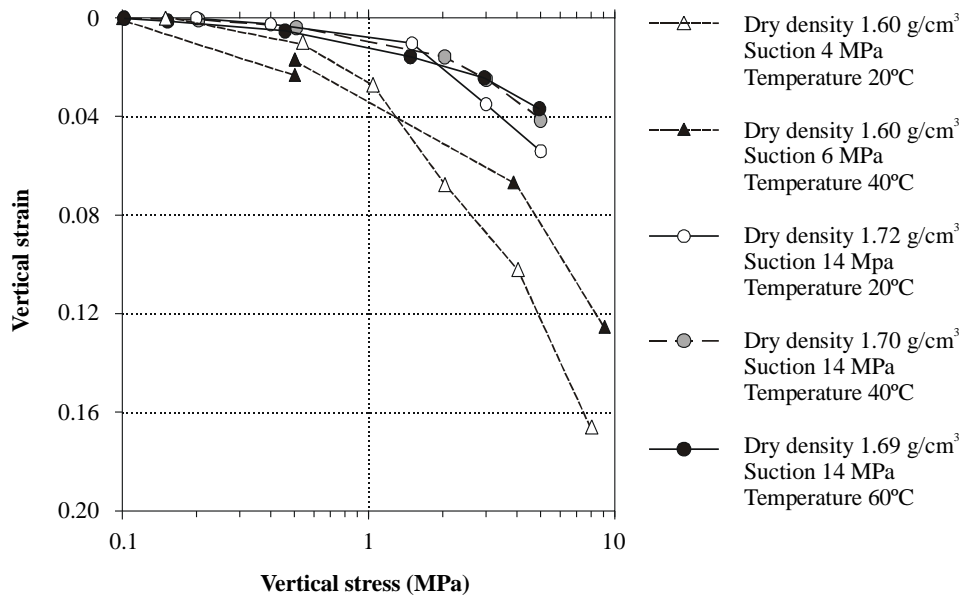


Figure 1-35 Loading paths in suction controlled oedometer tests carried out at different temperatures (ENRESA, 2000)

### 1.3.4 Tests in thermo-hydraulic cells

The objective of these tests is to analyse the properties of the bentonite and its behaviour under conditions similar to those that will be found in a repository; that is, to subject the material simultaneously to heating and hydration, in opposite directions, for different periods of time.

The tests have been performed in cylindrical hermetic cells of different dimensions:

- Large cells, in which the thickness of the bentonite and the thermal gradient are similar to those of the real case, and the time length of tests are 0.5, 1 and 2 years. No results are yet available.
- Intermediate cells. As saturation will probably not be reached in the large cells, cells of intermediate dimensions have also been used. In these cells, a single bentonite block measuring 13 cm in height and 15 cm in diameter is heated at the top at 100 °C, while being simultaneously hydrated with distilled or granitic water at the bottom, with an injection pressure of 1 MPa (Figure 1-36). The initial dry density and water content of the bentonite are 1.65 g/cm<sup>3</sup> and approximately 14 %, respectively. The quantity of sample is sufficient to allow the bentonite to be sliced into five sections at the end of the test (Figure 1-37). Then, the bentonite porewater is extracted by squeezing techniques. In this way, physical and geochemical characterisation of the solid phase (dry density, water content, soluble salts, exchangeable cations) could be carried out. The test program is devised for study of the phenomena induced separately by the thermal front and the hydration front, and by the coupling of both fronts, in tests of equal duration. Some results are given in the next Section. The data obtained in these cells have been used to calibrate THG modelling.
- Small cells. In this case, the bentonite specimen measure only 2.5 cm in thickness and 5.0 cm in diameter (Figure 1-38). Saturation is reached after a few days, under an injection pressure of 1 MPa. This has allowed a large number of tests of different duration and conditions to be performed. The initial dry density of the bentonite was 1.65 g/cm<sup>3</sup> and the water content was at equilibrium value under the laboratory relative humidity conditions (around 14 %). Two sets of temperatures (60-35°C and 100-60°C) applied at the heating and hydration ends have been examined, in order to ascertain the effect of temperature on the observed processes. The influence of the chemistry of the hydration water on the processes observed has been verified by using two types of water: granitic and saline (Table 1-5). The saline water has a chemical composition similar to that of the bentonite porewater under saturated conditions, but it is simplified to include only the major elements. The duration of the tests has been related to



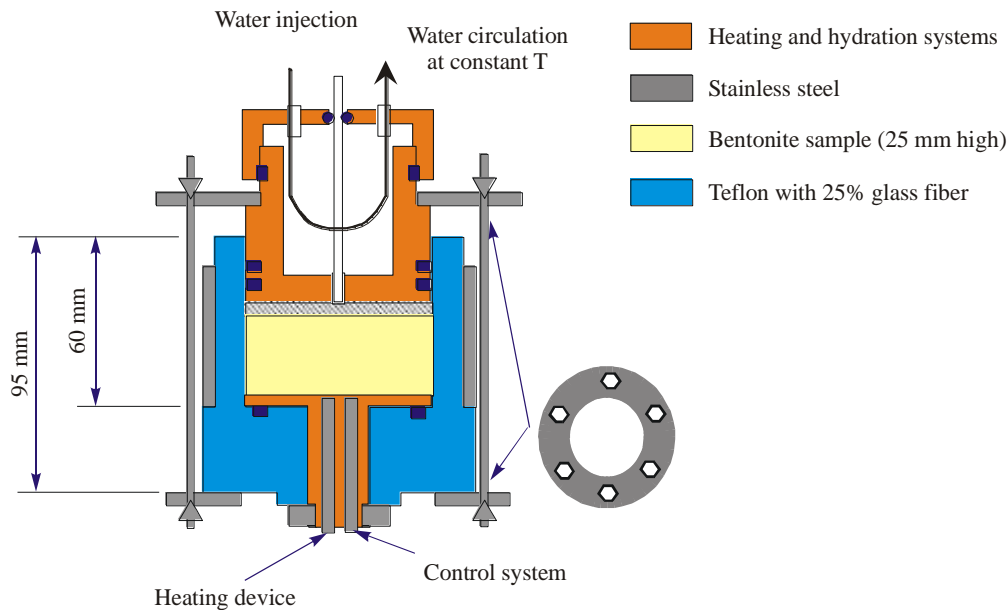


**Figure 1-38** Schematic design of the small cells for THG tests (ENRESA, 2000)

**Intermediate cells**

The main objective of these tests is to understand the fundamental mechanisms of water flow and solute transport occurring in a compacted bentonite subjected to simultaneous heating and hydration. Also, the chemical evolution of the bentonite porewater and the hydrogeochemical processes involved in the system (dissolution/precipitation and cation exchange reactions) are studied. Different tests have been performed, and some are still in progress (Table 1-13). The results presented belong to the transitory state, since saturated conditions have not been reached at the end of the thermohydraulic tests performed.

**Table 1-13** Tests performed with the intermediate cells

test number	test type	test time (days)	initial conditions				water uptake (cm <sup>3</sup> )
			mass (g)	$\rho_d$ (gcm <sup>3</sup> )	water content (%)	saturation degree (%)	
CT-22	heating + hydration	26	4298	1.65	13.4	56.7	275
CT-23	heating + hydration	183	4294	1.65	13.3	56.4	486
CT-24	heating	168	4690	1.62	26.5	100	---
CT-26	heating	147	4285	1.65	13.1	55.4	---
CT-27	hydration	148	4247	1.65	13.1	55.4	390
CT-28	heating + hydration	302	4315	1.65	13.9	58.8	
CT-30	hydration	302	4278	1.65	13.9	58.8	

Figure 1-39 and Figure 1-40 show the distribution of temperature and water content in each section analysed, for various tests. The heating source is at the top of the cell (at the right of the following figures) and the hydration supply is at the bottom (to the left of the figures).

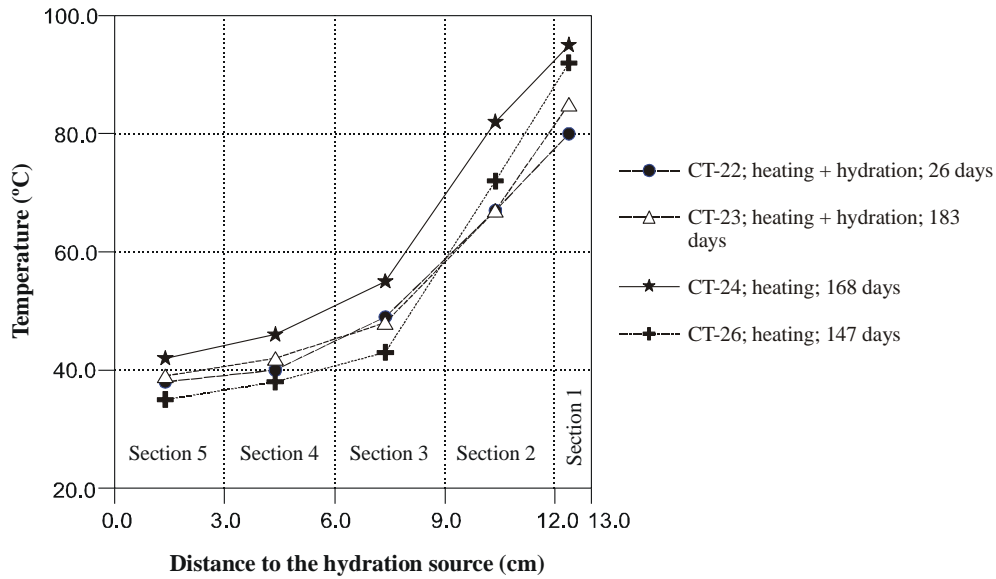


**Figure 1-39** Final temperature distribution in the intermediate cells tests (ENRESA, 2000)

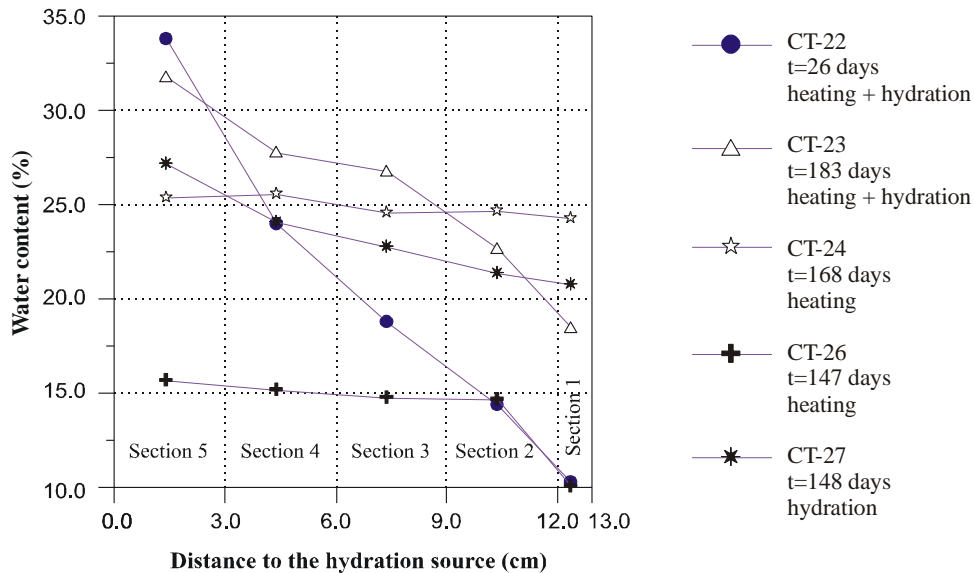


**Figure 1-40** Final water content distribution in the intermediate cells tests (ENRESA, 2000)

Significant changes in dry density, and therefore in porosity, are observed as hydration is induced in these experiments, probably due to the swelling of the bentonite (a slight deformation of the cell, with an increase of volume of the compacted bentonite block, was observed). Consequently, water contents (Figure 1-40) above the saturation water content of the bentonite block initially compacted to a dry density of 1.65 g/cm<sup>3</sup> (23.6 % of water content) were measured.



## 2 CRT - Material properties

### 2.1 Bentonite buffer

Below in Table 2-1 estimated averaged values for the different bentonite parts before the saturation phase are shown, a compact density of 2780 kg/m<sup>3</sup> has been used.

*Table 2-1 Initial conditions of the CRT experiment.*

Section	Density (kg/m <sup>3</sup> )	Water ratio	Dry density (kg/m <sup>3</sup> )	Void ratio	Degr. of saturation
Solid block	1991	0,172	1699	0,636	0,751
Ring shaped block	2087	0,171	1782	0,560	0,849
Bricks	1883	0,165	1616	0,720	0,637
Pellets I	1101	0,100	1001	1,778	0,156
Pellets II	1574	0,572	1001	1,778	0,895

### 2.2 Bentonite blocks

- MX-80
- Ring-shaped (Rx) or cylindrical (Cx)

Block name	Date of compaction (yy-mm-dd)	Water ratio	Density (kg/m <sup>3</sup> )	Weight (kg)	Average height (mm)	Degree of sat.	Void ratio
CRT NR R1	99-11-04	0.173	2091.9	1280.0	506.5	0.859	0.558
CRT NR R6	99-11-04	0.171	2102.7	1282.0	505.0	0.867	0.548
CRT NR R8	99-11-08	0.171	2099.8	1286.0	507.1	0.865	0.551
CRT NR R9	99-11-08	0.171	2098.3	1288.0	508.0	0.861	0.551
CRT NR R7	99-11-09	0.172	2099.5	1290.0	508.7	0.866	0.552
CRT NR R3	99-11-09	0.167	2102.7	1280.0	503.9	0.855	0.543
CRT NR R2	99-11-10	0.172	2095.4	1288.0	508.5	0.861	0.555
CRT NR R4	99-11-10	0.170	2116.3	1290.0	504.6	0.879	0.537
CRT NR R5	99-11-11	0.175	2086.5	1278.0	506.9	0.859	0.565
CRT NR R10	00-01-10	0.171	2069.1	1272.0	509.2	0.830	0.574
CRT NR C4	00-01-12	0.173	2016.4	2156.0	505.4	0.780	0.617
CRT NR C3	00-01-12	0.171	2004.8	2094.0	493.7	0.761	0.623
CRT NR C2	00-01-13	0.170	2003.1	2104.0	496.7	0.759	0.624
CRT NR C1	00-01-14	0.173	1987.7	2128.0	506.3	0.751	0.641

### 2.3 Bentonite pellets

- MX-80

- “Pillow-shaped”
- Width and length of 16.3 mm, thickness 8.3 mm.
- Bulk density of individual pellet 1970 – 2110 kg/m<sup>3</sup>.
- Water ratio ≈ 10 %



*Figure 2-1 Pellet geometry.*

## 2.4 Bentonite bricks

- MX-80
- Dimensions: 115×234×64 mm
- Average dry density: 1800 kg/m<sup>3</sup>
- Water ratio: ≈ 10 %

## 2.5 MX-80 properties

The used compact density of the bentonite is 2780 kg/m<sup>3</sup> /Börgesson et al., 1995/.

### 2.5.1 Thermal properties

The heat capacity  $c$  of the bentonite block and pellet-filled slot is  $c = 800 \text{ J}/(\text{m}\cdot\text{K})$ .

In /Börgesson et al. 1994/ the thermal conductivity of buffer materials was carefully characterized, and different models were compared. In Figure 2-2, taken from /Börgesson et al. 1995/, experimentally data of the thermal conductivity for MX-80 is given as a function of water saturation.

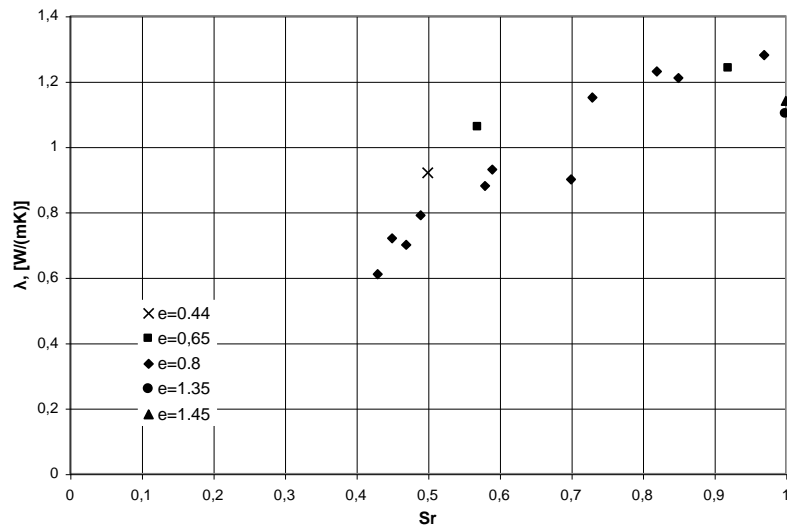


**Figure 2-2** MX-80 thermal conductivity as a function of the degree of saturation for different void ratios. From *Börgesson et al. (1995)*.

The work in /Börgesson et al. 1994/ concluded with a relation used in /Börgesson et al. 1995/ which is summarized in graphical form in Figure 2-3.

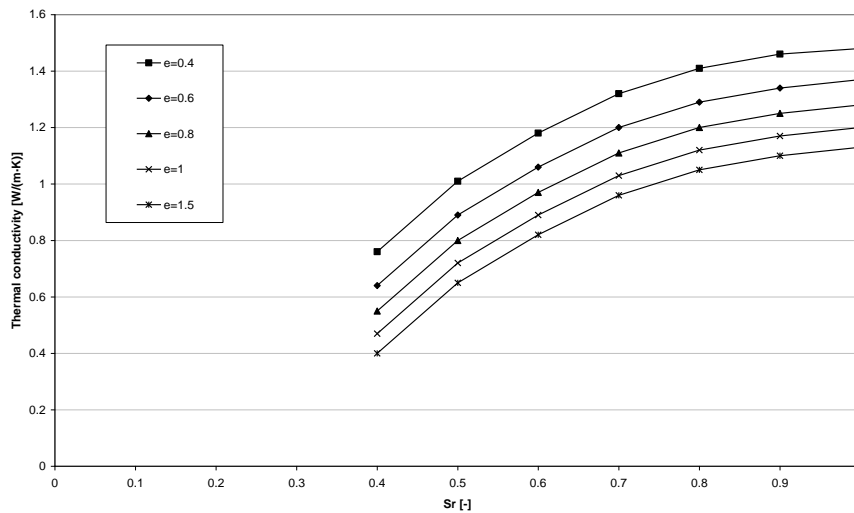


**Figure 2-3** Relation between void ratio, water saturation and thermal conductivity used in /Börgesson et al. 1995/.

In accordance with Figure 2-3 /Sugita et al., 2003/ found that the thermal conductivity for swollen pellets was slightly lower as compared to the thermal conductivity of blocks at comparable densities with the pellet cell. Figure 2-4 shows the results given in /Sugita et al., 2003/

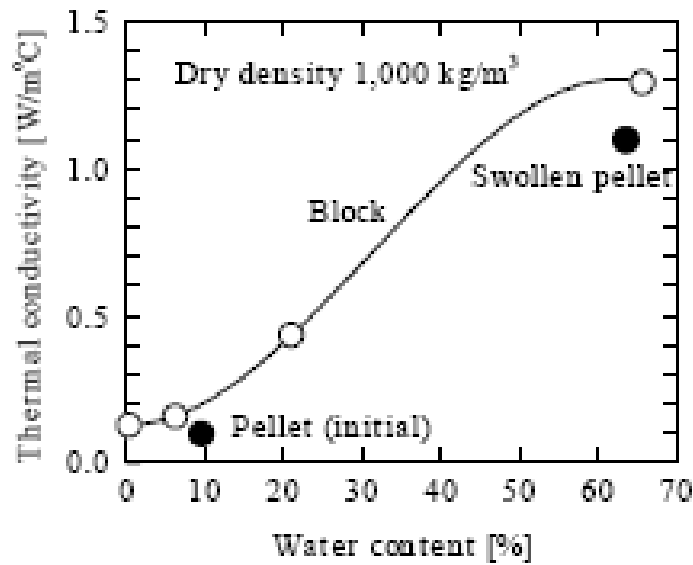


Figure 2-4 The thermal conductivity variation with water content for block and pellet. From Sugita et al. (2003).

### 2.5.2 Hydraulic properties

Figure 2-5 shows a compilation of experimental findings for the confined retention properties of MX-80 for a number of dry densities. The figure is taken from an earlier EBS task /EBS, 2005/ and is taken from an earlier EBS task. Below follows a short investigation of the retention.

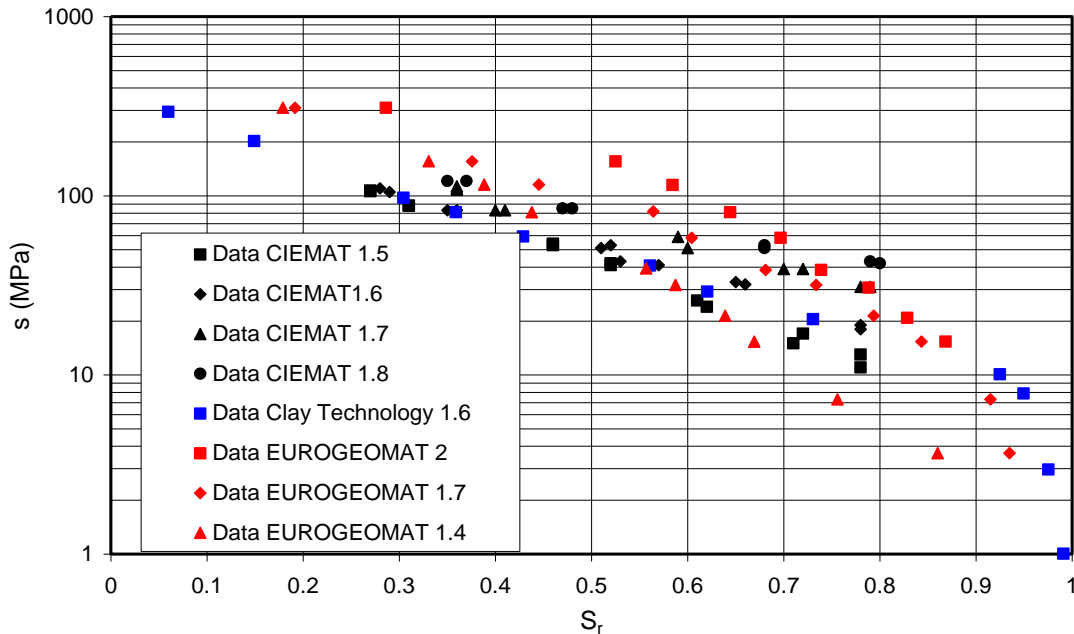


Figure 2-5 Retention of MX-80 at constant volume and several dry densities.

The retention of a free swelling sample can be estimated using the expression given below /Kahr et al. 1990/

$$S_{free}(w, w_0) = 1 \cdot 10^6 \exp(a(w_0) - b(w_0)w) \quad (1)$$



, where the constants  $a$  and  $b$  is dependent on the initial water ratio,  $w_0$ . Table 2-2 below show the constants  $(a,b)$ , taken from /Dueck 2007/, obtained for different initial water ratios  $w_0$ .

**Table 2-2**  $(a,b)$  parameter values in the retention expression for different initial water ratios.

$w_0$	0.100	0.175	0.270
$(a,b)$	( 6.3 , 16 )	( 7.25 , 20 )	( 7.5 , 20 )

Figure 2-6 shows that the expression (1) captures the retention behavior well in the range where the corresponding curve is shown. The parameters in Table 2-2 are fitted so that the response is close to the experimental data at high RH.

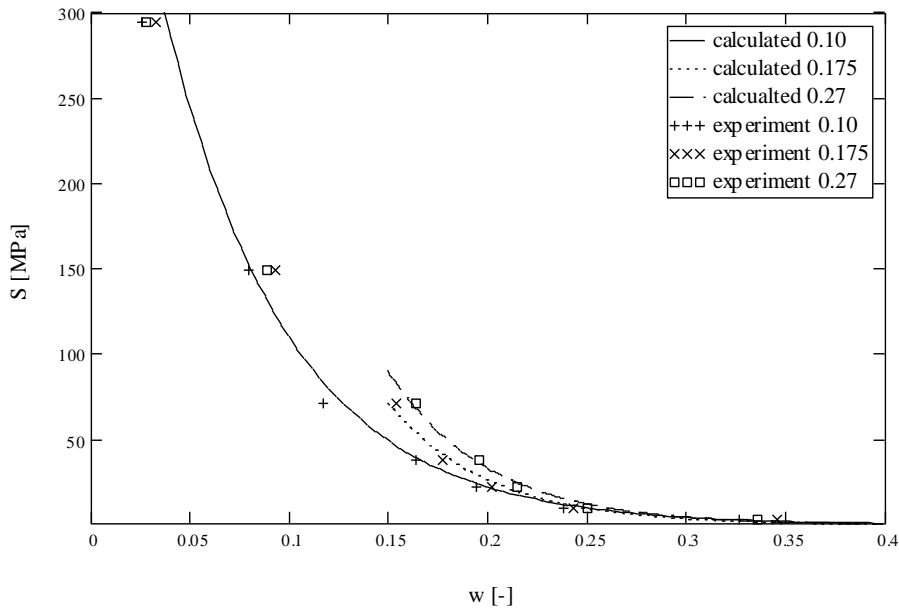


**Figure 2-6** *Experimental and model retention.*

It can be shown thermodynamically, see /Low et al., 1957/, that the swelling pressure,  $p_s$ , is related to the suction at full water saturation under free swelling conditions,  $S_{free}$ , according to

$$p_s(e, w_0) = S_{free}(w_f(e), w_0) \tag{2}$$

, where  $w_f(e) = \rho_w / \rho_s e$ . As Figure 2-7 shows, the experimental graph taken from /EBS 2005/, that the obtained swelling pressure - dry density relation resembles the experimental findings.

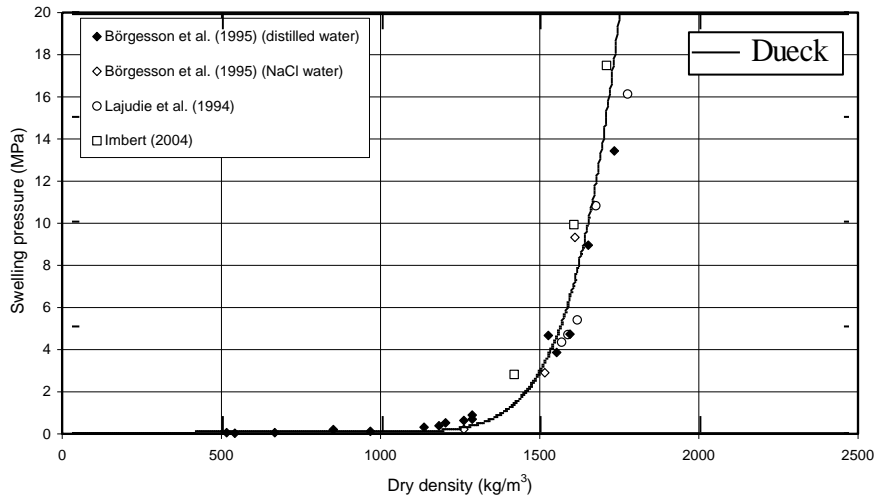


**Figure 2-7** Experimental and model swelling pressure.

To account for the effect of an external pressure,  $p$ , on the water retention (3) have been suggested, see /Crony et al. 1958/.

$$S_{conf}(w, w_0, e) = S_{free}(w, w_0) - \alpha p(w, w_0, e) \quad (3)$$

A simple assumption is that  $\alpha = 1$  and that the pressure depends linearly on the water ratio up to the swelling pressure, see /Börgesson, 1985/ and /Dueck, 2004/,

$$p(w, w_0, e) = p_s(e, w_0) \frac{w - w_0}{w_f - w_0} \quad (4)$$

(1) - (4) can be used to obtain an estimate of retention curves of bentonite under confined conditions with an initial water ratio  $w_0$  and void ratio  $e_0$ . In Figure 2-8 results obtained by using the equation above, with the dry densities 2000 kg/m<sup>3</sup> (black curves) and 1400 kg/m<sup>3</sup> (red curves) and the initial water ratio  $w_0 = 0$ , are shown together with the experimental data in Figure 2-5.

The model produces a process window containing most experimental points and the boundaries of the process window are not very far from the corresponding experimental points considering that the initial water ratio of the experiments is not known. The accuracy of the model is probably improved if the parameter set  $(a, b)$  corresponding to the correct initial water ratio is used.

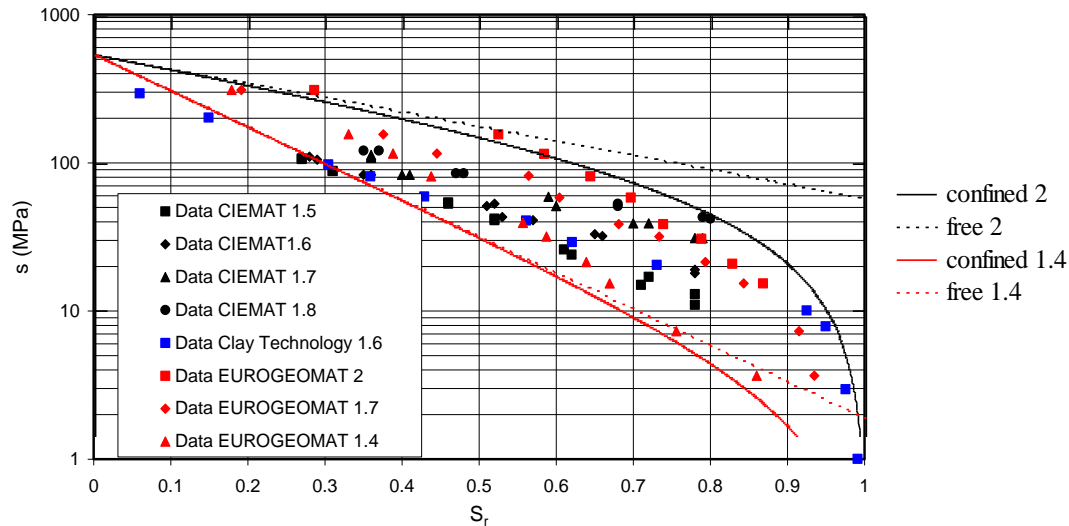


**Figure 2-8** Experimental and model data for confined retention. The model corresponds to a dry density of 2000 kg/m<sup>3</sup> and 1400 kg/m<sup>3</sup> respectively.

However, the analytical expressions (1) - (4) are considered to be accurate enough to give a possibility to calculate a process window inside which the bentonite block retention is likely to exist under the HM process. Below in Figure 2-9 such curves produced by (1) and (1) - (4) are shown together with the experimental retention data given earlier in Figure 2-5. The black curves show the initial state retention curve for  $e = e_0 = 0.564$ ,  $w_0 = 0.174$  and the red curves show the retention of an estimated final state where some swelling has occurred and therefore  $e = e_f = 0.75$ . The final void ratio  $e_f$  is estimated as the volume average of the initial void ratio, taking the inner slot, the bentonite and the pellet-filled slot into account. The dotted curves indicate free swelling retention and the solid lines indicate retention curves obtained under confined conditions. The arrow indicates the initial state.

A process window is also indicated with the shaded area. The three numbered boundaries are defined by:

1. A free swelling block from the initial condition.
2. An assumption of constant water ratio during expansion.
3. Confined swelling of the expanded block.

Note that the three steps above is not an actual process, it is just a way to obtain the boundaries of a possible process window.

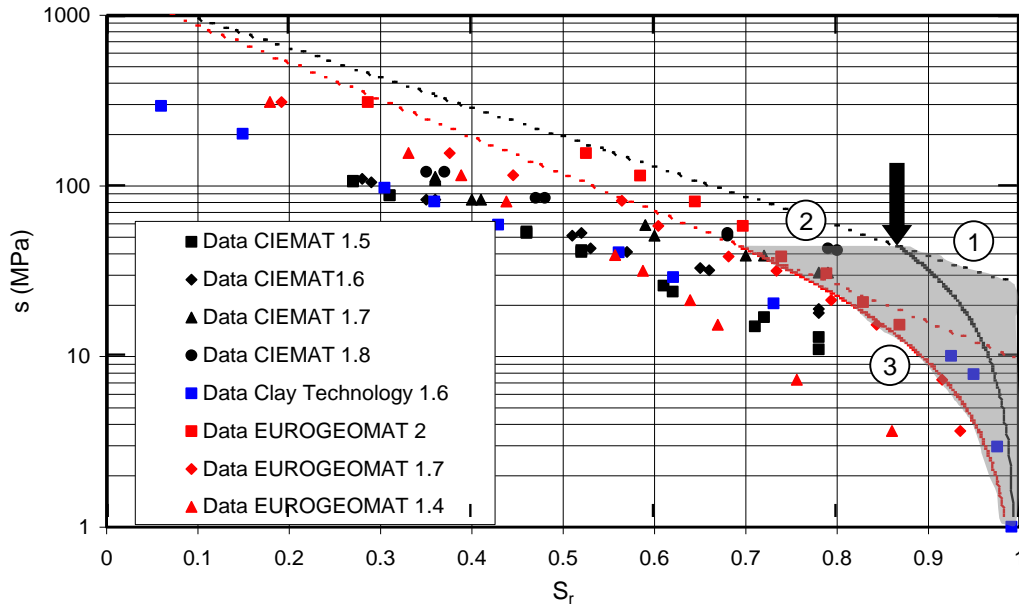


**Figure 2-9** Retention process window for bentonite block properties.

The same procedure is done for the pellet filled slot, but now with the initial state given by  $e = 1.78$ ,  $w_0 = 0.57$  and the final void ratio is assumed to be  $e_f = 0.75$  i.e. equal to the volume average initial pore volumes. Figure 2-10 shows the obtained retention curves, but the initial state is not contained in the graph and for a more complete view Figure 2-11 is also showing lower values of suction. When producing these results a parameter set  $(a,b) = (6.3, 14)$ , calibrated against an unpublished retention curve for  $w_0 = 0.63$ , has been used.

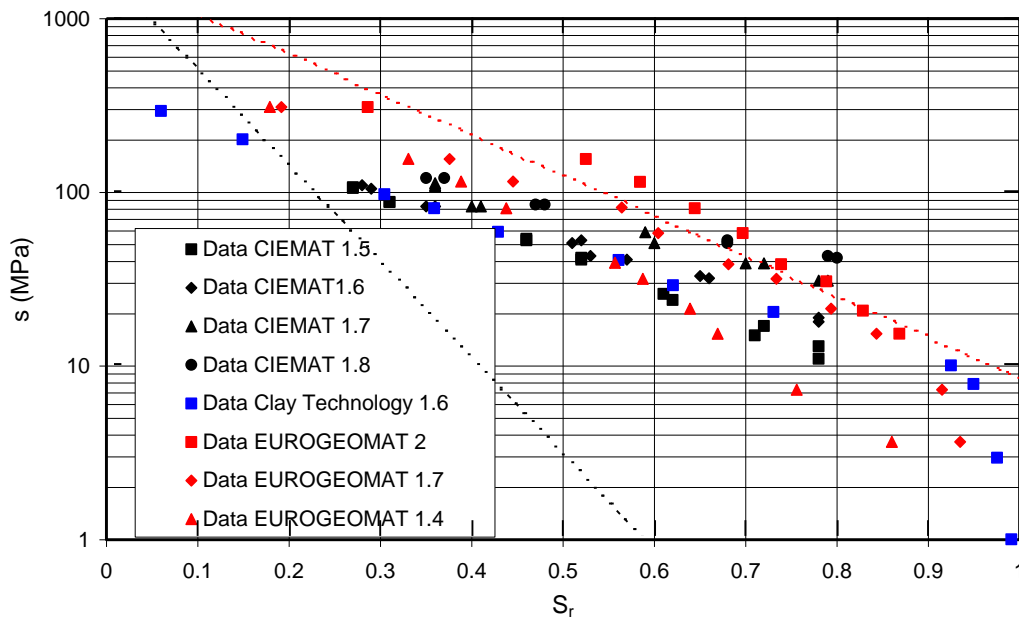


**Figure 2-10** Retention for homogenized pellet-filled slot. Experimental and model data.

Also here a process window is indicated. Here only one of the boundaries has a clear definition.

For the pellet-filled slot the estimated process window in retention is probably rather rough. The validity of the assumption of a homogenized media has not been confirmed. But as a point of departure the produced process window is considered to be of some relevance.

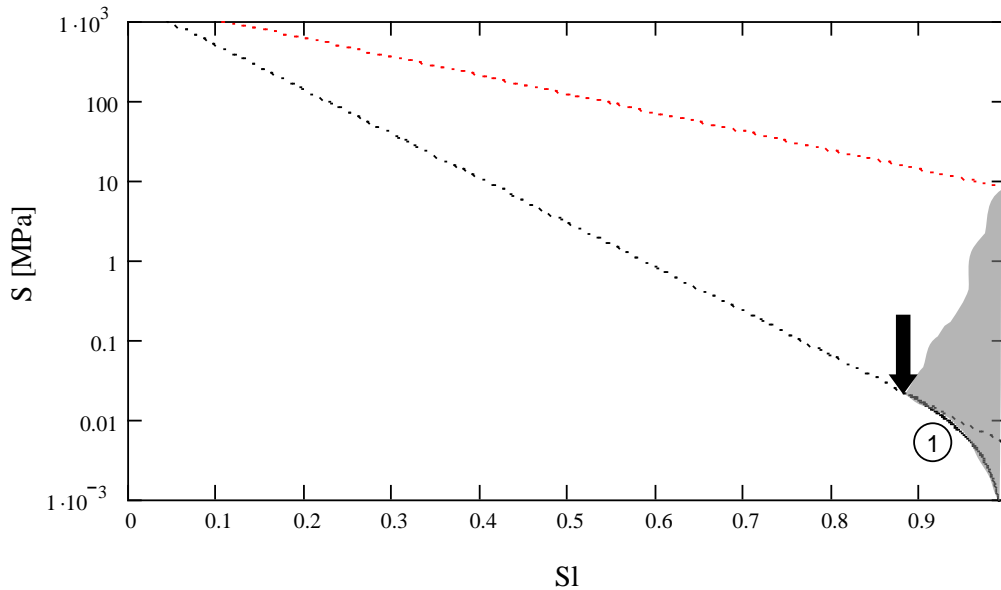


**Figure 2-11** Retention process window for homogenized pellet-filled slot.

In Figure 2-12, taken from /EBS, 2005/, a compilation of experimental results of the variation of the intrinsic permeability with porosity of MX-80 is shown.

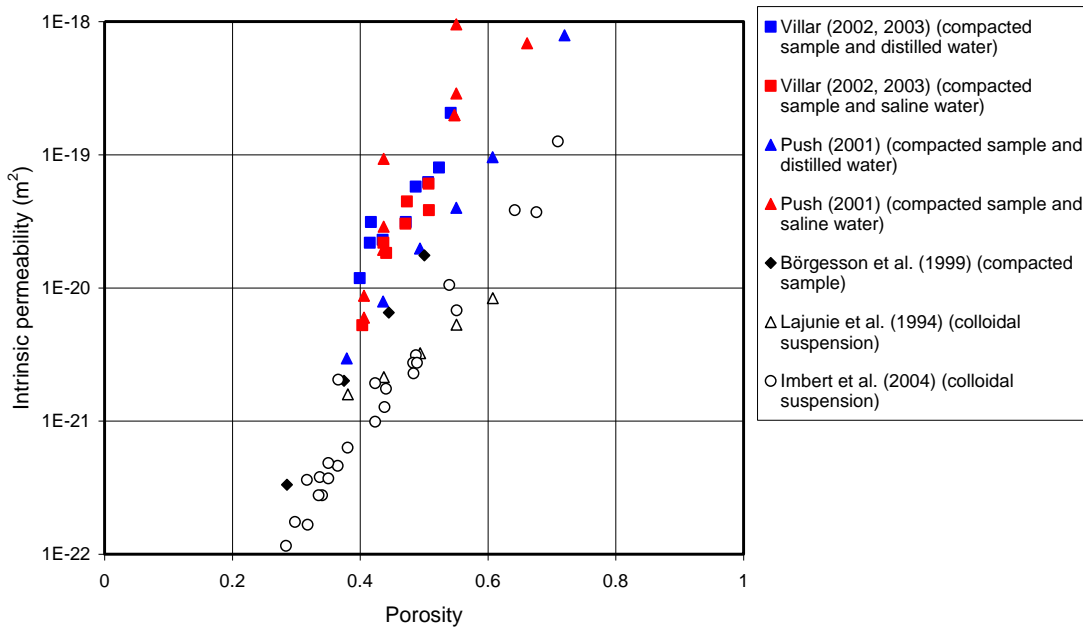


**Figure 2-12** Variation of intrinsic permeability with porosity as obtained by several laboratories in water-saturated samples.

### 2.5.3 Mechanical properties

In Figure 2-13, taken from /EBS, 2005/, the swelling pressure is given as a function of the dry density.

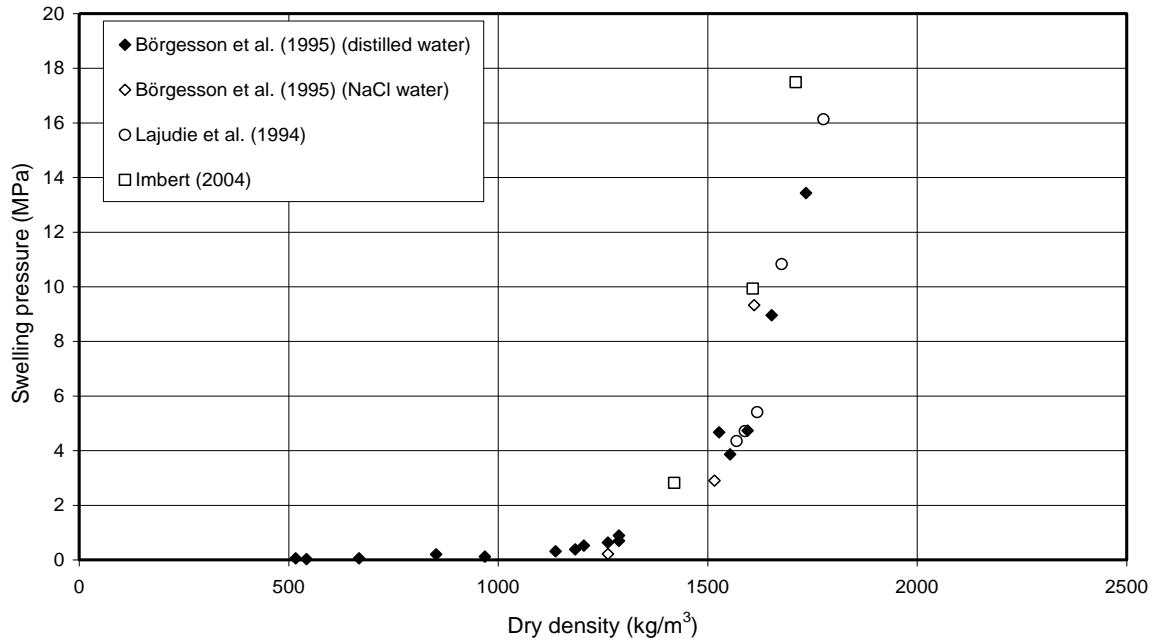


Figure 2-13 Swelling pressure vs dry density as obtained by different laboratories.

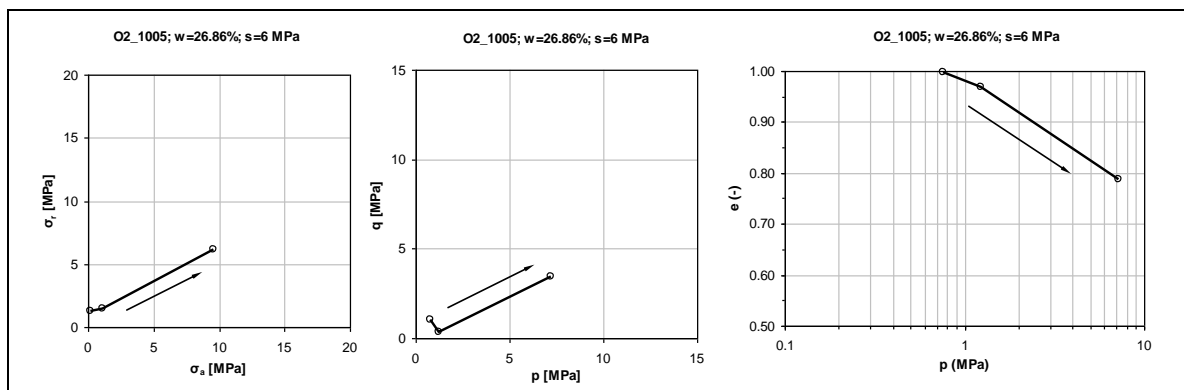
In Figure 2-14 the relation between pressure and void ratio is shown at different values of suction,  $S$ . The data is taken from /Dueck et al. 2006/.

The experimental setup from which the results were obtained consisted of a steel cylinder where a pre-compressed bentonite sample was inserted. The sample was then allowed to attain equilibrium with the suction  $S$ , given by the RH obtained from a salt solute, at a small prescribed axial stress. The sample was then subjected to different magnitudes of axial stress  $\sigma_a$ . From the recorded displacement of the loaded surface the void ratio  $e$  was obtained. The steel cylinder was also equipped with a force transducer in the radial direction from which the radial stress  $\sigma_r$  can be obtained. From the principal stresses,  $(\sigma_a, \sigma_r)$ , the pressure  $p = (\sigma_a + 2 \sigma_r)/3$  and deviatoric stress  $q = \sigma_a - \sigma_r$  can be calculated.

For each experiment, performed at a different level of suction, three graphs are showed in Figure 2-14.

- The left graph shows  $(\sigma_a, \sigma_r)$ , and is defining the prescribed load situation.
- The center graph shows  $(p, q)$ , which gives an overview of the load situation in the  $p - q$  space.
- The right graph shows  $(p, e)$ , where the  $p - e$  relation can be studied

The load path is indicated with arrows in the graphs.



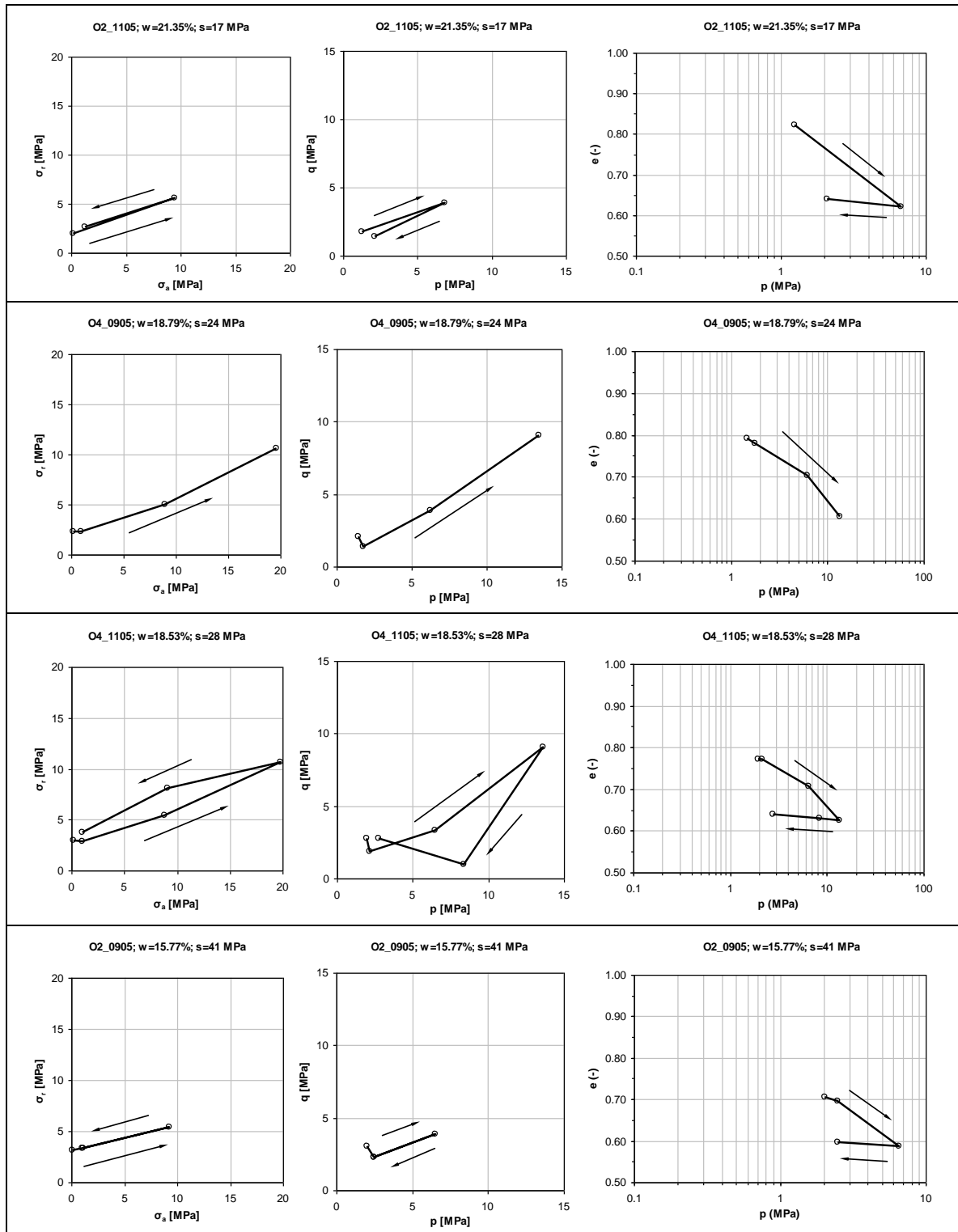
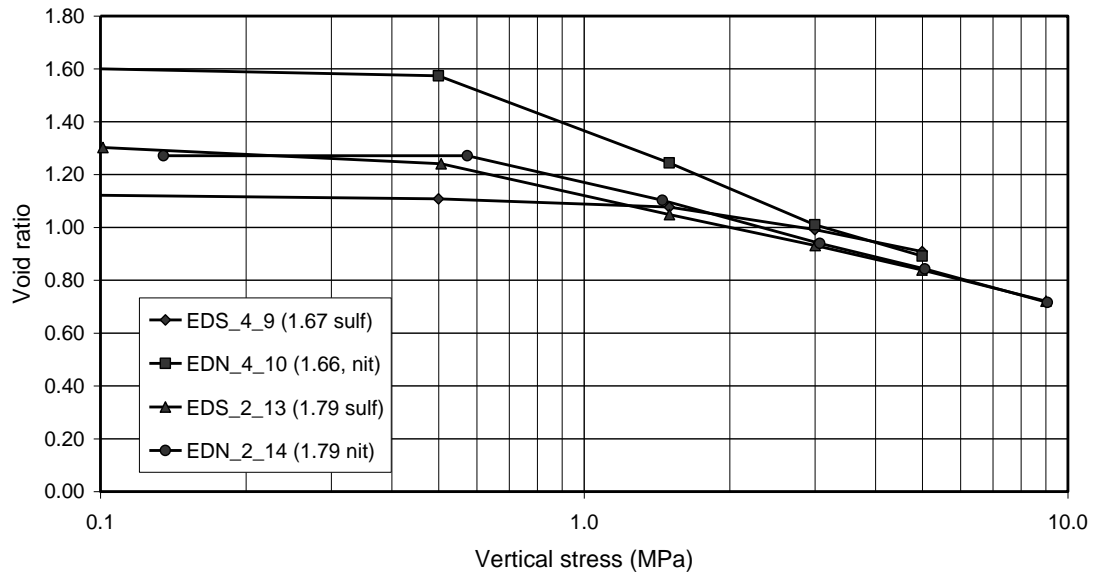


Figure 2-14 Pressure - void ratio relation at different levels of suction.

Below in Figure 2-15 the experimental results from /EBS, 2005/ are recapitulated.



**Figure 2-15** Compression lines obtained during the drained loading following the saturation stage for samples EDN\_4\_9, EDN\_4\_10, EDN\_2\_13 and EDN\_2\_14 /EBS, 2005/.

Below in Figure 2-16 the relation between void ratio,  $e$ , and suction,  $S$ , are shown at different levels of pressure  $p$ . The experimental data is taken from /Dueck et al., 2006/. The experimental setup is identical to the one described above used when the relation between void ratio and pressure at constant suction were investigated. The sample was subjected to a constant axial stress during changes in suction. The radial stress was recorded during the suction change and the corresponding level of pressure could then be calculated.

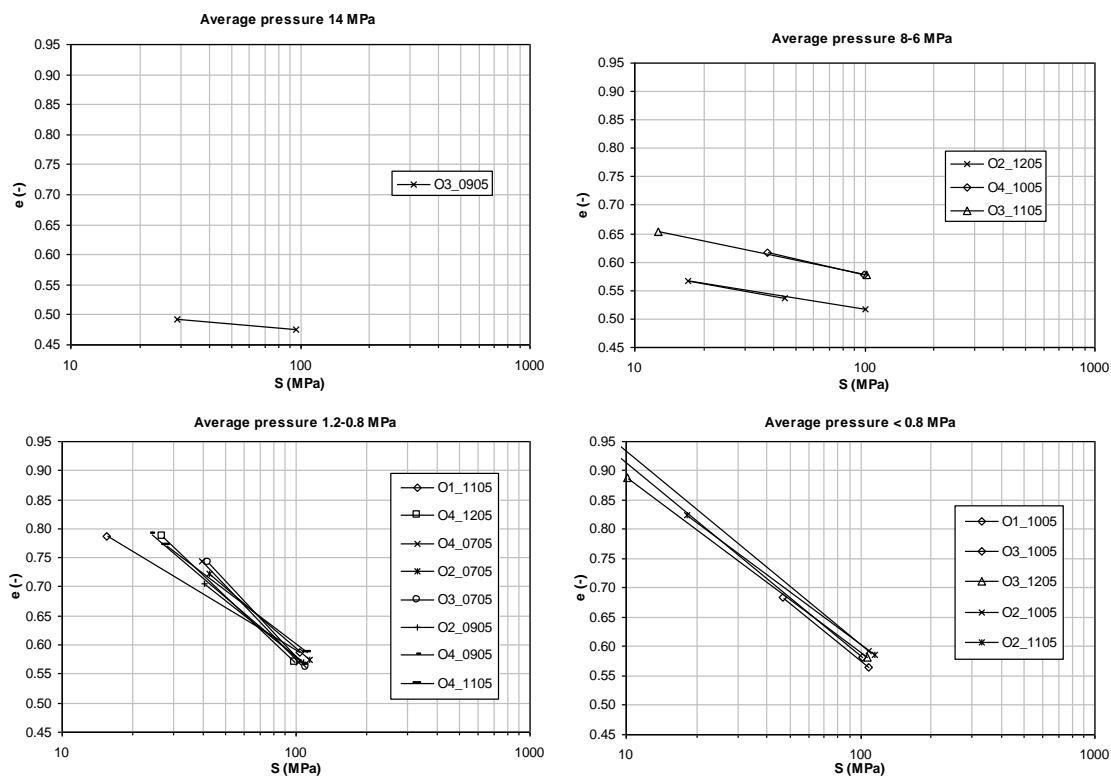


**Figure 2-16** The relation between void ratio and suction given at different pressure levels.

In Figure 2-17 below the relation between void ratio and suction is given at an axial load of 0.1 MPa, /EBS, 2005/.

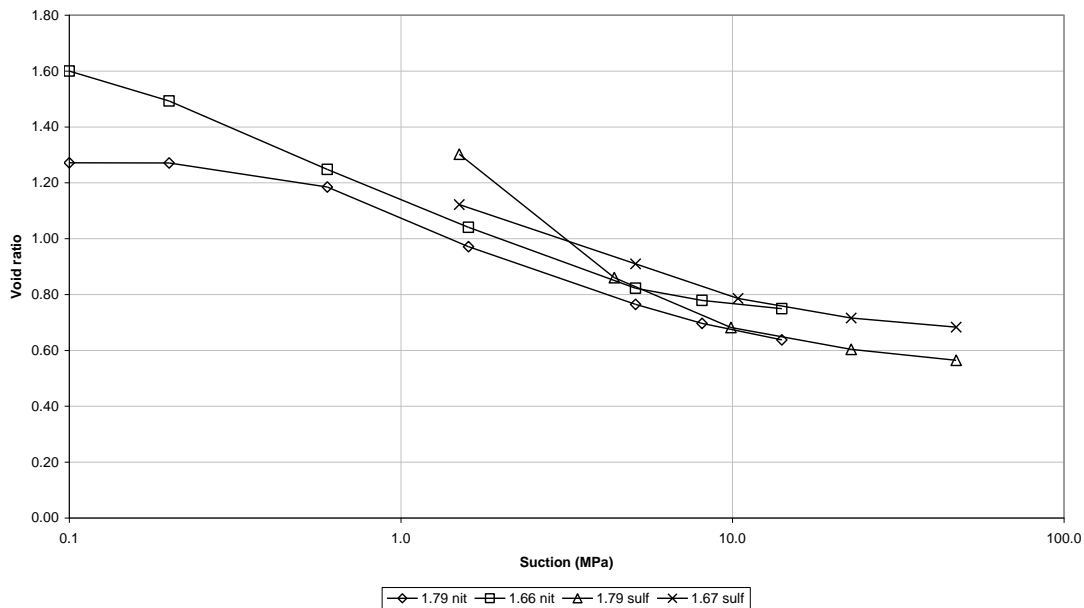


**Figure 2-17** Evolution of void ratio with applied suction during a wetting path performed in an oedometer cell under a constant load of 0.1 MPa /EBS, 2005/.

A thermal expansion coefficient of  $3 \cdot 10^{-6} \text{ }^\circ\text{C}^{-1}$  at  $T = 20 \text{ }^\circ\text{C}$  models the relation between temperature and void ratio well for a bentonite particle, /Börgesson et al., 1985/

## 2.6 Rock properties

The parameter values below are site data. No mechanical or hydraulic properties are presented since these processes are not considered necessary to model in the rock material for the experimental setup.

$$\rho = 2770 \text{ kg/m}^3$$

$$c = 770 \text{ J/(kg}\cdot\text{ }^\circ\text{C)}$$

$$\lambda = 2.6 \text{ W/(m}\cdot\text{ }^\circ\text{C)}$$

## 2.7 Concrete plug properties

Handbook values of concrete are presented, the reinforcement is not considered. No hydraulic properties are presented, since the concrete plug is protected from wetting by the impermeable rubber shield.

$$\rho = 2400 \text{ kg/m}^3$$

$$c = 770 \text{ J/(kg}\cdot\text{ }^\circ\text{C)}$$

$$\lambda = 2.7 \text{ W/(m}\cdot\text{ }^\circ\text{C)}$$

$$E = 30 \text{ GPa}$$

$$\nu = 0.15$$

$$\alpha = 10 \cdot 10^{-6} \text{ }^\circ\text{C}^{-1}$$

## 2.8 Steel lid properties

Handbook values for S355JR are presented below. Hydraulic properties are not considered to be necessary.

$$\rho = 7840 \text{ kg/m}^3$$

$$c = 460 \text{ J/(kg}\cdot\text{°C)}$$

$$\lambda = 47 \text{ W/(m}\cdot\text{°C)}$$

$$E = 206 \text{ GPa}$$

$$\nu = 0.3$$

$$\alpha = 12 \cdot 10^{-6} \text{ °C}^{-1}$$

## 2.9 Rock anchors properties

In Figure 2-18 below the total force acting on the plug is plotted against the plug displacement at the corresponding time. An assumption of a linear relation,  $\Delta F = k\Delta u$ , between the force and displacement seems appropriate. A stiffness  $k \approx 2.08 \text{ GN/m}$  is obtained for the red curve. Figure 2-18 was obtained using the average value of all three measured anchor forces and the “displacement2” measurement.

To check the measurements somewhat, Young’s modulus for the wires was calculated from knowing the force – displacement data in Figure 2-18 together with the known geometry (wire inclination =  $22^\circ$ , free wire length = 5 m and nominal anchor area =  $19 \cdot 98.7 \text{ mm}^2$ ). From the calculation the value  $E = 163 \text{ GPa}$  was obtained. In manufacturer data sheets for the wire the Young’s modulus is specified as approximately 197 GPa.

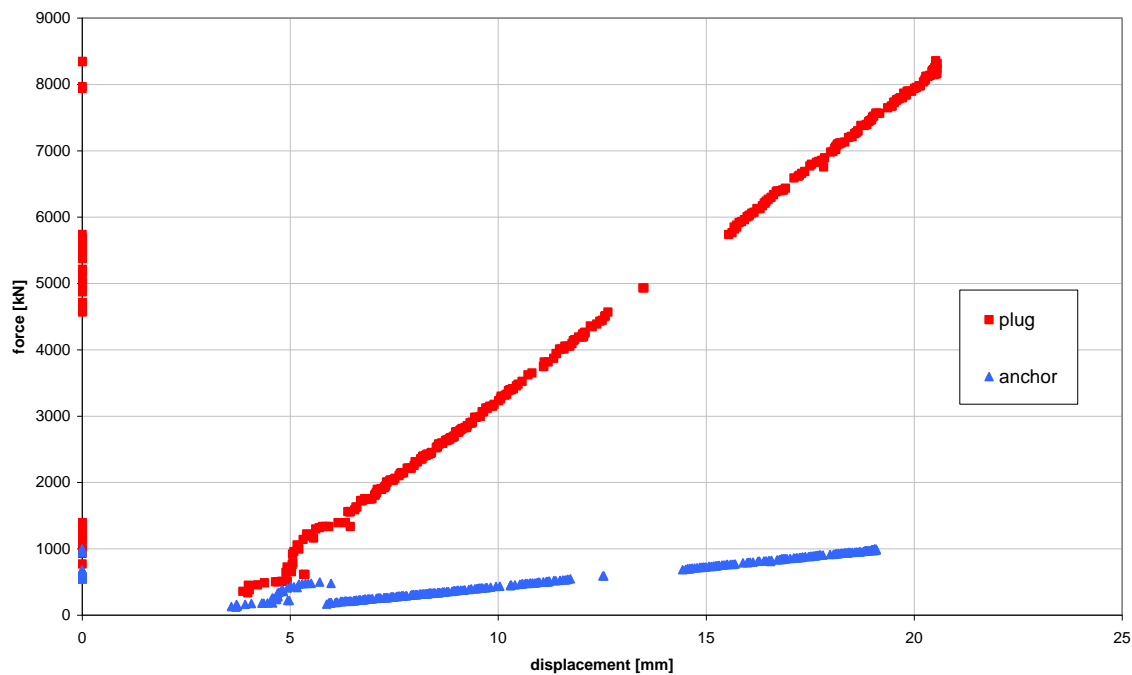


**Figure 2-18** The total force acting on the plug and the average force in all anchors plotted against total vertical displacement of the plug and the anchor elongation respectively.